413027

UNCLASSIFIED

FINAL DEVELOPMENT REPORT

PART II

FOR

THE DEVELOPMENT OF GAS LUBRICATED BEARINGS FOR USE IN BLOWER AND FAN MOTORS

THIS REPORT COVERS THE PERIOD 7 JUNE 1962 TO 7 JUNE 1963

ROTRON MANUFACTURING CO.
WOODSTOCK, N. Y.

NAVY DEPARTMENT BUREAU OF SHIPS ELECTRONICS DIVISION
Contract No. NObsr - 87522
25 JUNE 1963

UNCLASSIFIED

DESIGN MANUAL

FOR

SELF ACTING PLAIN CYLINDRICAL GAS JOURNAL BEARINGS

AND

THRUST BEARINGS

FOR USE IN

ELECTRICAL BLOWER MOTORS

ROTRON MANUFACTURING CO., Inc.

WOODSTOCK, NEW YORK

TABLE OF CONTENTS

	Page
I. INTRODUCTION	1
Use of the Gas Bearing Design Manual	2
Review of Basic Concepts in Gas Lubricated Bearings	3
II. DESIGN OF GAS-LUBRICATED JOURNAL BEARINGS	15
A. Load-Carrying Capacity with Static, Uni-Directional Loads	15
General Solution for Load Capacity	16
Journal Bearing Solutions for Low Values of Λ	31
Moment-Carrying Capacity of Journal Bearings	38
B. Evaluation of Friction in Full Journal Bearings	40
C. Attitude Angle in Full Gas-Lubricated Journal Bearings	46
D. Synchronous Whirl	60
Forces Due to Rotating Unbalance	60
Establishments of Limits for Rotating Unbalance	62
Synchronous Resonant Whirl	63
Translatory Synchronous Whirl Rotating Journal	64
Conical Synchronous Whirl Rotating Journal	66
Synchronous Translatory and Conical Bearing Whirl	68
Influence of External Vibration	73
E. Half-Frequency Whirl	76
Half-Frequency Whirl Stability for Liquid Lubricated Self-Acting Bearings	79
Half-Frequency Translatory Whirl Analysis for Small Values of Lambda	81

TABLE OF CONTENTS

	Page
E. Half-Frequency Whirl (cont'd)	
Half-Frequency Translatory Whirl of a Shaft in Infinitely Long Cylindrical Journal Bearings	91
Summary of Discussion on Half-Frequency, Translatory Shaft Whirl	97
Conical, Half-Frequency Whirl, Rotating Journal	98
Conical, Half-Frequency Bearing Whirl (Rotating & Non-rotating Bearing)	99
III. SELF-ACTING THRUST BEARINGS	107
A. Design of Self-Acting, Spiral Grooved Thrust Bearings	111
Film Stiffness in Spiral Grooved Thrust B Bearings	119
IV. BEARING LOADS	121
A. Magnetic Radial Bearing Loads	121
B. Bearing Moment Loads	125
V. BIBLIOGRAPHY	127

LIST OF ILLUSTRATIONS

Figure No.	Title	Page
1	Self-Acting Pressure Generation in a Journal Bearing (Ref. 1)	5
2	Experimental Pressure Distribution in a Journal Bearing (Ref. 2)	6
3	Journal in 360° Full Bearing	7
4	Schematic Diagram of Slider Thrust Bearing	8
5	Grooved Thrust Bearings (Ref. 2)	8
6	Example of Relationship between Load-Carrying Capacity W and Λ for a Self-Acting Gas Lubricated Journal Bearing (Data from Ref.2)	9
7	Load-Carrying Capacity of Self-Acting Gas Lubricated Journal Bearing as Influenced by Speed (Ref. 6)	10
8	Generalized Experimental Correlation of Dimensionless Load Parameter W' vs Λ , for l/d = 2 (Ref. 2)	11
9	Pressure Distribution for Compressible Fluids along a Straight Slider Bearing (Ref. 7)	13
10	Coordinate System for Journal Bearing	16
11	Theoretical Load-Carrying Parameter vs Compressibility Parameter for Full Journal Bearing for l/d = ∞ (Refs. 10 and 14)	18
12	Theoretical Load-Carrying Parameter vs Compressibility Parameter for Full Journal Bearing for l/d = ∞ (Ref. 11)	20
13	Theoretical Load-Carrying Parameter vs Compressibility Parameter for Full Journal Bearing for l/d = 2 (Ref. 14)	22

LIST OF ILLUSTRATIONS

Figure No.	Title	Page
14	Theoretical Load-Carrying Parameter vs Compressibility Parameter for Full Journal Bearing for l/d = 1 (Ref. 14)	24
15	Theoretical Load-Carrying Parameter vs Compressibility Parameter for Full Journal Bearing for l/d = ½ (Ref. 14)	26
16	Absolute Viscosity of Air (Refs. 16 & 17)	28
17	Theoretical Load-Carrying Capacity, 360° Journal Bearing	29
18	Discrepancy in Load Capacity between Theories based on Incompressible and Compressible Lubricants (Ref. 14)	31
19	1/S Plotted Against Eccentricity Ratio for $\Lambda \to 0$ (Data from Ref. 15)	33
20	1/S Plotted Against Eccentricity Ratio for $\Lambda \to 0$ (Data from Ref. 15)	34
21	Moment Capacity of Full Journal Bearings (Ref. 5)	37
22	Schematic Representation of Journal Bearing Sustaining an Applied Moment.	38
23	Relationship between Bearing Friction Torque and Journal Friction Torque(Ref.9)	40
24	Friction Factor for Full Bearing of Infinite Length (Ref. 15)	41
25	Effects of Slenderness and Eccentricity Ratios on Friction Factor (Ref. 15)	43
26	Typical Attitude-Eccentricity Locus for the Motion of the Center of a Journal in the Clearance of a Self-Acting Bearing	46
27	Attitude Relationship for Journal Bearing	46

LIST OF ILLUSTRATIONS

Figure No.	Title	Page
28	Attitude-Eccentricity Locus for Liquid Lubricated 180° Journal Bearing	48
29	Attitude-Eccentricity Locus Diagrams for Full Gas-Lubricated Journal Bearings(Ref.14)	49
30	Attitude Angle vs Compressibility Parameter for 1/d = ∞ (Ref. 13)	51
31	Attitude Angle vs Compressibility Parameter for 1/d = π (Ref. 13)	53
32	Attitude Angle vs Compressibility Parameter for 1/d = 2 (Ref. 13)	55
33	Attitude Angle vs Compressibility Parameter for 1/d = 1 (Ref. 13)	57
34	Attitude Angle vs Compressibility Parameter for 1/d = ½ (Ref. 13)	59
35	Force F, Resulting from Unbalance of Rotor Shaft Rotating with Shaft at Synchronous Speed	60
36	Schematic Representation of Orbiting Paths in a Journal Bearing	60
37	Orbital Eccentricity Ratio for Journal Subjected to an Unbalanced Radial Load (Data from Ref. 20)	62
38	Replot of Figure (17).	64
39	Indication of Synchronous Whirl of Shaft in Journal Bearing	66
40	Schematic Representation of Shaft Conical Synchronous Whirl	67
41	Conical Whirl of Bearing with Respect to Shaft	69

LIST OF ILLUSTRATIONS

Figure No.	Title	Page
42	Fixed Shaft and Rotating Bearing	70
43	Bearing Load Capacity under Sinusoidal Load Condition	75
44	Orbital Whirling Velocity of Shaft Center about Center of Bearing Compared to Shaft Spinning Velocity	77
45	Relationship of Radial Force F_r to Tangential Force F_θ for Several Values of Eccentricity Ratio	78
46	Ratio "C" Plotted Against Compressibility Number for Two l/d Ratios	85
47	"C" Plotted Against Λ and ω_1^* for l/d = ½	90
48	"C" Plotted Against Λ and ω_1^* for l/d = 1	90
49	Half-Frequency Whirl Stability Plot for $\varepsilon_o = 0.1$	93
50	Plot of Half-Frequency Translatory Whirl Threshold for Infinite Length 360^0 Journal Bearing	95
51	Schematic Representation of Rotating Bearing on Stationary Shaft	103
52	Dimensions of Hollow Cylinder for Equations (45) and (46)	103
53	Typical Forms of Self-Acting Thrust Bearing	107
54	Grooved Pumping Plate with Either Logarithmic or Archimedean Spiral	108
55	Grooved Thrust Bearings	108
56	Comparative Pressure Distribution for Compressible and Incompressible Lubrication	108

LIST OF ILLUSTRATIONS

Figure No.	Title	Page
57	Gas Pressure Distribution in Flat Tilted Pad Bearing	109
58	Schematic Representation of a Pumping Groove	109
59	Optimized Configuration for Spiral-Grooved Pumping Plate	111
60	Spiral-Grooved Thrust Plate Parameters	113
61	Thrust Bearing Capacity of A Single Bearing and also of a Double Acting Bearing with a Total Clearance of 0.001 Inches	117
62	Schematic Diagram of Double Acting Thrust Bearing	117
63	Thrust Load Characteristics of Double Acting Bearing with Total Clearance of 0.001 Inches	118
64	Motor Stator to Rotor Eccentricity	121
65	Flux Lines Linking Motor Rotor & Stator for Angular Positions of Stator Magnetic Field	122
66	Moment Produced by Non-Parallel Motor Rotor and Stator Centerlines	125
67	Magnetic Force Producing Moment Diagram	126

LIST OF TABLES

Table No.	Title	Page
I	Table of Radial Clearance to Molecular Mean Free Path	13
II	Compressibility Parameter vs Load Parameter for l/d of Infinity	19
III	Compressibility Parameter vs Load Parameter for l/d of π	21
IV	Compressibility Parameter vs Load Parameter for l/d of 2	23
V	Compressibility Parameter vs Load Parameter for l/d of 1	25
VI	Compressibility Parameter vs Load Parameter for l/d of ½	27
VII	Viscosity Data for Air	28
VIII	Values of 1/S vs ε, from Hays (15)	32
IX	Friction Factors for Full Bearings of Infinite Length	42
X	Attitude Angles for Liquid Lubricated, 180° Journal Bearing	48
XI	Attitude Angle vs Compressibility Parameter for l/d = ∞	50
XII	Attitude Angle vs Compressibility Parameter for l/d = π	52
XIII	Attitude Angle vs Compressibility Parameter for l/d = 2	54
XIV	Attitude Angle vs Compressibility Parameter for l/d = 1	56
XV	Attitude Angle vs Compressibility Parameter for l/d = ½	58

LIST OF TABLES

Table No.	Title	Page
XVI	Experimental Values of K*	69
XVII	Calculated and Observed Threshold Speeds for Half-Frequency Whirl	86
XVIII	Stability Data for Half-Frequency Whirl Threshold	88
XIX	Cross-Plotted Stability Data vs "C" and ω_1^* for $l/d = \frac{1}{2}$	88
XX	Cross-Plotted Stability Data vs "C" and ω_1^* for $l/d = 1$	89
XXI	Stability Data from Ref. 34 for Half-Frequency, Translatory Shaft Whirl, in 360° Cylindrical Journal Bearings of Infinite Length	94
XXII	Values of Spiral-Grooved Thrust Plate Parameters, θ and τ	113
XXIII	Computed Values of Thrust Capacity	116
XXIV	Net Load Capacity of Double Acting Thrust Bearings	116

LIST OF SYMBOLS

a_1 Thrust Plate Groove Width (in.)

a_2 Thrust Plate Land Width (in.)

b Thrust Plate Pumping Face Width (in.)

B Magnetic Flux Density (lines/in^2)

c Radial Clearance (in.)

c_f Friction Factor (Eq. 13)

c_t Thrust Plate Seal Belt Width (in.)

"C" Ratio of Predicted to Measured Half-Frequency Whirl

d Bearing Diameter (in.)

D Rotor Diameter (in.)

e Eccentric Distance of Shaft and Journal Center (in.)

f Frequency (cps)

f_{ts} Frequency-Synchronous Translatory Shaft Whirl (cps)

f_{cs} Frequency-Synchronous Conical Shaft Whirl (cps)

f_{tb} Frequency-Synchronous Translatory Bearing Whirl (cps)

f_{cb} Frequency-Synchronous Conical Bearing Whirl (cps)

$f_{\frac{ts}{2}}$ Frequency-Half-frequency Translatory Shaft Whirl (cps)

$f_{\frac{cs}{2}}$ Frequency-Half-frequency Conical Shaft Whirl (cps)

$f_{\frac{tb}{2}}$ Frequency-Half-frequency Translatory Bearing Whirl (cps)

F Force (pounds)

g Gravitation Constant (= 386 in/sec^2)

h Film Thickness (in.)

LIST OF SYMBOLS

h_o Minimum Film Thickness (in.)

H Parameter for Determination of Moment Loads (Eq. 11)

I_{ts} Transverse Moment of Inertia of Shaft System (lb.in.sec^2)

I_{ps} Polar Moment of Inertia of Shaft System (lb.in.sec^2)

I_{tb} Transverse Moment of Inertia of Bearing (lb.in.sec^2)

I_{pb} Polar Moment of Inertia of Bearing (lb.in.sec^2)

J Thrust Plate Radial Width (in.)

k Gas Bearing Film Stiffness for Translatory Synchronous Whirl (lb/in)

k_c Gas Film Restoring Moment for Conical Synchronous Whirl (lb/in)

K Parameter for Determination of Moment Loads (Eq. 12)

K_1 Shaft Mechanical Spring Stiffness (lb/in)

K_2 Gas Bearing Film Stiffness for Half-Frequency Translatory Whirl (lb/in)

K_{2c} Gas Film Restoring Moment for Half-Frequency Conical Whirl (lb.in)

l Bearing Length (in.)

l_r Rotor Length (in.)

l_m Motor Rotor Lamination Stack Length (in.)

L Distance between Bearing Centers (in.)

m_b Bearing Mass (lb.sec^2/in)

m_s Shaft Mass (lb.sec^2/in.)

M Moment (in.lbs)

LIST OF SYMBOLS

M_l Mass per Unit Length ($lb.sec^2/in^2$)

M_j Friction Moment (in.lbs)

n Ratio of Minimum Film Thickness to Molecular Mean Free Path

N Rotational Speed (rev/min)

N' Rotational Speed (rev/sec)

P_a Absolute Ambient Pressure (lb/in^2abs)

P_{avg} Average Pressure (lb/in^2)

r Journal Radius (in.)

r_m Mean Radius Thrust Plate (in.)

R Rotor Radius (in.)

S Sommerfeld Number (Eq. 4)

T Thrust Capacity per inch of Mean Circumference (lb/in)

u_o Linear Velocity at Mean Radius (in/sec)

U Surface Velocity (in/sec)

w Load per Unit Length (lb/in)

W Bearing Load (lbs)

W' Load Carrying Parameter = $\frac{W}{dlP_a}$

GREEK SYMBOLS

γ	Motor Air Gap Eccentricity (Eq.54)
δ	Bearing Misalignment Angle (radians)
δ_t	Thrust Bearing Groove Depth (in.)
Δ	Average Motor Radial Air Gap (in.)
ε	Eccentricity Ratio (Eq. 5)
ε_o	Eccentricity Ratio for Infinitely Long Bearing
θ	Thrust Bearing Parameter (Eq. 50)
Λ	Compressibility Bearing Parameter (Eq. 1)
μ	Viscosity ($lb.sec/in^2$)
σ	Motor Load Parameter (Eq. 53)
τ	Thrust Bearing Parameter (Eq. 51)
ϕ	Attitude Angle (degrees)
ω	Rotational Velocity (radians/sec)
ω_1^*	Stability Parameter (Eq. 34)

DESIGN MANUAL
for
Self-Acting Gas Lubricated Bearings for Use in Electrically Driven Blowers

I. INTRODUCTION

This manual is a direct outcome of the requirements set forth in BuShips Contract NObsr-87522 and is intended for use in the design of unit type self-acting gas bearings applicable to electrically driven blowers in the 10 to 500 cfm range. The work of preparing the manual was accomplished by the Rotron Manufacturing Company with Mr. D. D. Fuller serving as Consultant on gas bearings.

The information contained in the manual has been assembled utilizing the existing available literature for self-acting gas lubricated bearings. Insofar as possible, the data has been verified by additional test data accumulated at Rotron Manufacturing Company.

In its simplist form the construction of a radial, self-acting gas bearing can be thought of as a plain shaft running in a very close fitting bore and appears as a relatively simple problem. However, the clearances between shaft and bore must be carefully established so as to insure that the two elements are separated by a gas film during operation. This film carries the applied load and also acts as a spring with a definite spring rate. Therefore, besides determining the load carrying capacity, the problem resolves itself into the determination of the spring rate and the stability characteristics of the spring. As we consider the parameters responsible for the bearing characteristics, such as the pressure distribution in the gas film, the viscosity of the gas, and the speed and dimensional considerations, the complexity of the problem becomes more apparent.

Before reviewing the general concepts of gas lubricated bearings, it would do well to define some of the instabilities and terminology used in gas bearing design.

Self-Acting Bearing: A non-pressurized bearing that operates on a self induced gas film. It is generally termed "hydrodynamic bearing" to distinguish it from the pressurized "hydrostatic bearing".

Attitude-Eccentricity Locus: The path that the center of the rotating component follows under different load and speed conditions.

Synchronous Whirl: The orbital motion of the center of the rotating journal-bearing combinations around the center of the stationary member in the direction of rotation at a frequency equal to that of the spin speed. If the amount of unbalance present is small, it is possible to pass through this natural frequency by increasing the operating speed of the unit. At this point the spinning component will shift or invert from its geometrical center to its mass center or more specifically to its center of gravity. The speed at which this occurs is called the "inversion point" critical speed or alternately the "synchronous resonant whirl" critical speed.

Half-Frequency Whirl: The orbital motion of the center of the spinning member around the stationary member in the direction of rotation at a frequency of one-half or less of the spinning or rotational frequency.

As will become apparent in the design section of the manual, dimensional control of the clearances in a bearing and the type of loads the bearing must sustain are generally the key to successful operation of the bearing once the bearing design is established. This points out the desirability to design a specific piece of rotating equipment around the gas bearing in order to maintain the desired control within the bearing. In the case of electrically driven air moving devices, bearing location within the motor, electrical unbalance loads, air impeller location and resultant loads should be optimized in regard to their effect upon bearing performance to insure reliability of the equipment.

Use of the Gas Bearing Design Manual

Insofar as possible, all curves and formulations contained in this manual have been checked experimentally either at Rotron or by the experiments conducted by some of the referenced sources contained at the end of this manual. It should be understood, however, that experiments are conducted under ideal conditions with known loads generally applied through the bearing support center. Some variation in calculated results can be expected from the need to approximate the value of actual loads as well as from the variation in the true clearance in the bearing caused by taper or out-of-round conditions. It

is the attempt of this manual to provide the designer with the latest state-of-the art information on gas bearing design. Some good judgement on the part of the designer is required when considering his specific application. If these considerations are understood the manual should be a very useful guide for initiation of a gas lubricated blower design. Verification of the design will necessarily be accomplished by actual test.

The recommended procedure for utilizing the manual is to follow the order of presentation of the manual, i.e.: determine bearing size and load capabilities, and then determine bearing stability characteristics. An example is given for each computation to assist the designer in making use of the information. Included in the manual is a section on motor magnetic load influences of a two pole alternating current motor to assist the designer in predicting actual loads.

Review of Basic Concepts in Gas Lubricated Bearings

In order to make effective use of this design manual it is necessary for the designer to understand fully the basic concepts of gas lubricated bearings. Initially, it can be stated that a gas lubricated bearing is a type of bearing that has its running surfaces completely separated by a film of gas. Even when load is applied to the bearing, the surfaces are kept out of contact by this gas-film cushion.

As with liquid-lubricated, fluid-film bearings, the gas film is established by either of two basic actions. The first is characteristic of self-contained bearings operating in an open bath of liquid or gas. The relative motion of the sliding parts themselves, generates a film pressure within the clearance spaces of the bearing and insures separation of the surfaces and load-carrying capacity. This type of bearing is called the hydrodynamic (liquid) or self-acting (gas) bearing.

Figure (1) is an interesting drawing taken from Drescher (1) and shows schematically this phenomenon of self-acting pressure generation. An actual pressure trace for an experimental journal bearing is shown in Figure (2)

taken from Ford, Harris and Pantall (2). Since the viscosity of a gas is relatively low at room temperature, about 1/50 of that of water or 1/3500 of that of an SAE 10 petroleum oil, the load-carrying capacity resulting from this self-generated pressure is likewise relatively low. If the bearing has to start from rest under a static load and lift itself off the "ground" so to speak, and become gas borne, unit loads are generally limited to 1 to 2 psi based on the projected area of the bearing. If the load is applied after rotation has been established the unit load-carrying capacity may reach a practical maximum of about 10psi, again based on the projected area of the bearing, although higher values have been reported in laboratory test data. Cole and Kerr (3) list average pressures as high as 26.5 psi.

With the second basic type of bearing, the externally-pressurized or hydrostatic bearing, the limitation on load-carrying capacity no longer exists. In this type of bearing high pressure gas is supplied to the clearance space in the bearing and the surfaces are forced apart as a result. Limits on load-carrying capacity are dependent therefore only on the practical limits of gas pressure and gas volume that are conveniently available. Externally-pressurized gas bearings have been built with unit load-carrying capacities as high as 50 psi. There is, however, no reason why this figure of 50 psi cannot be exceeded if necessary. Since these bearings are not dependent on speed for the generation of pressure they can conveniently establish separation of surfaces and carry rated load with no rotation or sliding. There is always,of course, flow of gas through the bearing from the high pressure source to the lower ambient pressure. One of the conditions for successful operation of the externally-pressurized bearing therefore, requires that this volume of gas must be constantly supplied. In some applications where relatively high static loads are involved, hydrostatic gas may be needed only for starting. After normal operating conditions have been established the bearing may then continue to operate as a self-acting bearing.

However, in this manual we will consider only the self-acting gas-lubricated bearing.

Most of the complications that arise in the analysis and application of gas-lubricated bearings stem from two factors, first, the compressibility of the gas and, second,

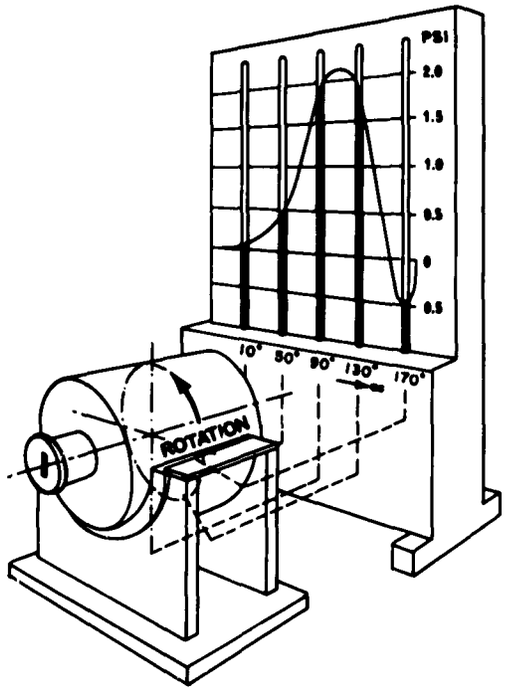

Fig. 1 - Self-Acting Pressure Generation in a Journal Bearing. (Ref. 1).

the low damping characteristics of the gas film. Some of the bearing characteristics that result and a number of the problems associated with these parameters will now be discussed.

When Harrison published his hydrodynamic analysis of a gas-lubricated journal bearing in 1913,(4), including the effect of compressibility, his equations showed the effect of ambient pressure and led to the establishment of a dimensionless group of variables that seemed to be significant in describing the performance characteristics of gas bearings.

For a journal bearing this was:

$$\frac{6\mu U r}{P_a c^2} \quad \text{or} \quad \frac{6\mu\omega}{P_a}\left(\frac{r}{c}\right)^2 \qquad (1)$$

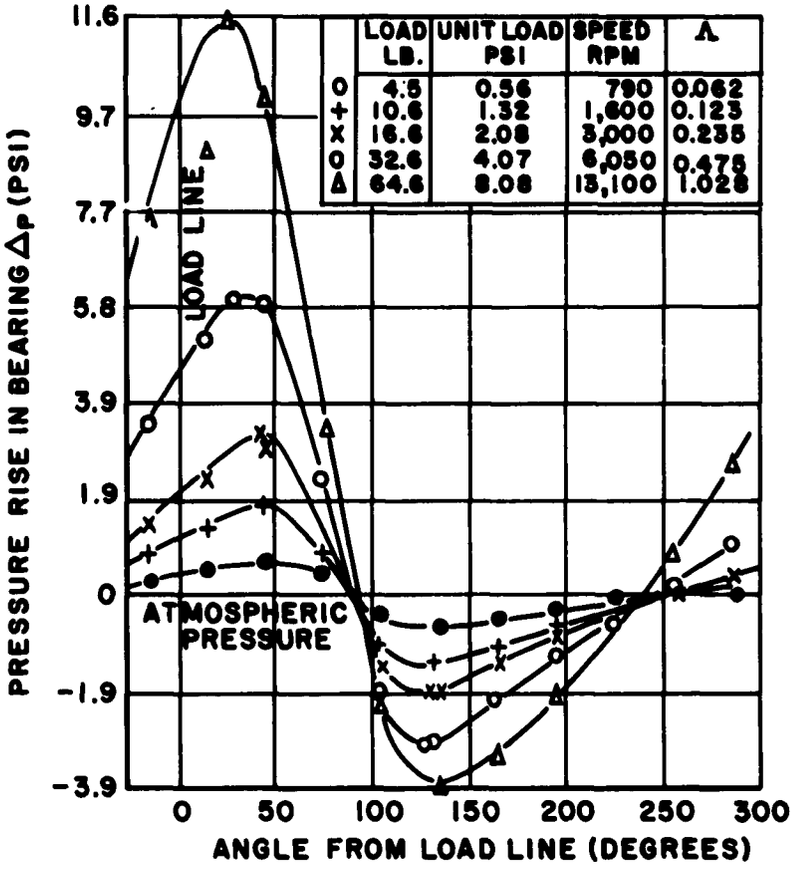

Fig. 2 - Experimental Pressure Distribution in a Journal Bearing. 4 x 2 Inch Diameter Bearing Operated By a Radial Clearance, C = 0.0012 Inch in Air At Atmospheric Pressure, (Ford, Harris & Pantall, Ref. 2)

With the usual units, μ is the absolute viscosity in reynes (lb.sec/in.^{2}); U is the surface velocity of the journal (in/sec); r is the radius of the journal (in.); P_a is the absolute ambient pressure (psia); c is the radial clearance (in.); and ω is the rotational velocity of the journal (radains/sec.). See Figure (3).

This dimensionless group of variables is designated by the Greek letter Λ, (capital lamda), and is termed the "compressibility bearing parameter". The same symbol Λ is used for similar compressibility bearing parameters for other types of gas-lubricated bearings.

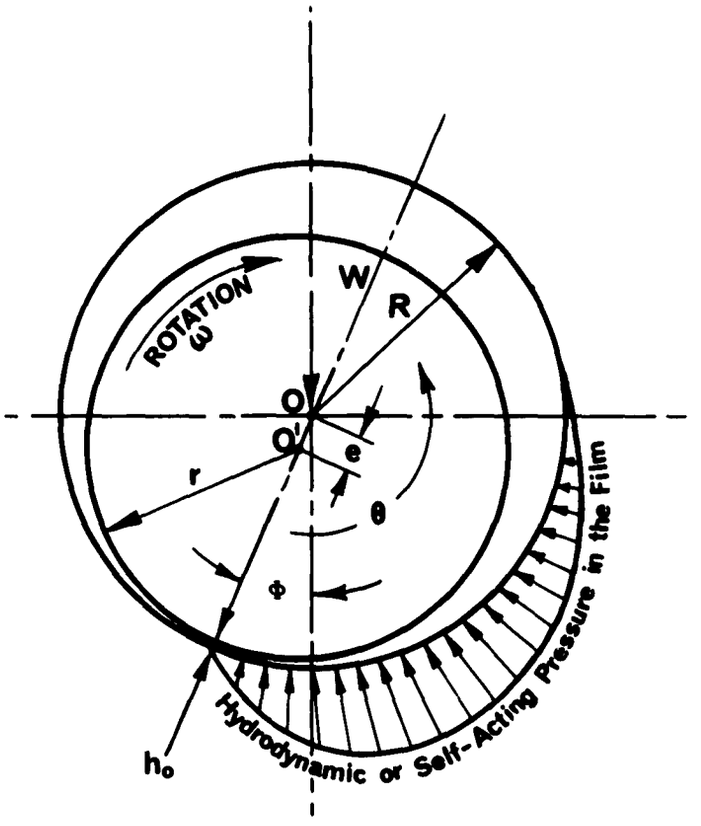

Fig. 3 - Journal in 360° Full Bearing.

For a thrust bearing the corresponding dimensionless group of variables is:

$$\Lambda = \frac{6\mu U l}{h_2^2 P_a} \qquad (2)$$

Where l is the length of the pad in the direction of motion (in.), h_2 is the minimum film thickness (in). Other symbols as defined above. Please see Figure 4.

For a spiral-grooved thrust plate, Λ may be described by:

$$\Lambda = \frac{6\mu U J}{h^2 P_a} \qquad (3)$$

where J is the radial dimension of the plate (in); U the mean surface speed (in/sec); and h the film thickness (in) which in this case is a constant. See Figure (5).

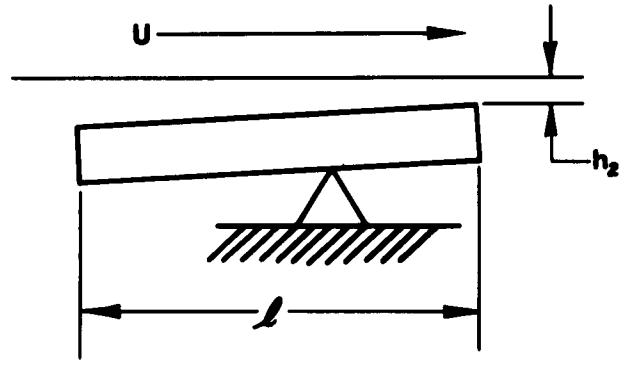

Fig. 4 - Schematic Diagram of Slider Thrust Bearing.

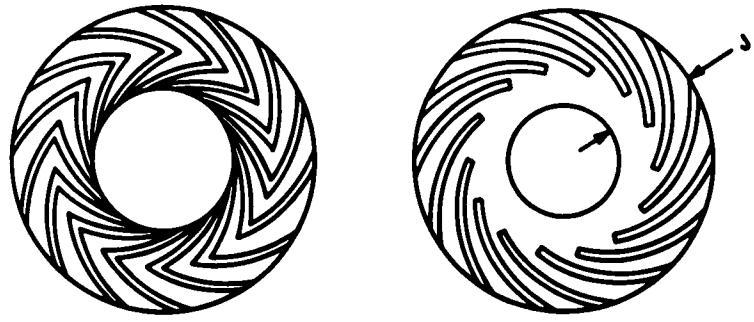

a. HERRING-BONE GROOVED b. SPIRAL GROOVED

Fig. 5 - Grooved Thrust Bearings. (Ref. 2).

It has been shown by Ford, Harris and Pantall,(2), by Ausman ,(5), and others that these dimensionless parameters designated by Λ are pertinent gas bearing parameters which define the state of operation of gas-lubricated bearings in a similar fashion to the Sommerfeld variable S for bearings operating with liquids or other incompressible lubricants.

$$S = \frac{\mu N'}{P_{avg}} \left(\frac{r}{c}\right)^2 \qquad (4)$$

N' is the journal rotational speed, (revs/sec); P_{avg} is the average pressure based on the applied load W, divided by the projected area of the journal, (W/dl), (psi); d is the journal diameter (in); other symbols as before.

The load-carrying capacity of these bearings, as well as other characteristics, can be expressed as a function of Λ. For example, Figure (6) shows a curve for a journal bearing at a fixed value of eccentricity ratio ε, indicating the general influence of variable ambient pressure.

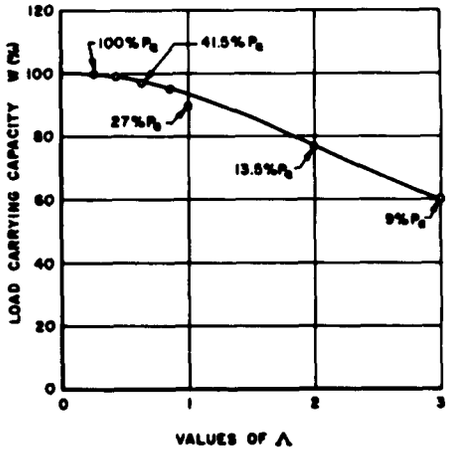

Fig. 6 - Example of Relationship Between Load-Carrying Capacity W and for a Self-Acting Gas Lubricated Journal Bearing. Speed, Viscosity and Eccentricity Ratio Held Constant. Ambient Pressure Varied. (Experimental Data from Ford, Harris & Pantell, Ref. 2).

When load is applied to a journal bearing the shaft moves to an eccentric position within the bearing clearances, Figure (3). The eccentricity ratio is a measure of how much the center of the shaft 0' displaces itself from the center of the bearing 0. Eccentricity ratio is defined as the eccentric distance e divided by the radial clearance c. Or,

$$\varepsilon = \frac{00'}{c} = \frac{e}{c} \qquad (5)$$

At light loads and high speeds, with small unbalance, the eccentric distance is very close to zero or e approaches 0 and consequently ε approaches 0 and the shaft is nearly concentric with the bearing. At heavier loads and lower speeds the shaft center becomes more displaced and when metal-to-metal contact occurs between the shaft and its bearing the eccentric distance e equals the radial clearance c and the eccentricity ratio ε is then 1. The limits on the magnitude of eccentricity ratio are therefore between zero and 1.

From a consideration of the variables included in Λ, one can gain an understanding of the pertinent parameters that influence the performance of self-acting, gas-lubricated bearings. The ambient pressure enters the analysis since the bearing acts as a pump and like all pumps, the ratio of its discharge pressure to supply pressure is limited. Thus a reduced ambient pressure and density around the bearing will result in a lower maximum pressure in the film. Naturally this means less load-carrying capacity.

Speed is also a factor in gas-lubricated bearings as it is in liquid-lubricated bearings but there is one distict difference. In the liquid-lubricated bearing the load capacity continues to rise directly as the speed increases, with no limit, assuming constant viscosity of the lubricant. With a gas bearing, however, although the load capacity does increase with speed, the rate of increase falls off at high speed due to compressibility effects, and the load-carrying capacity approaches a limiting value. At extreme speeds the load-carrying capacity becomes independent of viscosity and speed and is only a function of the ambient pressure surrounding the bearing. Figure (7) is from Pantall and Robinson, taken from (6).

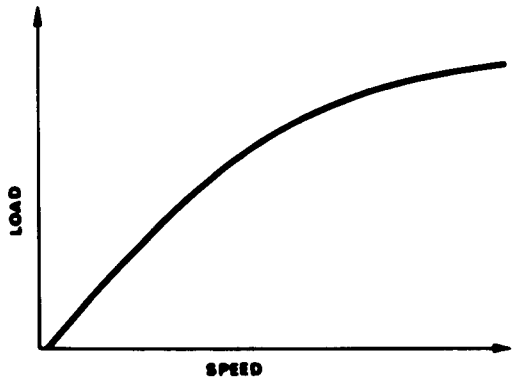

Fig. 7 - Load Carrying Capacity of Self-Acting Gas-Lubricated Journal Bearing As Influenced By Speed. (From Pantall and Robinson, Ref. 6)

In general, dimensionless plots of load-carrying parameter W' against Λ for various values of eccentricity ratio may be shown as in Figure (8), taken from (2). Design curves of this type are included in the design section of this manual.

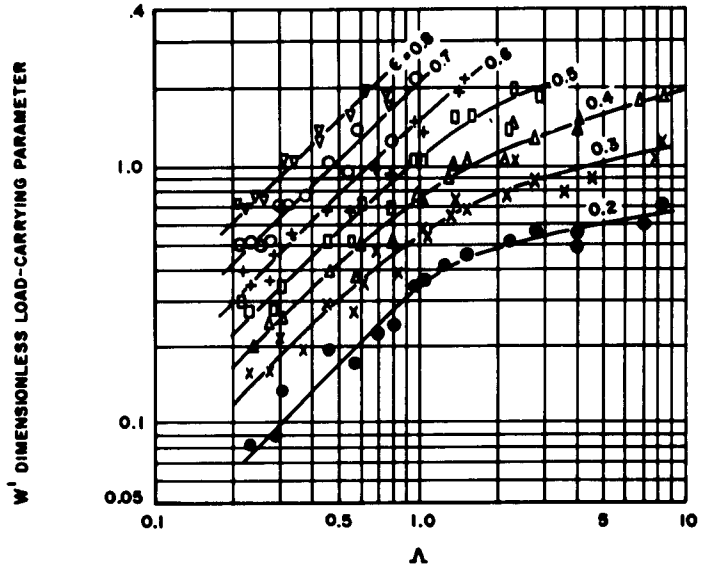

Fig. 8 - Generalized Experimental Correlation of Dimensionless Load Parameter W' vs Λ , for $l/d=2$. Departure from Straight Line Relationship When $\Lambda > 1$ Showing Compressibility Effect. (Ford, Harris & Pantall, Ref 2).

It will be noticed that for Λ greater than one, the plot no longer yields a straight line relationship. The deviation from the straight line indicates the point at which compressibility effects begin to exert their influence It is generally agreed, that for journal bearings, the compressibility and variable density influences are negligible as far as load-carrying capacity is concerned for values of Λ somewhat below 1 and the classical theory for incompressible lubricants may be used, if desired, without incurring a significant error.

This does not apply to attitude angle however, (angle ϕ of Fig.3), and this will be discussed in the design section.

Another point must be made regarding ambient pressures in the very low range, approaching those of a vacuum. The present theory of gas-lubricated bearings assumes that the gas can be considered as a continuous fluid. This assumption is no longer valid at very low pressures where the molecular mean free path of the gas becomes comparable in

magnitude to the film thickness in the bearing. When this happens, effects occur which can no longer be explained by continuum flow theory. Slip occurs at the boundary between the bearing surface and the gas. Therefore, instead of assuming vanishing velocities at the walls, slip velocities must be introduced. This has been done by Burgdorfer,(7).

If the ratio of minimum film thickness to mean free path is called n, it can be shown that for values of n less than 100 a noticeable effect on bearing pressure and load-carrying capacity may be expected. A typical graph is shown in Figure (9) from (7). This graph happens to be for a slider bearing. A similar condition would exist for a journal bearing.

Typical values of mean free path at atmospheric pressure, are:

Hydrogen	4.43×10^{-6} inches
Helium	7.32×10^{-6} inches
Air	2.52×10^{-6} inches
Neon	5.20×10^{-6} inches

Thus for n = 100 for air at atmospheric pressure, the film thickness at the entrance to a tilting pad bearing would be of the order of 2.52×10^{-4} inches (0.000252 inch).

Such values are not uncommon for self-acting bearings, even at atmospheric pressure. For low ambient pressures the effect would be even more marked and should be considered in any analysis and design for these operating conditions. This can be illustrated by a table (Table I) taken from (7) where the ratio of radial clearance to molecular mean free path was computed for a number of cases as reported by Wildmann, (8). It can be seen because of either the very small radial clearances in these journal bearings or because of the low ambient pressure, the value of this ratio in all cases is less than 100.

Another and different series of problems is associated with gas-lubricated bearings because of the low damping properties of the gas films. Because of this characteristic, certain dynamic instabilities need to be anticipated and controlled with machinery operating on gas-lubricated bearings.

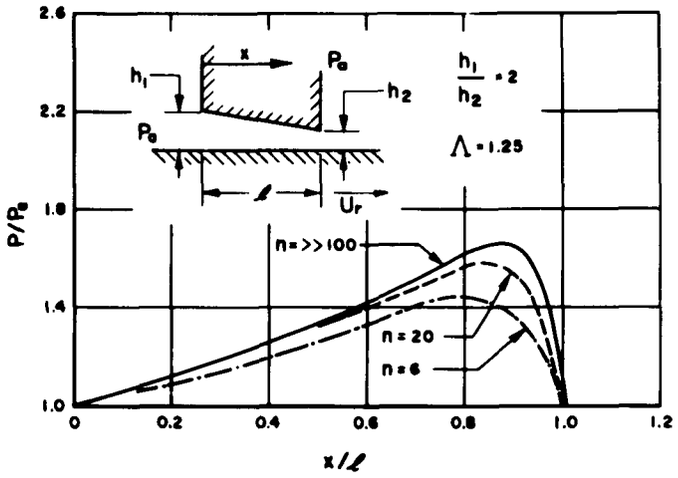

Fig. 9 - Pressure Distribution for Compressible Fluids Along a Straight Slider Bearing. (Ref. 7)

With liquid-lubricated bearings these might have been suppressed or they might have passed by unnoticed because of the greater damping action of liquids. With gas-lubricated bearings, however, these possible instabilities must be investigated, and in most cases design modifications can be made to avoid them or at least to mitigate their action.

The various types of these dynamic behavior characteristics will be described and analyzed in the design section of this report. The most important instabilities are half-frequency whirl and synchronous whirl.

TABLE I

Table of Radial Clearance To Molecular Mean Free Path

Bry. No.	Radial Clear. (micro-inch)	Ambient Pressure (psia)	Ambient Gas	Molecular Mean Free Path (micro-inch)	Ratio n Radial Clearance ÷ Molecular Mean Free Path
1	130	14.7	Air	2.52	52.5
2	210	14.7	Air	2.52	83.5
3	72	14.7	Air	2.52	28.6
5	135	14.7	Air	2.52	52.5
5	135	4	Air	9.26	14.5
5	135	14.7	Helium	7.32	18.5
5	135	3	Helium	35.90	3.76
5	135	14.7	Neon	5.20	25.6

II. DESIGN OF GAS-LUBRICATED JOURNAL BEARINGS

A. Load-Carrying Capacity with Static, Uni-Directional Loads

A typical journal bearing is shown in Figure (3). This is a schematic view with a greatly exaggerated clearance, running at some angular speed under the action of a load W. When starting, with solid contact between the shaft and the bearing at a point directly under the load, the shaft will start to run up the right side of the bearing. After rising a few degrees of arc it will enter a region where the gas comes between the bearing and the journal. Slip will begin. Then as the journal comes up to speed it will revolve faster and faster and build up a wedge-shaped film, which will then place the journal in the position shown in Figure (3).

A polar diagram of film pressures is shown in Figure (3) representing the positive film pressures in the loaded zone of the bearing. There will be negative pressures (below ambient pressure) in the unloaded zone of the bearing which will also contribute to the load-carrying capacity. These are not shown in Figure (3).

In general, the pressure generation in the clearance of a journal bearing is described for liquid lubricants by the Reynolds' equation, Ref.(9),

$$\frac{\partial}{\partial x}\left[\frac{h^3}{\mu}\frac{\partial p}{\partial x}\right] + \frac{\partial}{\partial Z}\left[\frac{h^3}{\mu}\frac{\partial p}{\partial Z}\right] = \frac{\partial}{\partial x}\left[6\ Uh\right] \qquad (6)$$

where
- p is the pressure at any point in the film
- h is the film thickness at any circumferential location
- μ is the absolute viscosity
- U is the surface speed of the journal
- x is the coordinate in the circumferential direction
- Z is the coordinate in the axial direction, please see Figure (10)

For a gas, the compressibility has to be included. This is represented by the mass density being a variable rather than a constant as with the liquid case so that the characteristic equation becomes, Refs. (10) and (11),

$$\frac{\partial}{\partial x}\left[\frac{\rho h^3}{\mu}\frac{\partial p}{\partial x}\right] + \frac{\partial}{\partial Z}\left[\frac{\rho h^3}{\mu}\frac{\partial p}{\partial Z}\right] = 6U\frac{\partial}{\partial x}\left[\rho h\right] \qquad (7)$$

where ρ is the mass density of the gas.

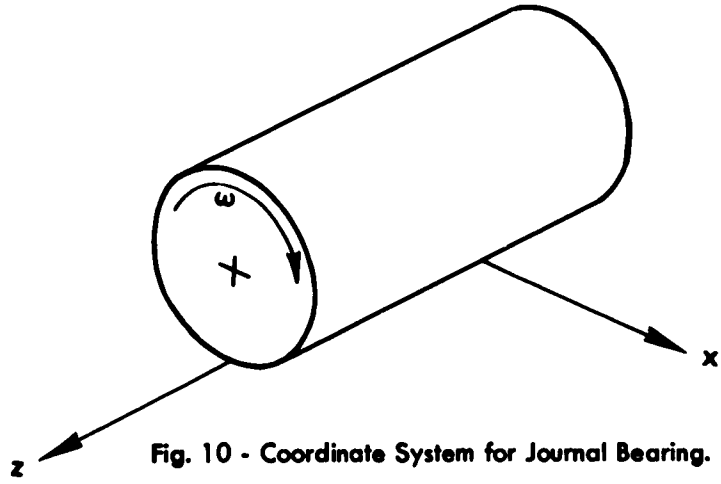

Fig. 10 - Coordinate System for Journal Bearing.

General Solution for Load Capacity

Exact solutions for Equations (6) and (7) cannot be obtained so that approximate methods have been used to develop design information. The best of these solutions have resulted from the application of digital computer techniques. The work of Elrod and Malanoski (12) and (13), Elrod and Burgdorfer (10), Raimondi (14), Hays (15) and Gross (11) will now be presented as a general design approach to 360° journal bearings.

Figures (11) through (15) show the load-carrying parameter, W/dlP_a, plotted against the compressibility bearing parameter, Λ, for various values of eccentricity ratio, ϵ.

W is the applied load, pounds
d is the journal diameter, inches
l is the journal length, inches
P_a is the ambient pressure, psia
Λ is defined by Equation (1)
ϵ is defined by Equation (5)

On each sheet is included the table of data from which the particular figure was drawn. There is one figure for each l/d ratio.

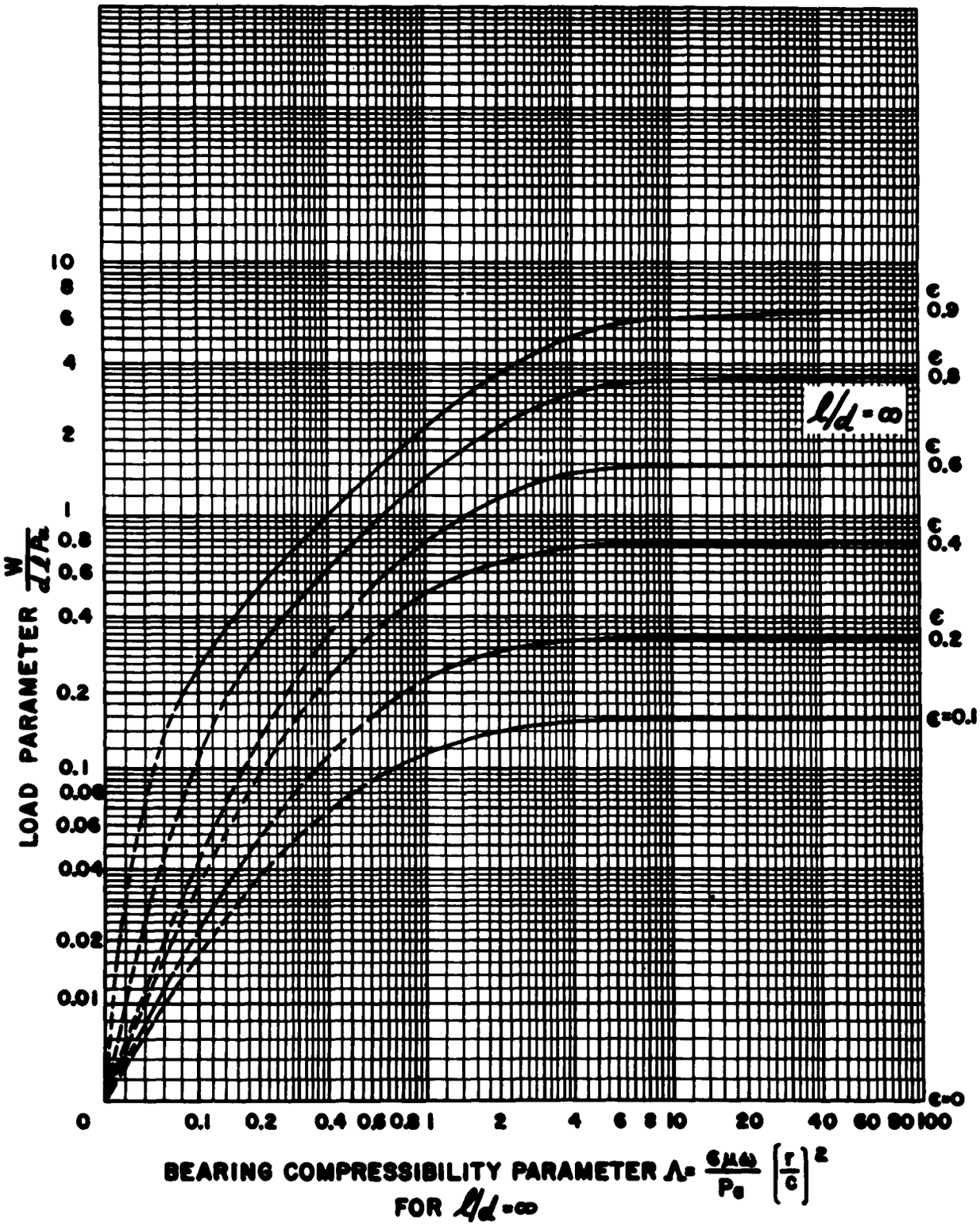

(REF. 10 AND 14)

Fig. 11 - Theoretical Load-Carrying Parameter vs Compressibility Parameter for Full Journal Bearing for $l/d = \infty$ (Ref. 10 and 14).

TABLE II

Compressibility Parameter vs Load Parameter for 1/d of Infinity

ε	Λ	W/dlP_a
0.1	0	0
	0.3	0.05
	0.6	0.09
	0.732	0.1
	1.8	0.14
	3.0	0.15
	6.0	0.155
	12.0	0.156
0.2	0	0
	0.962	0.2207
	1.979	0.2914
	4.012	0.3214
	8.058	0.3302
	∞	0.3335
0.4	0	0
	0.8209	0.4156
	1.859	0.6367
	3.976	0.7534
	8.110	0.7869
	∞	0.7966
0.6	0	0
	0.5418	0.4518
	1.460	0.9967
	3.643	1.440
	7.781	1.581
	∞	1.6349
0.8	0	0
	0.2052	0.3039
	0.6348	0.9537
	2.379	2.447
	6.256	3.379
	∞	3.6652
0.9	0	0
	0.0715	0.1708
	0.2221	0.5933
	1.017	2.298
	4.246	5.461
	∞	6.7234

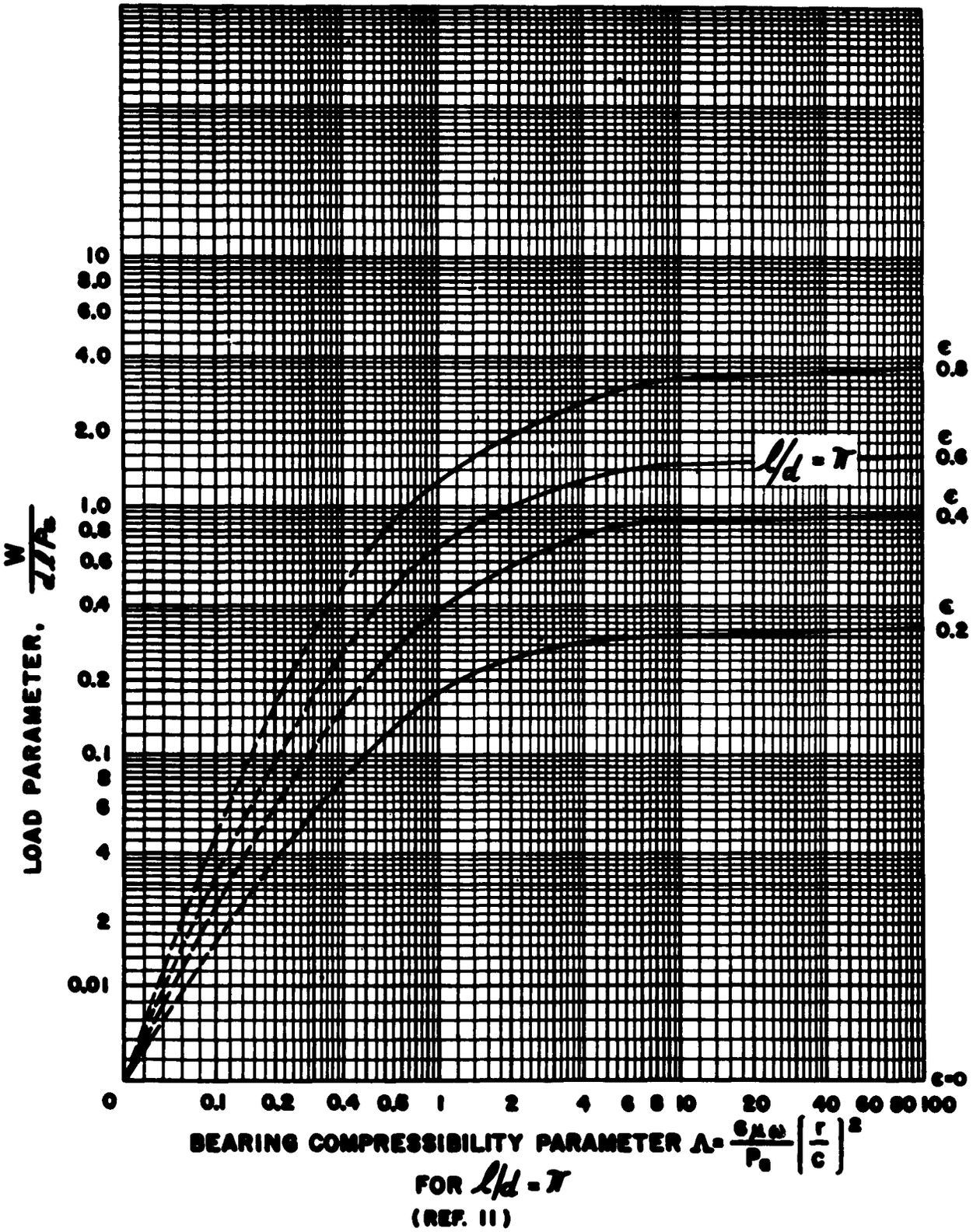

Fig. 12 - Theoretical Load-Carrying Parameter vs Compressibility Parameter for Full Journal Bearing for $l/d=\pi$ (Ref. 11).

TABLE III

Compressibility Parameter vs Load Parameter for $l/d = \infty$

ϵ	Λ	W/dlP_a	ϵ	Λ	W/dlP_a
0.2	0	0	0.6	0	0
	0.5	0.1027		0.5	0.349
	2.0	0.2438		2.0	0.969
	6.0	0.3001		6.0	1.411
	10.0	0.310		10.0	1.49
	∞	0.3337		30.0	1.557
				∞	1.625
0.4	0	0			
	0.5	0.203	0.8	0	0
	2.0	0.564		0.5	0.639
	6.0	0.822		2.0	1.880
	10.0	0.866		6.0	3.016
	30.0	0.9045		10.0	3.257
	∞	0.944		∞	3.66

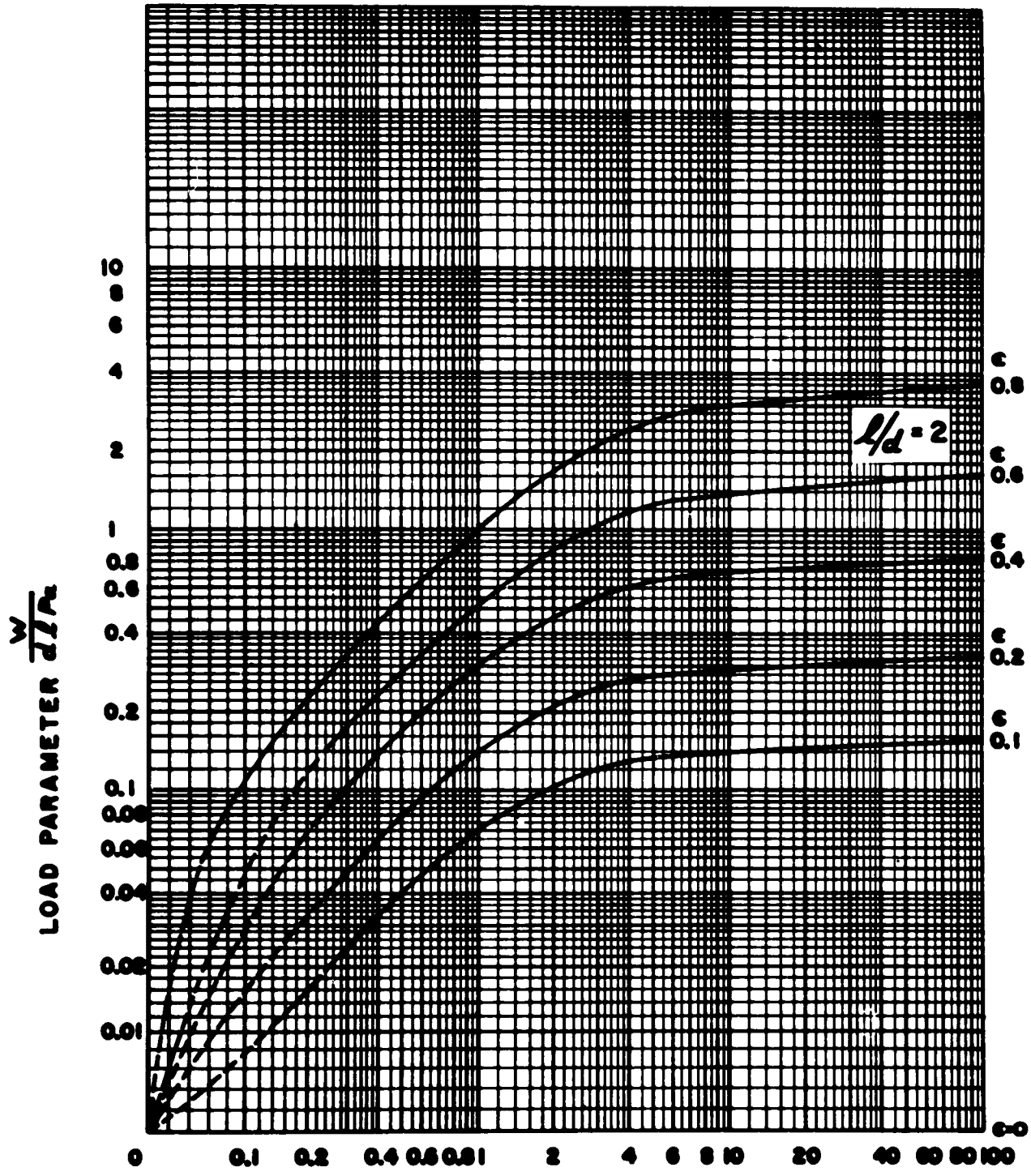

Fig. 13 - Theoretical Load-Carrying Parameter vs Compressibility Parameter for Full Journal Bearing for 1/d=2 (Ref. 14)

TABLE IV

Compressibility Parameter
vs
Load Parameter for $l/d = 2$

ϵ	Λ	W/dlP_a
0.1	0	0
	0.24	0.0194
	0.6	0.0462
	1.2	0.0794
	3.0	0.120
	6.0	0.136
	∞	0.1594
0.2	0	0
	0.24	0.0393
	0.6	0.0933
	1.2	0.161
	3.0	0.248
	6.0	0.283
	∞	0.3335
0.4	0	0
	0.24	0.0831
	0.6	0.197
	1.2	0.343
	3.0	0.561
	6.0	0.664
	∞	0.7966
0.6	0	0
	0.24	0.141
	0.6	0.335
	1.2	0.595
	3.0	1.04
	6.0	1.30
	∞	1.6349
0.8	0	0
	0.06	0.0641
	0.24	0.266
	0.6	0.645
	1.2	1.16
	3.0	2.14
	6.0	2.82
	∞	3.6652

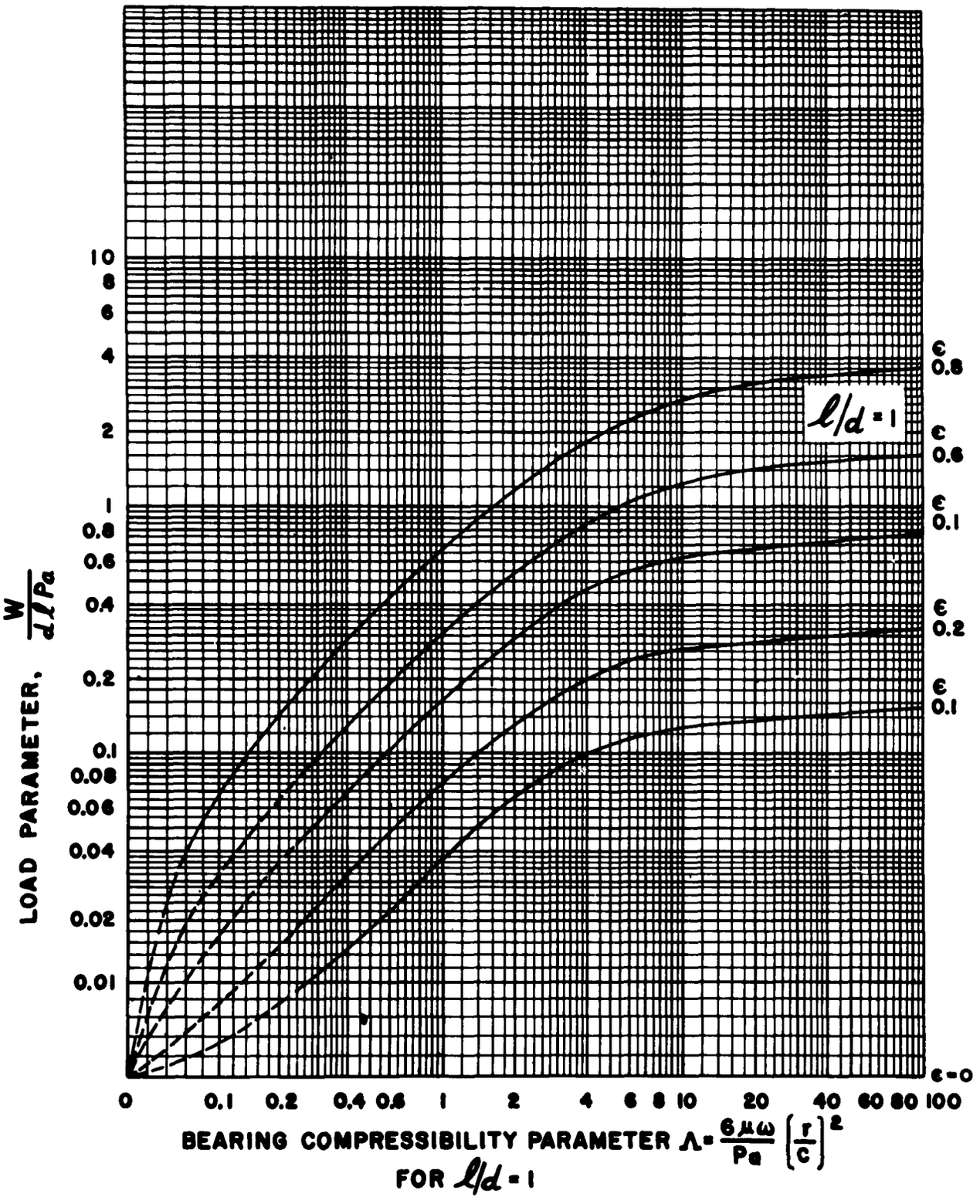

(REF 14)

Fig. 14 - Theoretical Load-Carrying Parameter vs Compressibility Parameter for Full Journal Bearing for l/d=1 (Ref. 14)

TABLE V

Compressiblity Parameter
vs
Load Parameter for 1/d = 1

ε	Λ	W/dlP_a	ε	Λ	W/dlP_a
0.1	0	0	0.4	0	0
	0.24	0.00902		0.24	0.0413
	0.6	0.0223		0.6	0.101
	1.2	0.0429		1.2	0.192
	3.0	0.0862		3.0	0.386
	6.0	0.116		6.0	0.545
	12.0	0.131		12.0	0.643
	∞	0.1594		∞	0.7966
0.2	0	0	0.6	0	0
	0.24	0.0186		0.24	0.0770
	0.6	0.0457		0.6	0.188
	1.2	0.0875		1.2	0.355
	3.0	0.176		3.0	0.720
	6.0	0.238		6.0	1.047
	12.0	0.273		12.0	1.280
	∞	0.3335		∞	1.6349
			0.8	0	0
				0.06	0.0404
				0.24	0.171
				0.6	0.428
				1.2	0.783
				3.0	1.555
				6.0	2.276
				12.0	2.835
				∞	3.6652

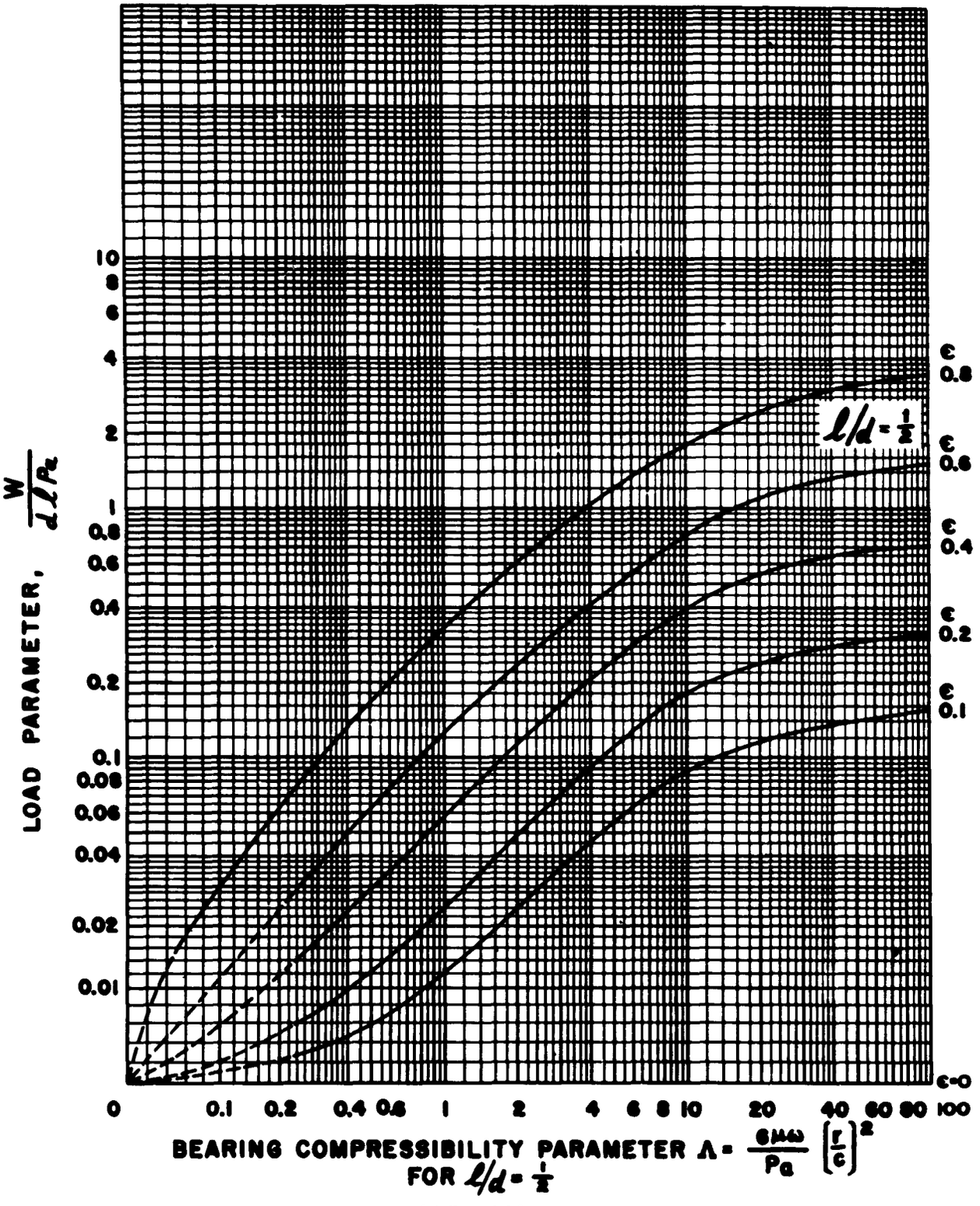

(REF. 14)

Fig. 15 - Theoretical Load-Carrying Parameter vs Compressibility Parameter for Full Journal Bearing for $1/d = \frac{1}{2}$ (Ref. 14)

TABLE VI

Compressibility Parameter
vs
Load Parameter for $l/d = \frac{1}{2}$

ϵ	Λ	W/dlP_a	ϵ	Λ	W/dlP_a
0.1	0	0	0.4	0	0
	0.24	0.00288		0.24	0.0141
	0.6	0.00719		0.6	0.0350
	1.2	0.0143		1.2	0.0693
	3.0	0.0348		3.0	0.163
	6.0	0.0634		6.0	0.288
	12.0	0.0974		12.0	0.449
	24.0	0.122		24.0	0.587
	∞	0.1594		∞	0.7966
0.2	0	0	0.6	0	0
	0.24	0.00599		0.24	0.0290
	0.6	0.0149		0.6	0.0721
	1.2	0.0297		1.2	0.141
	3.0	0.0717		3.0	0.325
	6.0	0.129		6.0	0.560
	12.0	0.199		12.0	0.873
	24.0	0.252		24.0	1.163
	∞	0.3335		∞	1.6349
			0.8	0	0
				0.06	0.0184
				0.24	0.0768
				0.6	0.201
				1.2	0.391
				3.0	0.834
				6.0	1.342
				12.0	1.991
				24.0	2.602
				∞	3.6652

Before proceeding with an example we will need some viscotiy data for air. It should be understood that knowing the viscosity, the solutions presented in this report are applicable to other gases as well as air. Table VII is a summation of data from References (16) and (17).

TABLE VII

Viscosity Data for Air

Absolute Viscosity in Reyns ($lb.sec/in^2$) x 10^{9}

Pressure psia → / Temp. °F ↓	14.7	294	735	1000
70	2.65	2.75	2.88	2.95
122	2.86	2.895	2.962	3.02
212	3.18	3.205	3.24	3.275
302	3.465	3.48	3.50	3.52

Thus the viscosity of air at 70°F and 14.7 psia is 2.65×10^{-9} reyns.

Figure (16) is a plot of the viscosity data from Table VII.

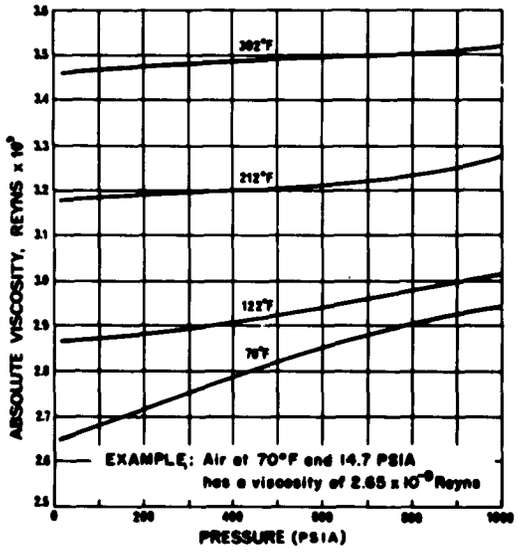

Fig. 16 - Absolute Viscosity of Air. (Refs. (16) and (17).

Example 1: Load Capacity for Bearings with $\Lambda > 1$. Suppose we wished to determine the operating eccentricity ratio and minimum film thickness for a journal bearing with the following specifications:

Rotor Weight	0.118 lb.(for one bearing)
Speed	24,000 RPM
Ambient Pressure	14.7 psia
Lubricating Fluid	Air
Ambient Temperature	100°F
Bearing Length	0.50 in.
Bearing Diameter	0.50 in.
Bearing Radial Clearance	0.00025 in.

Bearing Calculations:

$$\Lambda = \frac{6\mu\omega}{P_a}\left(\frac{r}{c}\right)^2$$

$\mu = 2.68 \times 10^{-9}$ reyns Fig. (16)

$\omega = \frac{24,000}{60} \times 2\pi = 2513$ rads/sec.

$r = 0.25$ inches

$P_a = 14.7$ psia

$c = 0.00025$ inches

Therefore $\Lambda = \frac{6\pi 2.68 \times 10^{-9} \times 2513}{14.7}\left(\frac{0.25}{0.00025}\right)^2$

But $\frac{r}{c} = \frac{0.25}{0.00025} = 1000 = 10^3$

$$\Lambda = \frac{6\pi 2.68 \times 10^{-9} \times 2513 \times 10^6}{14.7}$$

$\Lambda = 2.75$

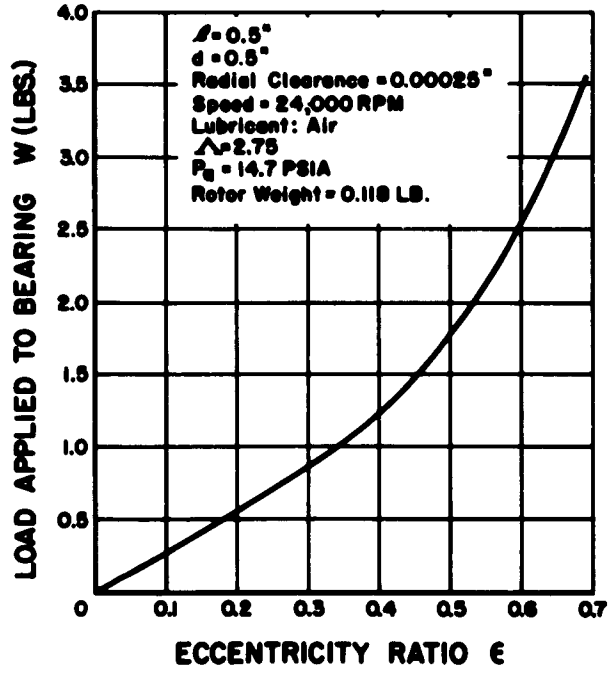

Fig. 17 - Theoretical Load-Carrying Capacity 360° Journal Bearing.

For 1/d = 1, and $\Lambda = 2.75$, in Figure (14) we may be able to establish the operating eccentricity ratio, once we have evaluated W/dlP_a.

$$W = 0.118 \text{ lb.}$$

$$dlP_a = 0.5 \times 0.5 \times 14.7 = 3.675 \text{ lb.}$$

Then $$\frac{W}{dlP_a} = 0.118/3.675 = 0.0321$$

Then in Figure (14) with $W/dlP_a = 0.0321$ and $\Lambda = 2.75$ we find that the operating ϵ has a value of somewhere between $\epsilon = 0.1$ and $\epsilon = 0$. Probably a value of $\epsilon = 0.05$ is about as close as it can be estimated.

The minimum film thickness is then, from Figure (3)

$$h_o = c\,[1-\epsilon] \qquad (8)$$

$$= 0.00025\,[1-0.05]$$

$$= 0.00025 \times 0.95$$

$$= 0.0002375$$

$$h_o = 0.00024 \text{ inches}$$

This bearing would need to be checked for at least half-frequency whirl stability and for the possibility of synchronous vibration before the design would be considered as complete. (See appropriate sections in manual). If the bearing were subjected to a range of steady-state loads, as for example if the unit were being subjected to a wide acceleration spectrum, then the performance pattern could be calculated by assuming different values of W/dlP_a, for the same speed and ambient pressure conditions. Thus, in this case Λ = a constant of value 2.75

Assumed Acceleration Condition, "G's"	W(lbs) Resultant	W/dlP_a	ϵ
1	0.118	0.0321	0.05
2	0.236	0.0642	0.075
3	0.354	0.0816	0.1
4	0.472	0.1285	0.15
5	0.590	0.1605	0.2
6	0.708	0.1927	0.24
7	0.8255	0.2245	0.29
8	0.944	0.257	0.31
9	1.061	0.289	0.35
10	1.18	0.321	0.37
20	2.36	0.642	0.58
30	3.54	0.963	0.69

These results are plotted in Figure (17).

Journal Bearing Solutions for Low Values of Λ

It can be observed in Figures (11) through (15) that for low values of Λ, much below a value of one, the probable accuracy that can be obtained from the use of these figures is considerably reduced. It has also been shown by Ford, Harris and Pantall (2), (Figure 8) that for journal bearings the compressibility and variable density influences are negligible as far as load-carrying capacity is concerned for values of Λ somewhat below one and the classical theory for incompressible lubricants may be used.

This has also been shown very clearly by Raimondi (14) and Figure (18) is reproduced from his paper.

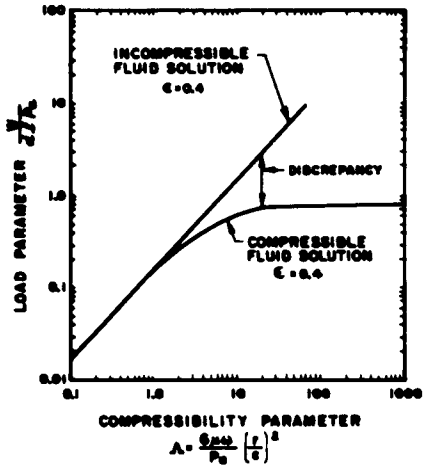

Fig. 18 - Discrepancy In Load Capacity Between Theories Based On Incompressible and Compressible Lubricants. (Ref. 14).

For convenience therefore, and in some instances for increased accuracy, a solution based on incompressible lubricants may be used. One of the best of these is due to Hays, Ref. (15). His solution is based on the use of the Sommerfeld variable, S, Equation (4). For the case of $\Lambda \to 0$, we have the following relationships between ε, $1/S$, and l/d ratio:

TABLE VIII

Values of 1/S vs ϵ, From Hays (15)
$\Lambda \to 0$

1/d	ϵ=0.05	ϵ=0.1	ϵ=0.2	ϵ=0.4	ϵ=0.6	ϵ=0.8	ϵ=0.9
0.1	-	0.01	0.042	0.102	0.228	0.710	6.5
0.2	-	0.065	0.165	0.398	0.882	2.625	9.5
0.3	-	0.17	0.363	0.870	1.885	5.305	14.2
0.4	0.15	0.3	0.625	1.485	3.14	8.352	19.0
0.6	0.25	0.55	1.30	3.019	6.08	14.60	25.5
0.8	0.42	0.9	2.09	4.755	9.18	20.31	31.0
1.0	0.65	1.3	2.92	6.513	12.16	25.25	39.0
1.25	0.9	1.75	3.91	8.56	15.46	30.35	48.0
2.50	1.65	3.4	7.25	15.17	25.33	44.0	59.0
5.0	2.25	4.65	9.52	19.49	31.42	51.85	66.0
10.0	2.95	5.5	10.69	21.69	34.50	55.80	71.0

From Equation (4),

$$\frac{1}{S} = \frac{P_{avg}}{\mu N'} \left(\frac{c}{r}\right)^2 \qquad (9)$$

Converting $N' = \frac{\omega}{2\pi}$ $P_{avg} = \frac{W}{dl}$

we have $$\frac{1}{S} = \frac{W/dl\ 2\pi}{\mu\ \omega} \left(\frac{c}{r}\right)^2$$

multiplying by $\frac{6}{6}$ and $\frac{P_a}{P_a}$ we have

$$\frac{1}{S} = \frac{W/dl\ 2\pi}{\mu\ \omega} \left(\frac{c}{r}\right)^2 \times \frac{6}{6} \times \frac{P_a}{P_a}$$

$$\frac{1}{S} = \frac{P_a}{6\mu\omega} \left(\frac{c}{r}\right)^2 \times \frac{W}{dlP_a} \times 12\pi$$

$$\frac{1}{S} = \frac{1}{\Lambda} \times W' \ 12\pi \quad \text{where } W' = \frac{W}{dlP_a}$$

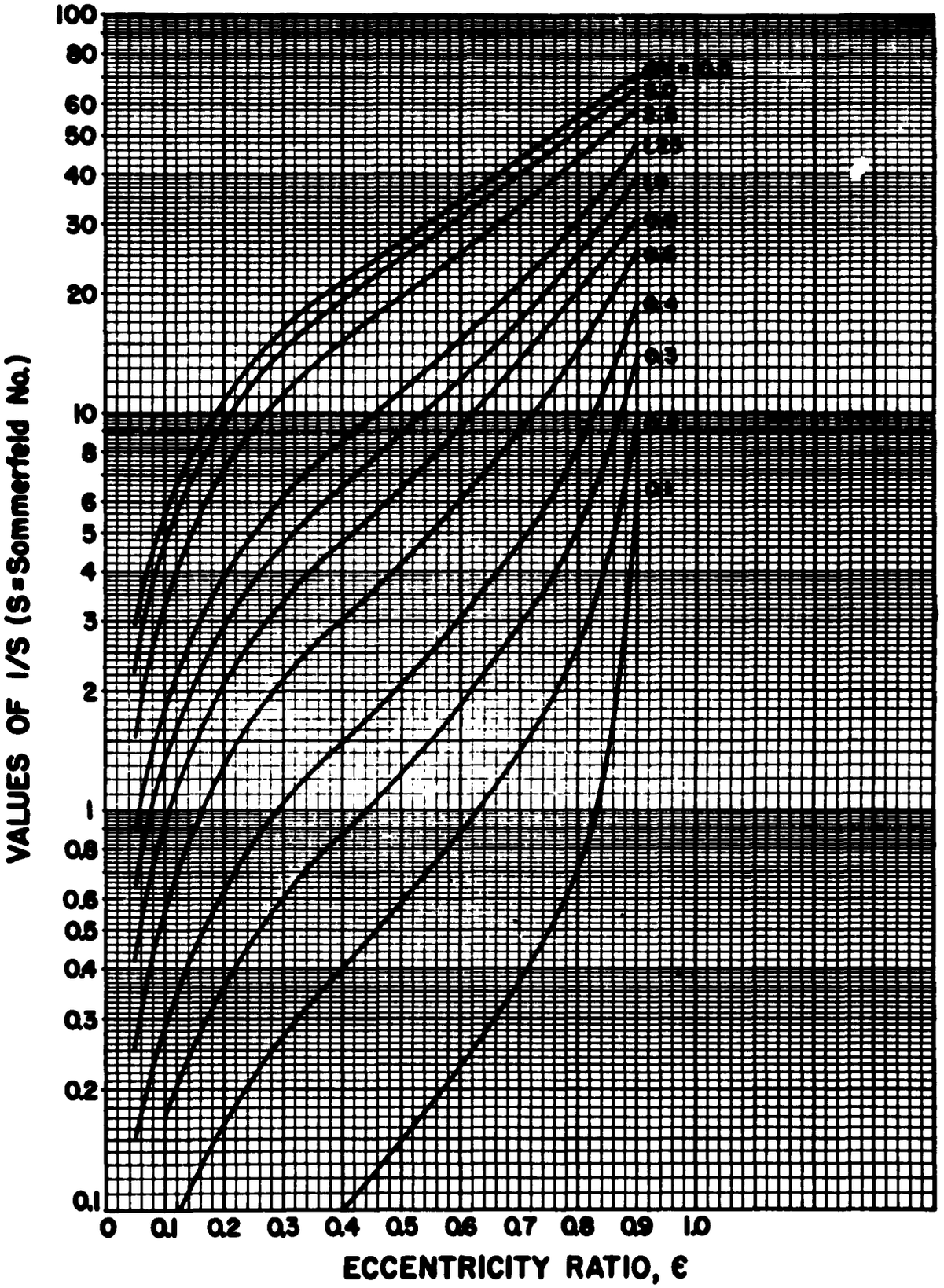

Fig. 19 - 1/S Plotted Against Eccentricity Ratio for Λ Approaching Zero. (Data from Ref. 15)

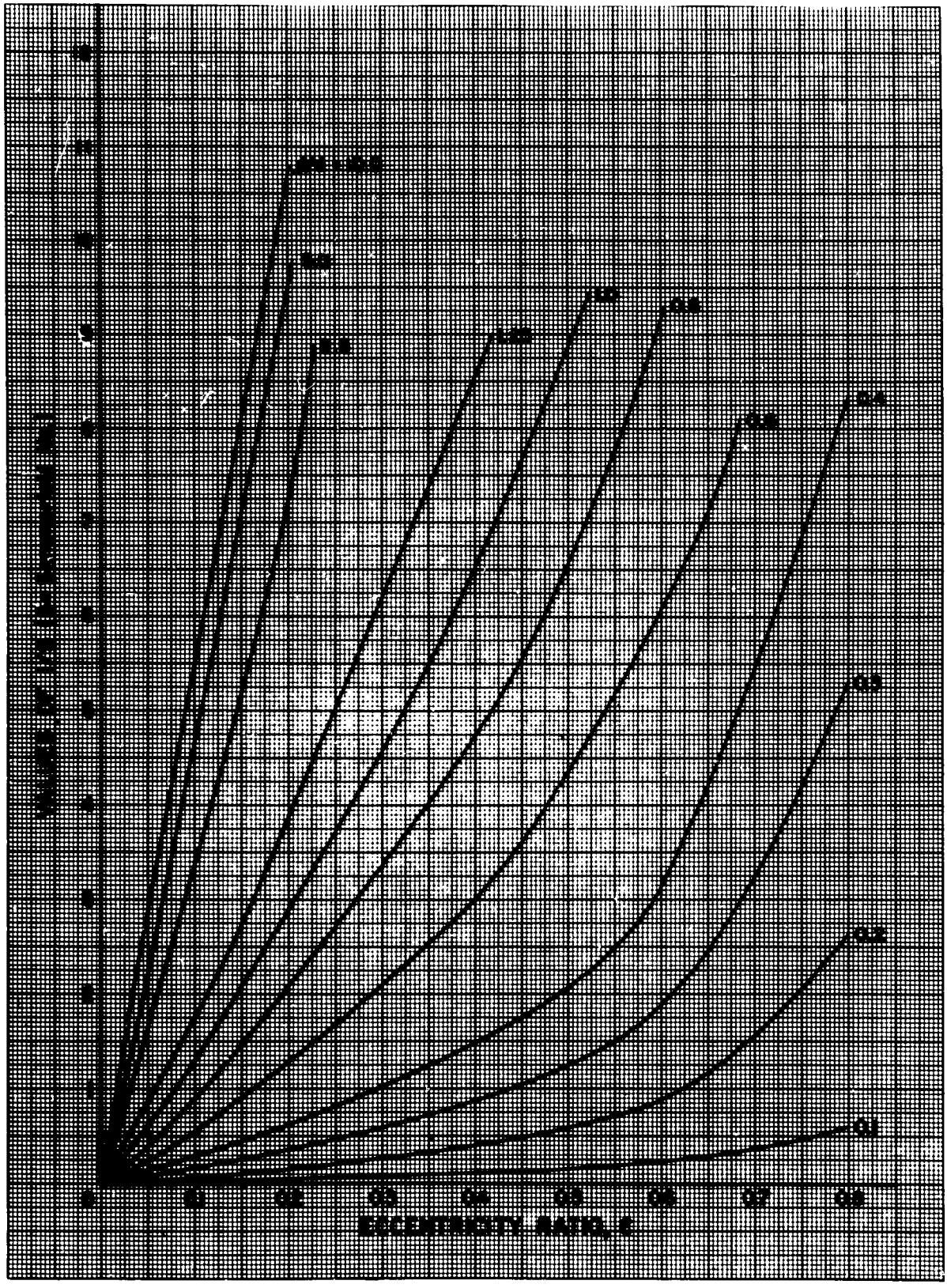

Fig. 20 - I/S Plotted Against Eccentricity Ratio for Λ Approaching Zero.
(Data from Ref. 15)

or $$\frac{1}{S} = \frac{12\ W'\pi}{\Lambda} \qquad (10)$$

This provides the relationship between the Sommerfeld number S and the compressibility parameter Λ (for low values of Λ)

Data from Table VIII are plotted in Figure (19) and the lower left hand corner of Figure (19) is expanded in Figure (20) to permit more accurate evaluation at very low values of eccentricity ratio ϵ.

Example 2: Let us compute the load-carrying capacity of a gas-lubricated journal bearing for which Λ is less than one. Air at 70°F and 14.7 psia is to be used.

$\mu = 2.65 \times 10^{-9}$ from Fig. 16
$l = 0.75$ in.
$d = 0.375$ in.
$c = 0.00025$ in.
$N = 3150$ RPM
$W = 4$ ounces; $P_{avg} = \frac{4}{16 \times 0.375 \times 0.75} = 0.89$ psi
$U = 61.9$ in/sec.
$r = 0.375/2 = 0.1875$ in.
$P_a = 14.7$ psia

Compute value of Λ. From Equation (1),

$$\Lambda = \frac{6\mu Ur}{c^2 P_a}$$

$$\Lambda = \frac{6 \times 2.65 \times 10^{-9} \times 61.9 \times 0.1875}{(0.00025)^2 \times 14.7}$$

$$\Lambda = 0.201$$

Now the l/d ratio is $0.75/0.375 = 2$.

Use first Figure (13) which includes the effect of compressibility and for a given Λ and W/dlP_a find ϵ.

$$\frac{W}{dlP_a} = \frac{4/16}{0.375 \times 0.75 \times 14.7} = 0.0604$$

Then from Figure (13), $\epsilon = 0.4$

The minimum film thickness, Equation (8), is

$$h_o = c\ [1-\epsilon]$$
$$= 0.00025\ [1-0.4]$$
$$= 0.00025 \times 0.6$$
$$h_o = 0.00015 \text{ in.}$$

Next use the Hays solution for incompressible lubricants corresponding to $A \to 0$. From Equation (9)

$$\frac{1}{S} = \frac{p_{avg}}{\nu N'} \left(\frac{c}{r}\right)^2$$

$$\frac{1}{S} = \frac{0.89}{2.65 \times 10^{-9} \times \frac{3150}{60}} \left(\frac{0.00025}{0.1875}\right)^2$$

$$\frac{1}{S} = 11.37$$

Now in Figure (19), with $1/S = 11.37$ and $1/d = 2$, we find that $\epsilon = 0.4$, which is the same as calculated above from Figure (13).

Incidentally, the alternate form of $1/S$ from Equation (10) yields

$$\frac{1}{S} = \frac{12\nu W'}{A} \quad \text{where } W' = \frac{W}{dlP_a} = 0.0604 \text{ from above.}$$

Therefore

$$\frac{1}{S} = \frac{12 \times \nu \times 0.0604}{0.201}$$

$$\frac{1}{S} = 11.35 \text{ the same result as from Eq. (9).}$$

Example 3: Ausman, Ref.(18), cites experimental data from a number of sources. The first is given below from Scheinberg. Data are for an l/d ratio of 1.1 and $A = 2.5$.

W/dlP_a	Experimental ϵ	Calculated ϵ $(l/d=1)$	Calculated ϵ $(l/d=2)$	Calculated ϵ By Interpolation
0.35	0.33	0.4	0.3	0.39
0.585	0.5	0.58	0.44	0.57
0.82	0.62	0.66	0.56	0.65
1.12	0.72	0.75	0.65	0.74

The agreement is quite satisfactory.

Also from (18) we have data from Sternlicht and Elwell for $A = 1.3$ and $l/d = 1.5$:

W/dlP_a	Experimental ϵ	Calculated ϵ $(l/d=1)$	Calculated ϵ $(l/d=2)$	Calculated ϵ By Interpolation
0.11	0.15	0.25	0.15	0.2
0.26	0.39	0.47	0.32	0.395
0.4	0.55	0.62	0.43	0.525
0.5	0.65	0.68	0.51	0.595
0.68	0.82	0.76	0.63	0.695

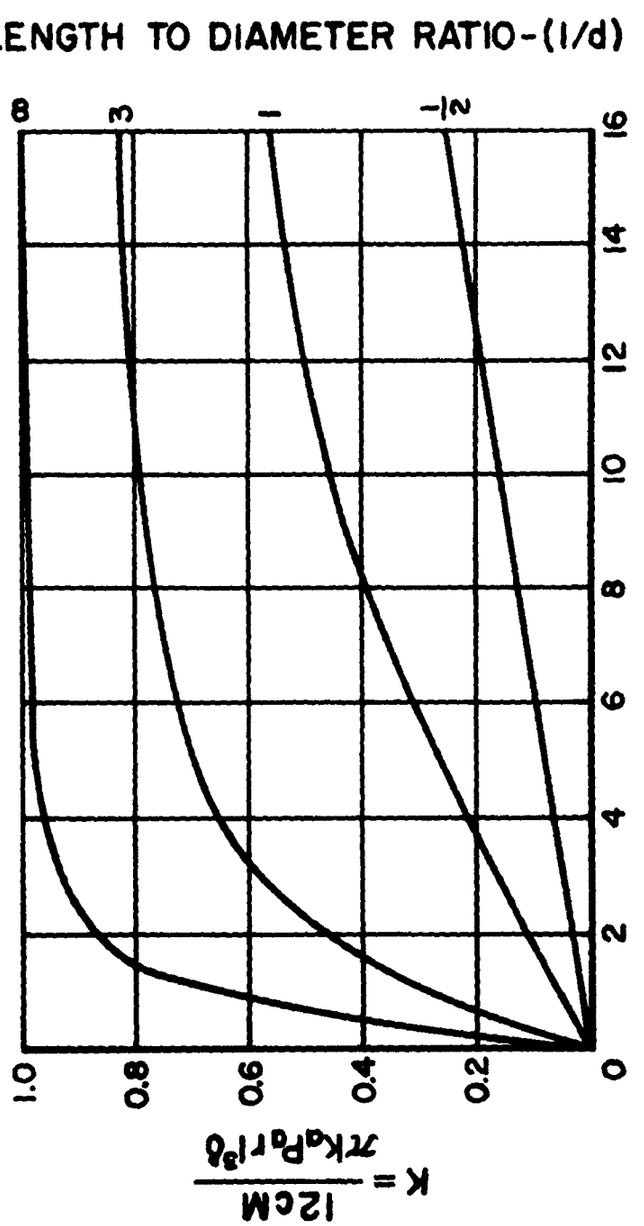

Fig. 21 - Moment Capacity of Full Journal Bearings. (Ausman, Ref. 5).

Now repeat these last calculations of ε using Figure (19) and the approach based on incompressible lubricants even though Λ is 1.3 and is higher than the recommended limit of one.

W/dlP_a	$\frac{l}{d}$	Calculated Fig. 19 ε	Experimental ε
0.11	3.18	0.14	0.15
0.26	7.54	0.32	0.39
0.4	11.6	0.46	0.55
0.5	14.5	0.53	0.65
0.68	19.7	0.63	0.82

Agreement is only fair, especially at higher values of ε.

Moment-Carrying Capacity of Journal Bearing (Overhung Static Load)

To estimate the moment-carrying capacity of a full journal bearing we may use the analysis of Ausman (18). There is little experimental verification of these predictions. However, the results may be used to show what bearing variables are significant in producing a moment-carrying characteristic.

Figure (21) is reproduced from Ausman's paper. In it is plotted a dimensionless parameter H, against another dimensionless parameter which we can call K. This is done for various values of l/d ratio of the bearing.

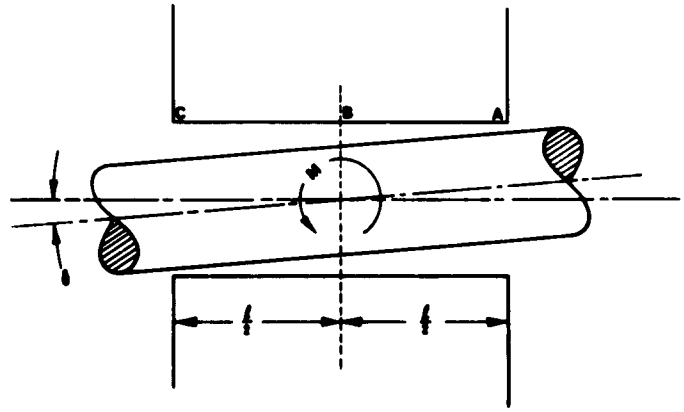

Fig. 22 - Schematic Representation of Journal Bearing Sustaining An Applied Moment, M.

$$H = \frac{6\mu\omega r^2}{k_a P_a c^2} \qquad (11)$$

$$K = \pi \frac{12cM}{k_a P_a r} \left(\frac{1}{d}\right)^3 \delta \qquad (12)$$

k_a = coefficient of polytropic expansion of gaseous lubricant which for our purposes is isothermal air so that $k_a = 1.0$

M = moment applied to the bearing (in.lbs)

δ = misalignment angle or angular displacement of journal (see Fig.22) radians

Other variables as before.

Example 4: Consider a journal bearing with the following specifications:

l = 1-1/8 in.
d = 0.375 in.
W = 1.63 oz.
N = 3150 RPM
P_a = 14.7 psia
c = 0.000375 in.
ν = 2.65×10^{-9} (Air at 14.7 psia & 70°)

Substitute in Equation (11) for H,

$$H = \frac{6\nu\omega r^2}{kP_a c^2}$$

$$H = \frac{6 \times 2.65 \times 10^{-9} \left[\frac{3150}{60}\right] \times 2\pi \times \left[\frac{0.375}{2}\right]^2}{1.0 \times 14.7 \times 0.000375^2}$$

$$H = 0.0893$$

From Figure (21) we use a linear interpolation for low values of H.

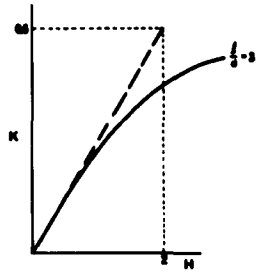

Now K is given as Equation (12), solving for M we have

$$K = \frac{12\, c\, M}{\pi k_a P_a r\, l^3 \delta}$$

$$0.0267 = \frac{12 \times 0.000375 \times M}{\pi \times 1.0 \times 14.7 \times 0.1875 \times 1.125^3 \times \delta}$$

$$M = \frac{0.0267 \times \pi \times 1.0 \times 14.7 \times 0.1875 \times 1.125^3 \times \delta}{12 \times 0.000375}$$

$$M = 73.44$$

Thus the moment depends upon the permissible angular misalignment δ between the central axis of the journal and the central axis of the bearing. One can look at the situation in either of two ways; by considering the δ that would result from the application of a known moment M, or estimate the maximum angular displacement that might be tolerated and interpret this in terms of a maximum allowable moment that might be applied to the journal bearing.

For this example let us use the latter approach. For the concentric position of the journal in its bearing the film thickness at point B, Figure (22), will be equal to the radial clearance c, or 0.000375 inches. We might then assume a deflection as shown with a minimum film thickness at point A, Figure (22), of 0.00005 in. and a maximum film thickness at point C of 0.00070 inches.

The total length of the bearing is 1-1/8 in. so that the angle to be used becomes

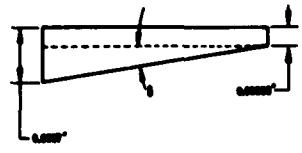

$$\tan \delta = \frac{0.0007 - 0.00005}{1.125}$$

$$\tan \delta = 0.000578 \text{ or very closely,}$$

$$\delta = 0.000578 \text{ radians}$$

Now substituting in the equation,

$$M = 73.44$$

$$M = 73.4 \times 0.000578$$

$$M = 0.0424 \text{ inch lbs.}$$

B. Evaluation of Friction in Full Journal Bearings

Of interest in some designs is the power loss in the bearing due to friction resulting from the viscous drag effects of the gas. In gas bearings the friction is described from the friction factor c_f which is defined as follows:

$$c_f = \frac{M_j}{\frac{2\pi\mu U r^2 l}{c}} \qquad (13)$$

where M_j is the friction moment in inch pounds, other symbols the same as before.

The friction moment being considered arises from the hydrodynamic film forces acting on the journal of a bearing during steady state operation, designated M_j. As evidenced on Figure (23), when a load W_A is applied through the center of the bearing O, the reaction load W (which is equal and opposite to W_A) occurs at the journal center O' creating a moment equal to WOO' sin ϕ. If the lubricant film in the bearing clearance space is considered a free body, then the friction moment of the journal acting on the lubricant film will be M_j and the friction moment of the bearing will be M_b. Summing up the clockwise and counterclockwise moments we have:

$$M_b + WOO' \sin \phi = M_j$$

from Equation (5) $OO' = \varepsilon c$ $\quad \therefore M_j = M_b + W \varepsilon c \sin \phi$

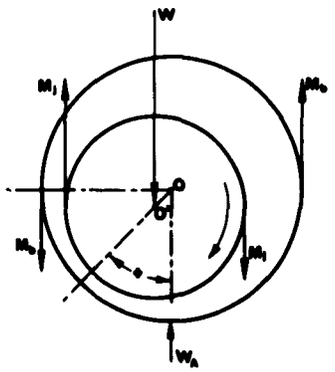

Fig. 23 - Relationship Between Bearing Friction Torque and Journal Friction Torque (9).

It should be noted that the journal friction is greater than the bearing friction if friction measurements are being made through the bearing. Of consideration also is the fact that the journal friction varies with the angle ϕ, which is called the attitude angle of the bearing or simply attitude, as well as with the eccentricity ratio ε.

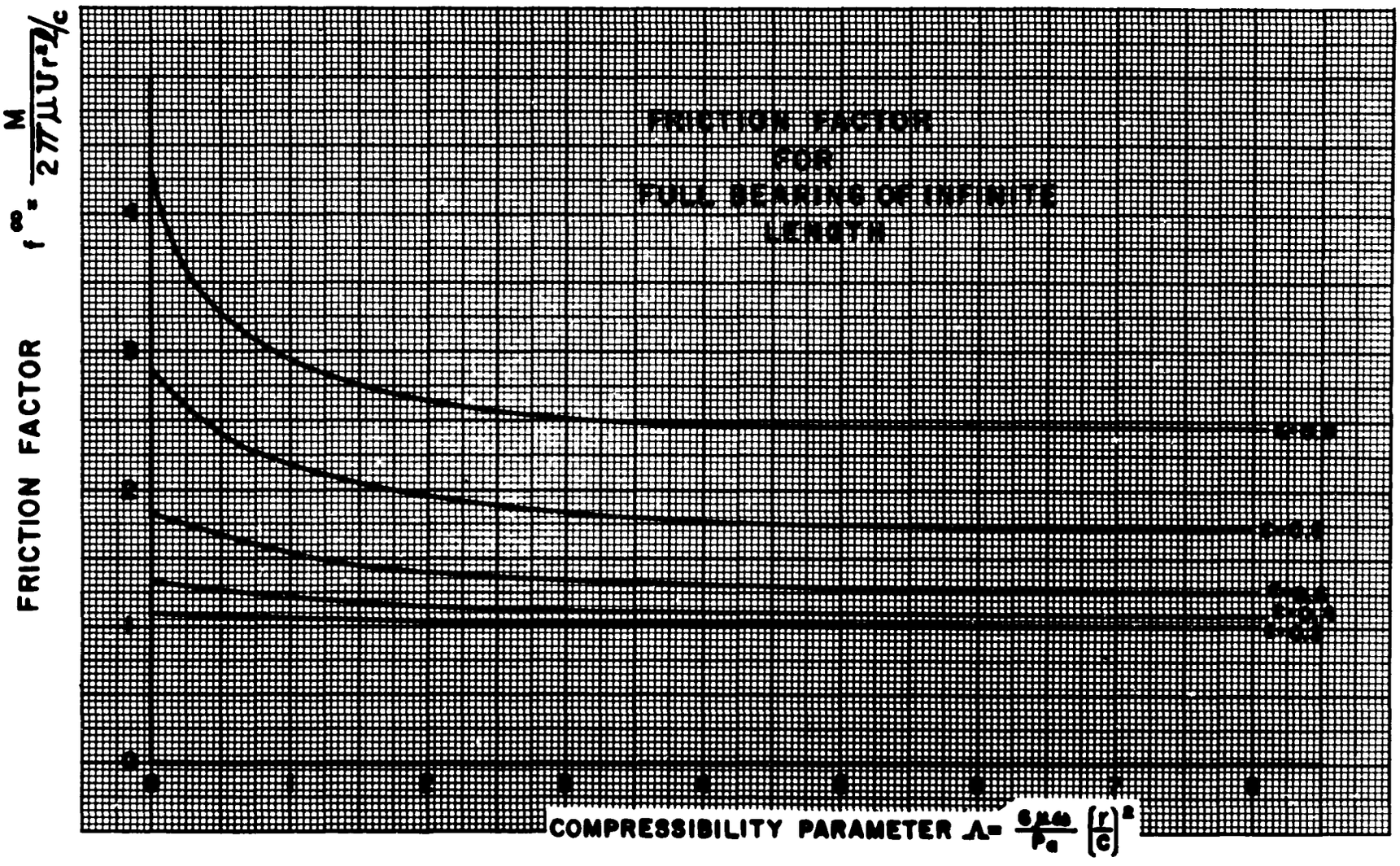

Fig. 24 - Friction Factor for Full Bearing of Infinite Length (Ref. 15).

The friction loss of a 360° journal bearing is rather independent of Λ at values of ε up to about 0.5. This means that for low ε the values of friction as obtained for the case of incompressible lubricants ($\Lambda \to 0$) may be used. This can be seen graphically for example in Figure (24) which is reproduced from Ref. (12) for the infinitely long bearing.

Table IX is a compilation of data for the infinitely long bearing for all values of Λ up to 8. Values for $\Lambda = 0$ were obtained from References (15), (14), and (9).

TABLE IX

Friction Factors for Full Bearings of Infinite Length

ε	Λ	c_f^{∞}
0.0	0	1.0
0.2	0	1.09
0.4	0	1.33
0.6	0	1.82
0.8	0	2.87
0.9	0	4.30
0.2	0.9622	1.0518
0.4	0.8209	1.2346
0.6	0.5418	1.6536
0.8	0.2052	2.6722
0.9	0.0715	4.0505
0.2	1.979	1.0331
0.4	1.859	1.1528
0.6	1.460	1.4501
0.8	0.6348	2.3268
0.9	0.2221	3.6303
0.2	4.012	1.0242
0.4	3.976	1.1090
0.6	3.643	1.3090
0.8	2.379	1.8987
0.9	1.017	2.9412
0.2	8.058	1.0214
0.4	8.110	1.0956
0.6	7.781	1.2648
0.8	6.256	1.7220
0.9	4.246	2.4733

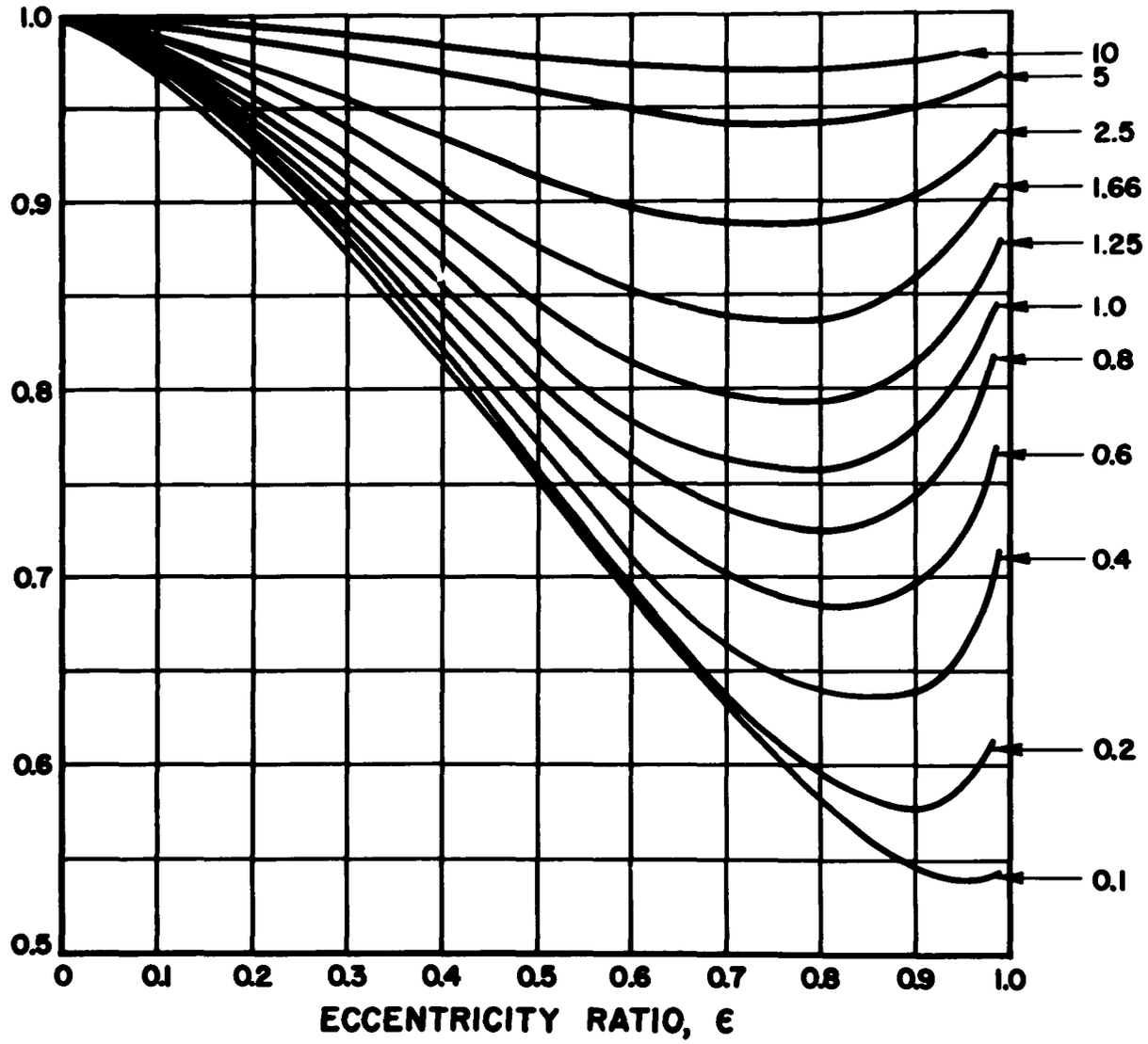

Fig. 25 - Effects of Slenderness and Eccentricity Ratios on Friction Factor. (Ref. 15).

For bearings of finite length a correction must be applied to the value of c_f^∞ as obtained from Table IX and Figure (24). The value of the correction, although calculated for the case where $\Lambda = 0$, may also be applied to bearings with values of Λ up to about 6. A graph of such correction factors is shown in Figure (25). The data for this graph were obtained from Ref. (15). c_f is the friction factor for the journal bearing of finite length.

Raimondi (14) also shows the influence of compressibility effects on the friction of finite journal bearings.

In summary, the following rules may be used to obtain values of the friction factor:

1. For $0 \leq \Lambda \leq 6$ use Elrod's values of c_f^∞, Fig. 24, corrected for 1/d ratio from Hays' Figure 25.
2. For $6 \leq \Lambda \leq 12$ use $c_f = c_f^\infty$ from Fig. 24. No correction for 1/d ratio being required.
3. For $\Lambda \geq 12$ use $c_f = \frac{1}{1-\epsilon^2}$ (Ref. 13).

Example 5: Suppose we consider the bearing of Example 1.

$$\Lambda = 2.75,\ 1/d = 1,\ \epsilon = 0.05$$

From Figure (24), $c_f^\infty = 1.0$

From Figure (25), the correction factor $\frac{c_f}{c_f^\infty} = 1.0$. No correction at low values of ϵ.

Therefore, $c_f = 1.0 \times c_f^\infty$

$$c_f = 1.0$$

Then from Equation (13)

$$c_f = \frac{M_j}{2\pi\mu U r^2 l/c}$$

or
$$M_j = \frac{2\pi\mu U r^2 l c_f}{c} \qquad (14)$$

For this example, $\mu = 2.68 \times 10^{-9}$ reyns
$U = 2510$ rads/sec x 0.25 in.lb.= 627.5 in/sec.
$r = 0.25$ in.
$l = 0.50$ in.
$c = 0.00025$ in.

Substituting in Equation (14),

$$M_j = \frac{2\pi \times 2.68\times10^{-9}\times627.5\times(0.25)^2\times0.50\times1.0}{0.00025}$$

$$M_j = \frac{2\pi \times 0.268\times0.6275\times0.0625\times0.50}{25}$$

M_j = 0.00132 inch lb., friction torque.

Or translated into horsepower at a speed of 24,000 RPM,

$$\text{F.H.P.} = \frac{2\pi MN}{33,000} = \frac{2\pi\times0.00132\times24,000}{12 \times 33,000}$$

It is always possible to get a good, order-of-magnitude check on the friction in a journal bearing by using Newton's definition of absolute viscosity. As shown in Reference (9) Equation (6), page 8,

$$M = \frac{\mu A r U}{h} \qquad (15)$$

μ = absolute viscosity in reyns (lbs.sec/in^2)
A = the swept area, $2\pi rl$(in^2)
U = the surface speed of the journal (in/sec)
h = the radial film thickness which is c

Thus using the parameters from Example 5,

$$M = \frac{2.68\times10^{-9}\times2\pi\times0.25\times0.50\times0.25\times627.5}{0.00025}$$

M = 0.00132 inch lb. friction torque

In this case the answer is identical to the previous result obtained for Example 5 since the only difference between Equations 15 and 16 is the absence of the c_f factor from Equation (15). Thus when $c_f \to 1$, both equations yield the same result.

C. Attitude Angle in Full Gas-Lubricated Journal Bearings

It is clear from the discussions outlined in the introduction that the journal center does not coincide with the bearing center under steady operating conditions. There is actually a locus of points that the journal center will follow depending upon the bearing geometry. Figure (26) shows a typical locus of motion of the center of a journal in the clearance of a self-acting journal bearing. The angle ϕ is the attitude angle formed between the direction of applied load and the line joining the bearing and shaft centers. This angle is shown in Figures (23), (26) and (27) and is of importance in establishing both the mathematical and physical criteria for stability in hydrodynamic (self-acting) journal bearings.

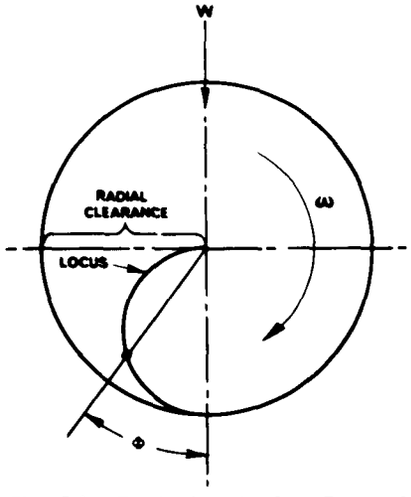

Fig. 26 - Typical Attitude - Eccentricity Locus for the Motion of the Center of a Journal in the Clearance of a Self-Acting Bearing.

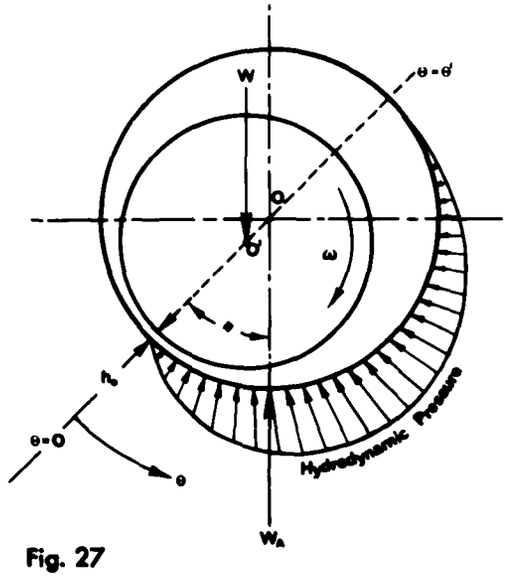

Fig. 27 - Attitude Relationships for Journal Bearing.

To determine the parameters affecting attitude angle it is necessary to examine the hydrodynamic pressure profile in the bearing. In Figure (27) an applied load W_A is subjected to the bearing through the bearing center O, and the reactive load is taken at the journal center O'. The resultant film force W has a component along the line of centers OO' equal to W cos ϕ.

The hydrodynamic pressure at any point in the film is a variable, p, a function of speed, viscosity, clearance, angular position in the clearance, eccentricity ratio, etc.

W cos ϕ is then opposed by that component of the pressure film force acting along the line of centers 00'.

$$W \cos \phi = \int_{\theta=0}^{\theta=\theta'} p \cos \theta \, r \, l \, d\theta \qquad (16)$$

And in the same way for the component of the resultand film force W perpendicular to the line of centers 00', we have,

$$W \sin \phi = \int_{\theta=0}^{\theta=\theta'} p \sin \theta \, r \, l \, d\theta \qquad (17)$$

For purposes of this explanation sideflow or variation of p in the axial direction is neglected.

Dividing Equation (17) by Equation (16) yields,

$$\frac{W \sin \phi}{W \cos \phi} = \frac{\int_{\theta=0}^{\theta=\theta'} p \sin \theta \, r \, l \, d\theta}{\int_{\theta=0}^{\theta=\theta'} p \cos \theta \, r \, l \, d\theta} = \tan \phi \qquad (18)$$

or in general, tan ϕ is a function only of eccentricity ratio ε . This function is unique for any particular bearing. For example, with a liquid lubricated journal bearing, assuming a pressure arc of 180°, (Ref. 19),

$$\tan \phi = \frac{\pi \sqrt{1-\varepsilon^2}}{2 \varepsilon} \qquad (19)$$

Evaluating Equation (19) we have Table X.

TABLE X

Attitude Angles for Liquid Lubricated, 180° Journal Brg.

ε	tan ϕ	ϕ degrees
0	∞	90
0.1	15.65	86.35
0.2	7.70	82.6
0.3	5.0	78.7
0.4	3.6	74.5
0.5	2.72	69.8
0.6	2.095	64.5
0.8	1.18	49.7
0.9	0.762	37.3
0.95	0.517	27.35
0.98	0.319	17.7

When plotted on polar coordinates as shown in Figure (28), the resultant curve is known as an attitude-eccentricity locus and represents the path along which the center of the journal will always traverse.

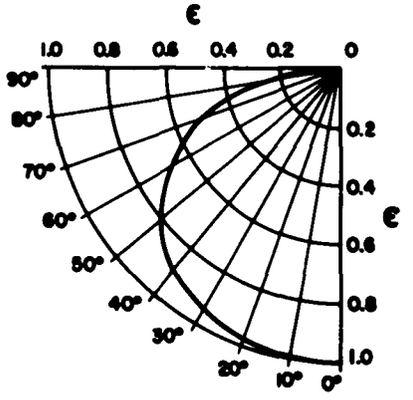

Fig. 28 - Attitude-Eccentricity Locus for Liquid-Lubricated, 180° Journal Bearing.

In a similar fashion, the attitude angles for certain gas lubricated bearings have been calculated including the compressibility effects of the gas. Thus the attitude angles for gas-lubricated bearings become a function of Λ as well as ε. Figure (29) shows attitude angle patterns for full, gas-lubricated journal bearings as found in Ref. (14). Notice the effect of Λ on these locii. These diagrams are similar to Figure (28) where the eccentricity ratio, $\varepsilon = 1$, is replaced by the radial clearance.

For quantitative evaluation of these angles, charts from Elrod, Ref. (13), are used since they cover a greater range of Λ values with higher accuracy and also include one additional l/d ratio. Tables of these values are also included.

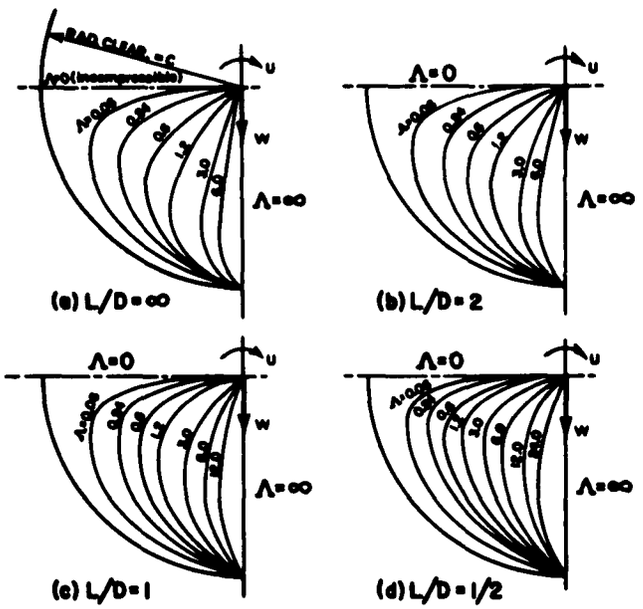

Fig. 29 - Attitude-Eccentricity Locus Diagrams for Full, Gas-Lubricated Journal Bearings. (Ref. 14).

Example 6: With a bearing having an l/d ratio of 1 and a value of $\varepsilon = 0.6$, the following attitude angles are obtained from Figure (33) or Table XIV:

Λ	ϕ
0	90°
0.1	85
0.2	79
0.4	69
0.6	62
1.0	52
4.0	25
8.0	15
20.0	8
60.0	3.9
100.00	2.7

The dependency of attitude angle ϕ on Λ is obvious.

It can be seen in these figures that considerable difference exists in the attitude angle between fluid theory for incompressible lubricants ($\Lambda \to 0$) and fluid theory for compressible lubricants, even for very small values of the compressibility parameter (or bearing number)Λ. This is not like the case for load-carrying capacity where there is little difference in predicted values between liquids and gaseous lubricants up to a value of Λ about one.

For gas-lubricated bearings the value of the attitude angle ϕ must always be determined through Figures (30) to (34) by means of the compressibility parameter.Λ.

TABLE XI

Attitude Angle, ϕ (deg.) for $1/d \to \infty$

Λ	ϵ=0.2	Λ	ϵ=0.4	Λ	ϵ=0.6	Λ	ϵ=0.8	Λ	ϵ=0.9
0	90	0	90	0	90	0	90	0	90
.9622	45.75	0.8209	47.97	0.5418	52.78	0.2052	54.53	0.0715	52.88
1.979	26.93	1.859	28.10	1.460	30.73	0.6348	35.05	0.2221	32.49
4.012	14.03	3.976	14.38	3.643	15.10	2.379	17.23	1.017	19.80
8.058	7.130	8.110	7.160	7.781	7.310	6.256	7.660	4.246	8.270
12	4.808	12	4.866	12	4.736	12	4.016	-	-
24	2.408	24	2.436	24	2.369	24	2.006	-	-
30	1.927	30	1.949	30	1.895	30	1.605	-	-
40	1.446	40	1.462	40	1.422	40	1.203	-	-
50	1.156	50	1.170	50	1.137	50	0.963	-	-
60	0.964	60	0.975	60	0.948	60	0.802	-	-
70	0.826	70	0.835	70	0.812	70	0.688	-	—
80	0.723	80	0.731	80	0.711	80	0.602	-	-
90	0.642	90	0.650	90	0.632	90	0.535	-	-
100	0.578	100	0.585	100	0.569	100	0.481	-	-
	0	∞	0	∞	0	∞	0	-	-

$\epsilon \to 0$

Λ	ϕ	Λ	ϕ
0	90	30	1.91
0.1	84.30	40	1.43
0.24	76.50	50	1.15
0.6	59.03	60	0.96
1.2	39.80	70	0.82
3	18.43	80	0.72
6	9.46	90	0.64
12	4.76	100	0.58
24	2.38	∞	0

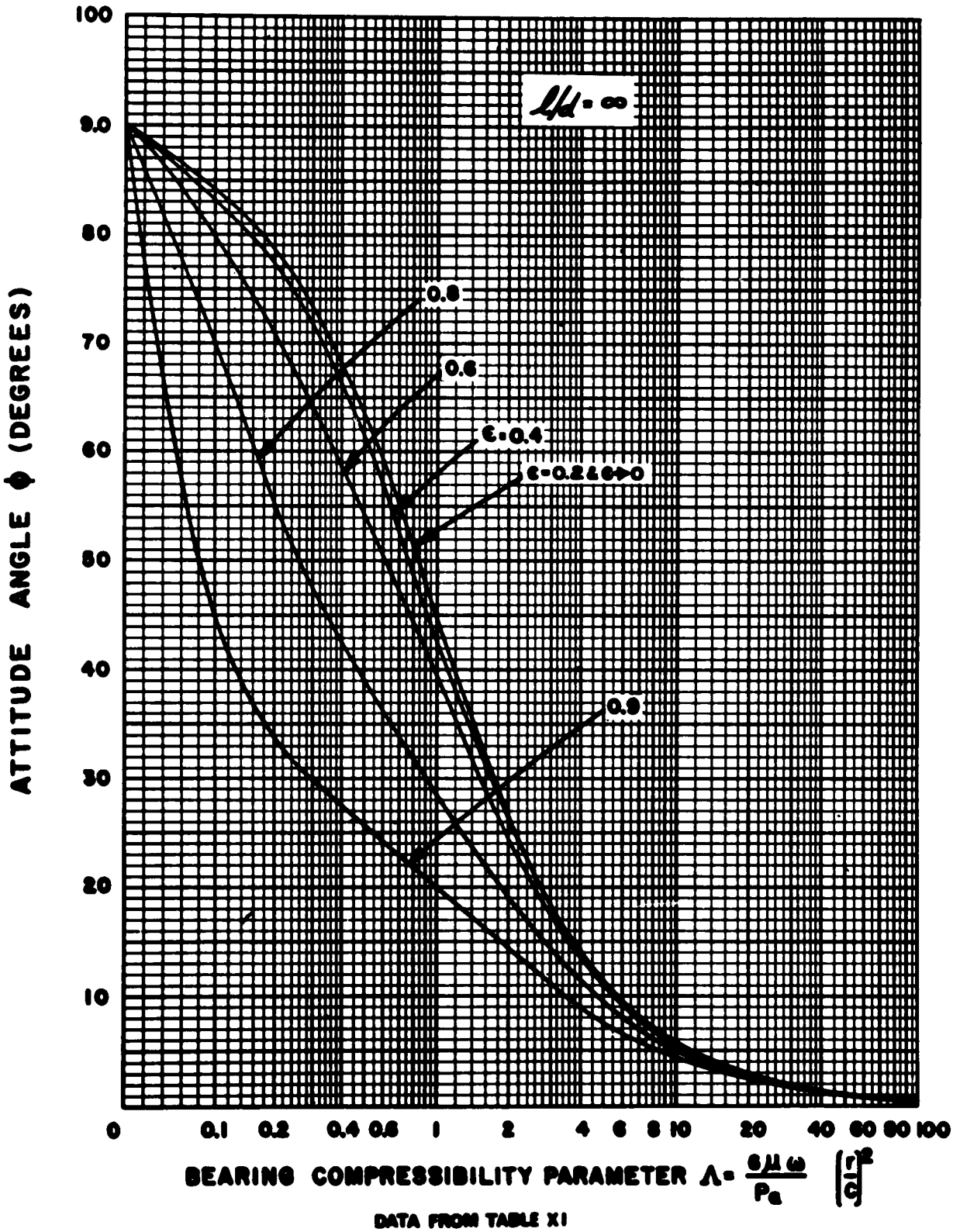

Fig. 30 - Attitude Angle vs Compressibility Parameter for $1/d = \infty$ (Ref. 13).

TABLE XII

Attitude Angle, ϕ (deg.) for $1/d = \pi$

Λ	$\epsilon \to 0$	$\epsilon = 0.2$	0.4	0.6	0.8
0	90	90	90	90	90
0.1	85.58	-	-	-	-
0.24	79.50	-	-	-	-
0.5	68.95	67.58	64.13	55.80	38.43
1	52.76	-	-	-	-
2	34.35	33.43	31.87	27.43	19.40
6	14.75	14.20	13.45	11.72	8.77
10	9.87	9.42	8.80	7.57	5.65
20	5.82	5.86	5.32	4.49	3.28
24	5.09	5.08	4.59	3.84	2.78
30	4.32	4.29	3.84	3.19	2.28
40	3.52	3.46	3.08	2.52	1.77
50	3.01	2.94	2.60	2.10	1.46
60	2.65	2.58	2.27	1.82	1.25
70	2.39	2.32	2.03	1.62	1.10
80	2.18	2.11	1.84	1.46	0.98
90	2.02	1.95	1.69	1.34	0.89
100	1.88	1.82	1.57	1.23	0.82
∞	0	0	0	0	0

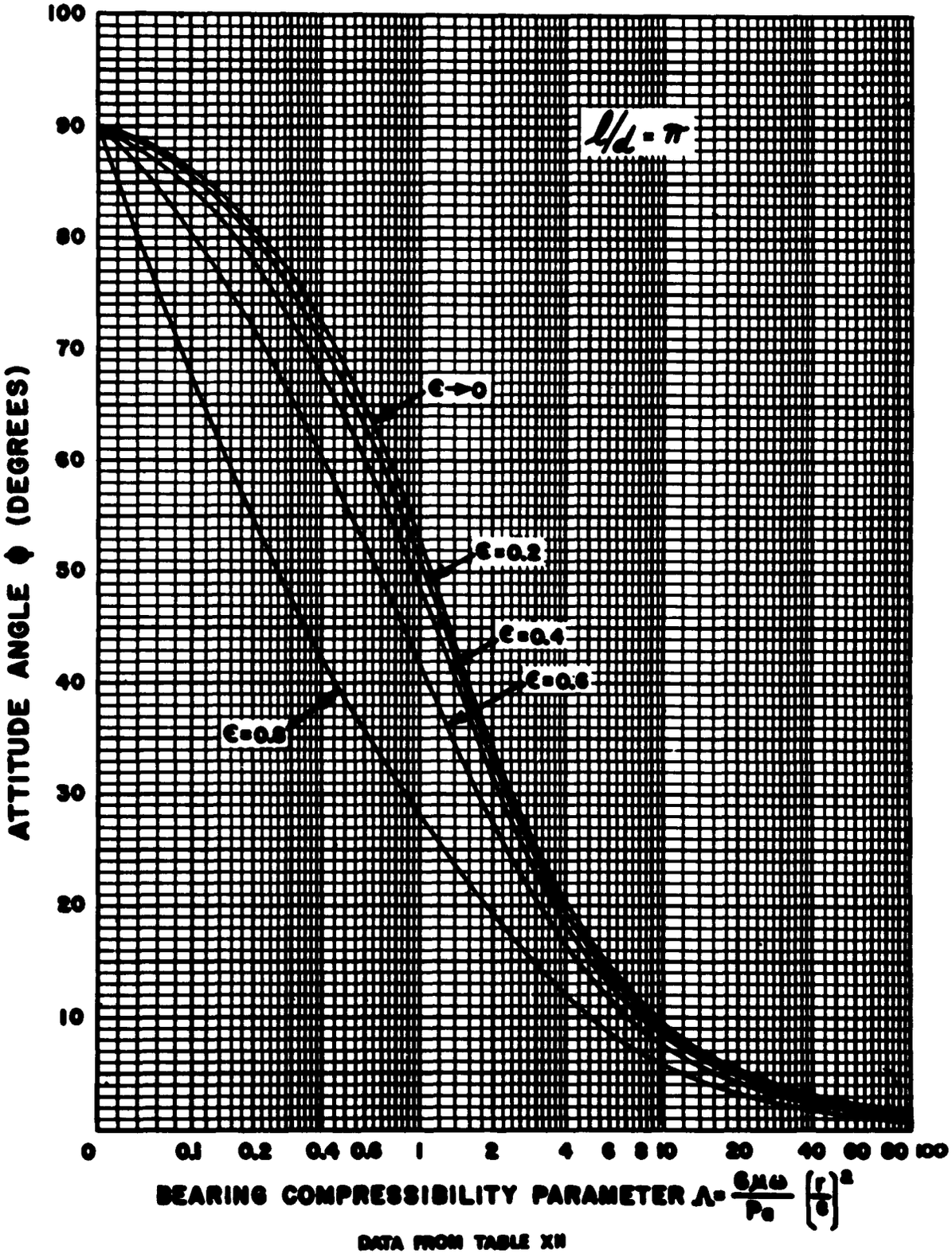

Fig. 31 - Attitude Angle vs Compressibility Parameter for $l/d=\pi$ (Ref. 13).

TABLE XIII

Attitude Angle, ϕ (deg.) for l/d = 2

Λ	$\varepsilon \to 0$	$\varepsilon = 0.2$	0.4	0.6	0.8
0	90	90	90	90	90
0.06	-	-	-	-	76.56
0.1	86.55	-	-	-	-
0.24	81.77	81.28	78.80	71.94	52.48
0.6	70.17	68.98	64.47	54.58	36.37
1.2	54.46	53.22	48.63	39.99	26.60
3	30.58	29.94	27.47	22.92	15.94
6	18.26	17.74	16.10	13.43	9.370
12	11.00	11.33	10.20	8.486	6.068
24	6.745	6.715	5.907	4.750	3.254
30	5.794	5.720	4.998	3.976	2.687
40	4.780	4.675	4.050	3.180	2.110
50	4.130	4.014	3.456	2.686	1.757
60	3.671	3.552	3.042	2.346	1.518
70	3.327	3.208	2.737	2.097	1.343
80	3.059	2.940	2.501	1.905	1.210
90	2.842	2.726	2.311	1.752	1.105
100	2.662	2.548	2.155	1.627	1.019
∞	0	0	0	0	0

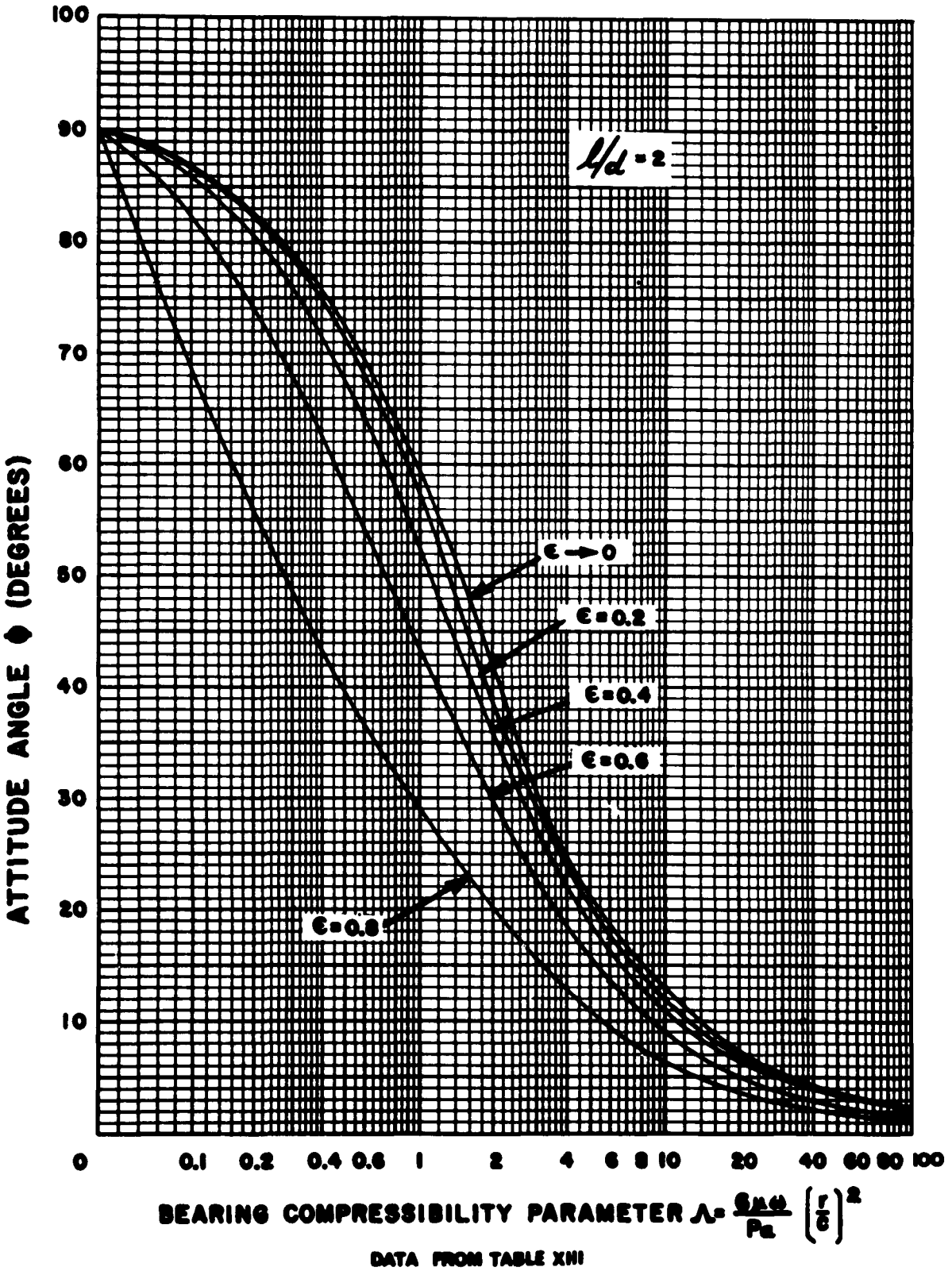

Fig. 32 - Attitude Angle vs Compressibility Parameter for 1/d=2 (Ref. 13).

TABLE XIV

Attitude Angle, ϕ (deg.) for l/d = 1

Λ	$\varepsilon \to 0$	$\varepsilon = 0.2$	0.4	0.6	0.8
0	90	90	90	90	90
0.06	-	-	-	-	77.77
0.1	88.38	-	-	-	-
0.24	86.11	85.62	83.53	76.92	54.01
0.6	80.35	79.33	74.43	62.09	37.36
1.2	71.24	69.32	62.19	47.96	27.87
3	49.96	47.93	41.11	30.50	17.94
6	31.60	30.33	26.01	19.55	11.90
12	18.81	17.95	15.32	11.58	7.140
24	11.77	11.66	9.924	7.500	4.687
30	10.21	10.02	8.474	6.343	3.909
40	8.528	8.279	6.950	5.146	3.118
50	7.430	7.168	5.987	4.397	2.630
60	6.648	6.383	5.312	3.878	2.297
70	6.058	5.798	4.810	3.494	2.053
80	5.594	5.340	4.419	3.197	1.865
90	5.218	4.970	4.104	2.959	1.716
100	4.904	4.663	3.844	2.763	1.594
∞	0	0	0	0	0

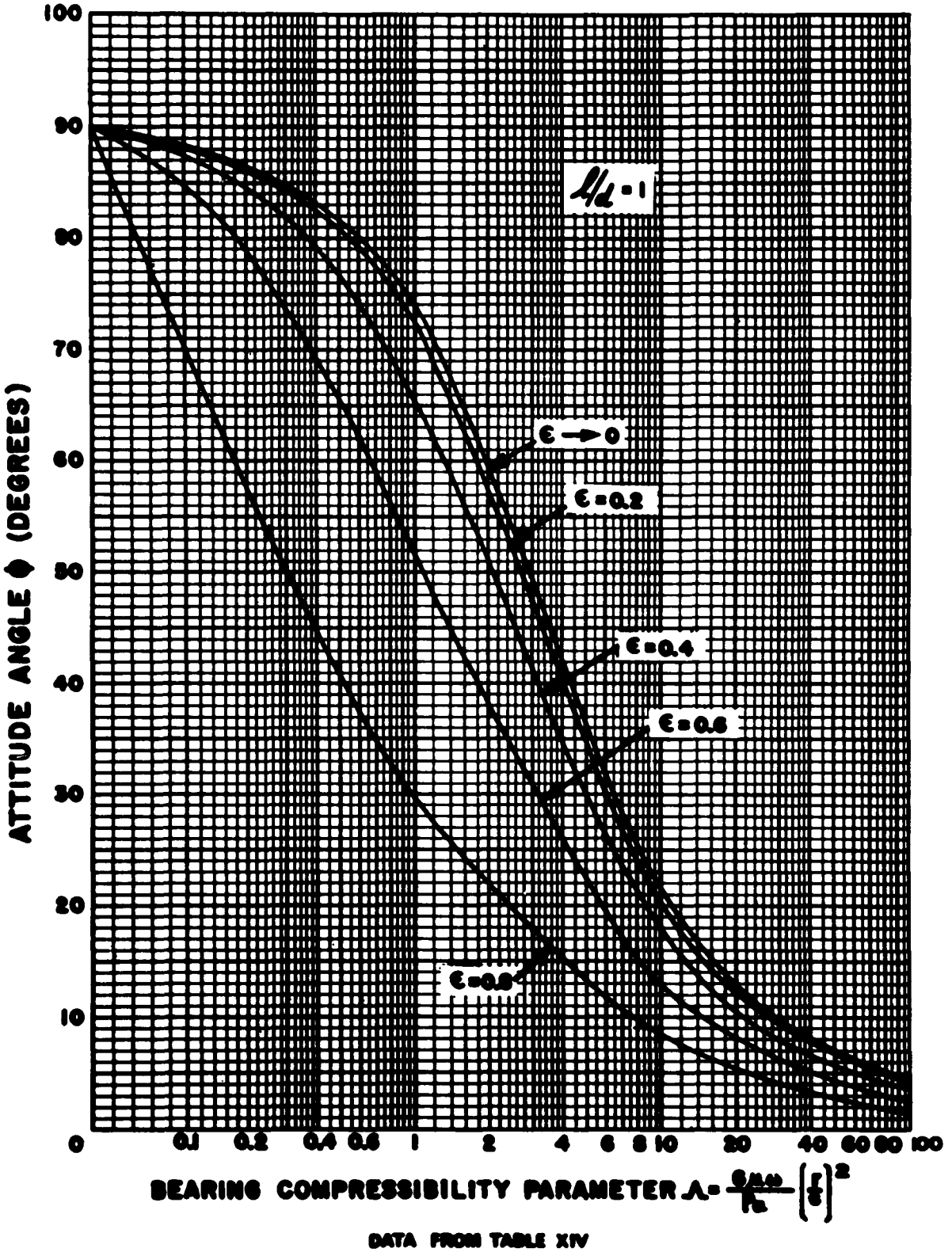

DATA FROM TABLE XIV

Fig. 33 - Attitude Angle vs Compressibility Parameter for 1/d=1 (Ref. 13).

TABLE XV

Attitude Angle, ϕ (deg.) for $l/d = \frac{1}{2}$

Λ	$\epsilon \to 0$	$\epsilon = 0.2$	0.4	0.6	0.8
0	90	90	90	90	90
0.06	-	-	-	-	81.51
0.1	89.48	-	-	-	-
0.24	88.75	88.54	87.48	83.41	61.56
0.6	86.88	86.37	83.73	74.44	43.46
1.2	83.75	82.78	77.82	63.16	32.60
3	74.79	72.45	63.63	45.53	22.36
6	61.54	58.62	48.78	33.29	16.60
12	43.04	40.81	33.32	22.72	11.74
24	26.03	24.62	20.24	14.07	7.450
30	21.93	20.32	16.95	12.16	6.898
40	17.71	16.75	13.85	9.844	5.507
50	15.15	14.47	11.91	8.405	4.659
60	13.44	12.87	10.55	7.414	4.082
70	12.21	11.68	9.546	6.686	3.661
80	11.26	10.74	8.760	6.119	3.336
90	10.50	9.987	8.136	5.668	3.078
100	9.866	9.368	7.615	5.298	2.868
∞	0	0	0	0	0

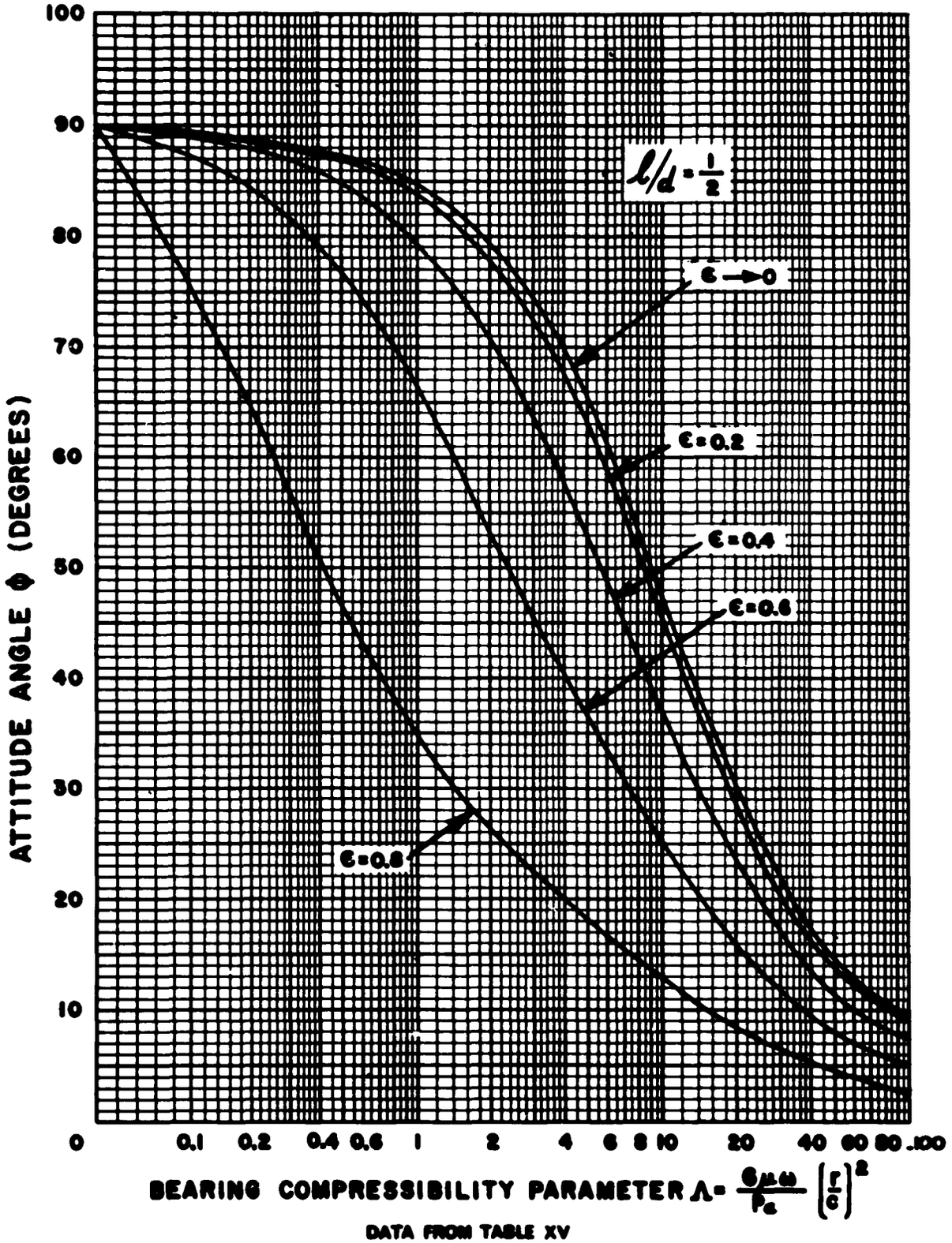

DATA FROM TABLE XV

Fig. 34 - Attitude Angle vs Compressibility Parameter for $l/d=\frac{1}{2}$ (Ref. 13).

D. Synchronous Whirl

Forces Due to Rotating Unbalance

In addition to unidirectional constant radial forces, the second most common type radial load that a journal must carry is mass unbalance of the rotating component. Such an unbalance produces a radial force that rotates at shaft speed as depicted on Figure (35) with a magnitude dependent upon both the amount of unbalanced mass in the system and the rotational speed.

As with a steady, unidirectional load, a rotating force will produce a displacement of the journal within the bearing. In this case, however, the center of the journal will not be displaced to a fixed point in space but will describe a somewhat circular orbit because of the angular motion of the force. It is clear that this angular motion occurs at the same frequency as the shaft rotational speed and therefore it is generally termed 'synchronous whirl'. If all other radial forces were removed from the journal then the center of the circular orbit of the shaft center would correspond closely to the center of the bearing as seen on Figure (36)path A. On the other hand, if a steady unidirectional radial load acts on the journal to displace the journal center to some point 0' (Fig.36), then the center of the circular orbit due to unbalance would also shift to 0' and the new path described by the journal center would approximate path B.

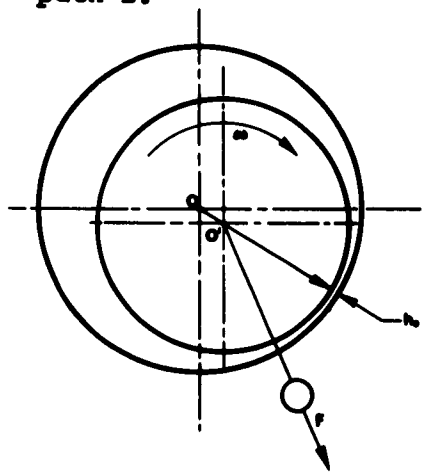

Fig. 35 - Force F, Resulting from Unbalance of Rotor Shaft Rotating with Shaft At Synchronous Speed.

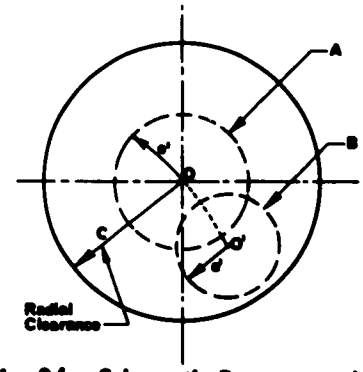

Fig. 36 - Schematic Representation of Orbiting Paths in a Journal Bearing, Path A Due to Unbalance. Path B Due to a Steady Load Plus Unbalance.

In order to determine the minimum bearing film thickness of a journal bearing containing unbalance of the rotating member it is necessary to determine the radius e' of the circular orbit of the shaft center.(See Fig. 36). For small values of e' the eccentricity ratio ε and e' may be calculated as though the rotating load were a stationary load of the same magnitude. This has been shown to be quite accurate if ε does not exceed a value of about 0.4 to 0.5. Thus the analysis to predict the load-carrying capacity of a static load may be applied to a load due to rotating unbalance with satisfactory accuracy provided that the value of eccentricity ratio ε does not exceed about 0.4 or 0.5. (Ref. 20). For eccentricity ratios greater than these values dynamic responses occur in the gas film involving squeeze film forces and other time dependent actions so that the static equivalency described above becomes more inaccurate.

To review the accuracy of considering the unbalance load as a fixed load the following example taken from Ref. 20 by Sternlicht and Elwell is presented.

Example 7: A 360° gas-lubricated, self-acting journal bearing was tested on a vertical shaft. Attitude angle and eccentricity ratio were measured for the shaft while in operation. For the following conditions, the eccentricity ratio for a rotating unbalance may be computed assuming the analysis for a steady load condition is applicable:

$l/d = 1$
Diameter = 2"
Length = 2"
Speed = 6000 rpm
Radial Clear.= 0.000504
Viscosity = 2.61×10^{-9} reyns
Unbal. @ 6000 rpm = 12.5 lb/brg
Amb.pressure = 14.7 psia

$$A = \frac{6\mu u}{P_a}\left[\frac{r}{c}\right]^2$$

$$A = \frac{6 \times 2.61 \times 10^{-9} \times \frac{6000 \times 2\pi}{60}}{14.7}\left[\frac{1}{0.000504}\right]^2$$

$$A = 2.63$$

$$\text{and } \frac{W}{dlP_a} = \frac{12.5}{14.7 \times 2 \times 2} = 0.2125$$

Using Figure (14) or Table V, the calculated value of $\varepsilon = 0.27$. The measured value of $\varepsilon = 0.275$ indicating excellent agreement. To make a more complete analysis several other points were calculated with the following results:

Speed (rpm)	Force-lbs.	$W/P_a dl$	A	Calculated ε	Measured ε (Ref.20)
2,000	1.5	0.0255	0.876	0.08	0.08
4,000	5.05	0.0859	1.755	0.15	0.15
6,000	12.5	0.2125	2.63	0.27	0.275
8,000	22	0.374	3.505	0.37	0.405
10,000	35	0.595	4.38	0.47	0.53

The results are shown in Figure (37) compared with experimental data.

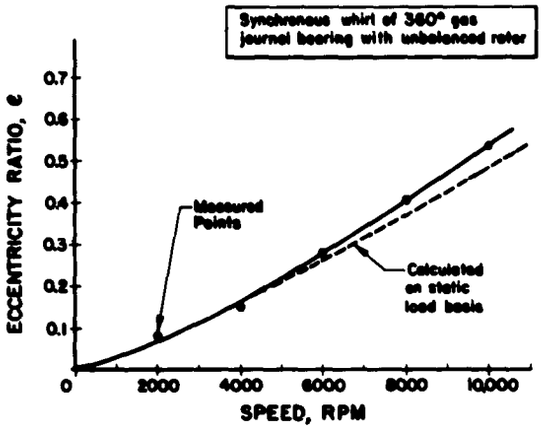

Fig. 37 - Orbital Eccentricity Ratio for Journal Subjected To An Unbalanced Radial Load. Experimental Data from Ref. 20.

Establishment of Limits for Rotating Unbalance

The method of analysis just discussed also provides a means for establishing the limits on unbalance that can be tolerated in any particular rotating assembly. This limit will be measured in terms of the eccentricity ratio that the unbalance produces and the corresponding minimum film thickness.

Example 8: As an illustration of this, reconsider Example 7 that has just been described as having an eccentricity ratio of $\epsilon = 0.27$. The specific bearing in Example 7 had a length and diameter of 2 inches each with a radial clearance of 0.000504 inches. If it is desirable to maintain the minimum film thickness of this bearing at 0.00037 inches at 6,000 RPM then the maximum eccentricity ratio allowable may be calculated using Equation (8)

$$h_o = c\,[1-\epsilon] \text{ or } 1 - \frac{h_o}{c} = \epsilon$$

$$\epsilon = 1 - \frac{.00037}{.000504}$$

$$= 1 - .734$$

$$\epsilon = 0.266 \text{ or approximately } 0.27$$

For this eccentricity ratio and the calculated bearing compressibility number $\Lambda = 2.63$, the maximum load may be determined from Figure (14) to be 12.5 pounds per bearing. This force is the result of an unbalance which can be determined from the relation

$$F_{\text{unbalance}} = \frac{W}{g}\,\omega^2\,r$$

where W is the magnitude of the unbalance, ω is the rotational speed in radians per sec., "g" is the gravitational constant and r is the effective radius of the unbalance.

Thus for this example, substituting the numerical values, we have:

$$12.5 = \frac{W}{386}\left[\frac{6000}{60} \times 2\pi\right]^2 \times r$$

$$Wr = 0.0122 \text{ lb.in.}$$

$$\text{or} \quad Wr = 0.195 \text{ oz.in. of unbalance}$$

The allowable unbalance becomes a function of bearing clearance, size and speed, for a given lubricant viscosity, and in most cases would be established by the limits on minimum film thickness that would be acceptable. In a majority of applications a minimum film thickness, resulting from unbalance, of perhaps from 3/4 to 2/3 of the radial clearance would probably be allowable, i.e. $\epsilon = .25$ to $\epsilon = 0.34$.

Synchronous Resonant Whirl (Inversion-Point Critical Speed)

If the gas film in the bearing is considered as a spring supporting the rotating element, then any disturbing force will create a deflection of this spring. In the case of an unbalance force, the disturbing force varies angularly in direction at a frequency equal to that of the rotating speed of the rotor. At any specific point in the gas film the unbalanced force thus acts as a vibrating force with a frequency equal to the rotational speed. The rotating shaft system which is considered supported on a gas spring, has a natural frequency at which it will resonate. If the frequency of the unbalanced vibrational force corresponds to the lowest natural frequency of the shaft and support system, a forced vibration phenomenon occurs which is frequently termed "synchronous resonant whirl" or "inversion point critical speed". Both of the terms imply that the rotor is acting as a rigid body and is vibrating on the relatively soft gas "springs" in the bearings. (Ref. 21)

Extensive observations have been made on this type of instability (Ref. 22). By means of capacitance probes monitoring the motion of the journal in its bearing, it can be shown that below this resonant "critical speed" the shaft-rotor system is rotating about its geometric axis. After passing through this resonant condition, the shaft-rotor system begins to spin about its center of gravity axis. This inversion, or shift in the center of rotation, can be observed on the screen of an oscilloscope and hence the origination of the term "inversion-point critical speed".

Translatory Synchronous Whirl Rotating Journal

The response of a gas film spring is non-linear, consequently, there is no spring "constant" but rather a spring rate which will increase with eccentricity ratio for this type of bearing. The actual spring rate therefore, at a given eccentricity ratio, may be obtained by drawing a tangent to the curve of load-carrying capacity plotted against eccentricity ratio for a given bearing at a fixed speed (Refs. 22 and 23). Such a curve would be typical of Figure (17).

Example 2: Figure (17) is redrawn in Figure (38) including as an additional abscissa the minimum film thickness corresponding to the various values of ε. These are calculated from Equation (8)

$$h_o = c\,[1-\varepsilon]$$

For the bearing described in Figure (17), c = 0.00025 inches.

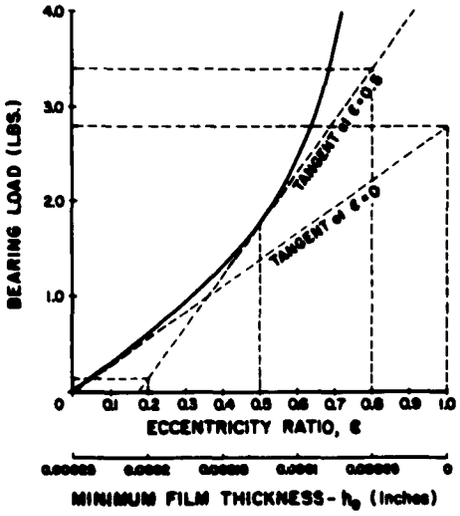

Fig. 38 - Replot of Data from Example 1 and Fig. 17.

If the rotor is on a vertical shaft or in a zero gravity field the bearing load would be zero and the eccentricity ratio would also be zero. The slope of the above curve at $\varepsilon = 0$ is the film stiffness k.

$$k_{\varepsilon=0} = \frac{2.8\ \text{lbs.}}{0.00025\ \text{in.}} = 11{,}200\ \text{lb./in.}$$

The natural frequency of vibration, still considering the shaft-rotor system as a simple rigid body, would then be:

$$f = \frac{1}{2\pi}\sqrt{\frac{2k}{m_s}} \qquad (20)$$

where k = film stiffness of one bearing (lb/in). See Figure (40), assuming translation only.

m_s = total mass of rotating system (shaft) (W/g or lb.sec^2/in)

f = natural frequency (cycles/sec)

In the case of this rotor the weight is 0.118 lb. or $m = \frac{0.118}{386}$.

$m = 0.000306$ lb.sec^2/in for one bearing

For a two bearing system

$$m = 0.000306 \times 2 \text{ lb.sec}^2$$

The natural frequency then is, from Equation (20),

$$f = \frac{1}{2\pi}\sqrt{\frac{11,200 \times 2}{0.000306 \times 2}}$$

$$f = \frac{1}{2\pi}\sqrt{36.6 \times 10^6}$$

$f = 964$ cycles/sec or 57,800 cycles/min.

Since this device is designed to run at 24,000 RPM there will be no need to pass through this particular critical speed.

As a further illustration, suppose the shaft-rotor system was loaded by some force, so that ε was equal to 0.5. A tangent to the curve in Figure (38) would yield a film stiffness k of:

$$k = \frac{(3.4 - 0.13)\text{lb.}}{(0.0002\text{-}0.00005)\text{ in.}} = \frac{3.27}{0.00015}$$

$k = 21,800$ lb/in.

And the natural frequency corresponding to the synchronous resonant whirl or inversion point critical speed would be in this case from Equation (20),

$$f = \frac{1}{2\pi}\sqrt{\frac{21,800 \times 2}{0.000306 \times 2}}$$

$f = 1345$ cycles/sec.or 80,600 cycles/min.

Although this phenomenon is rare in oil-lubricated bearings because of the high damping in oil films, it has been observed and identified in oil-lubricated shaft journal bearings with overhung compressor wheels operating at fairly high speeds. One case involved a shaft 3.3 inches in diameter operating at 12,000 RPM with a rotor weighing about 100 pounds. Because of the low damping properties of gas films however, such instabilities are not suppressed and consequently will appear if the dynamic conditions are appropriate.

Conical Synchronous Whirl Rotating Journal

It was assumed in the previous discussion that the journal axis remains parallel to the bearing axis as depicted on Figure (39A). This is termed the cylindrical mode or translatory mode of vibration. It is also quite possible for the shaft rotor system to vibrate in a conical mode as illustrated in Figure (39B). In this case the journal axis generates a conical surface with the apex in the plane of the center of mass. The difference between the two modes of vibration is determined by the distribution of the rotor mass and for the case of a two bearing support system, the distance between the bearings.

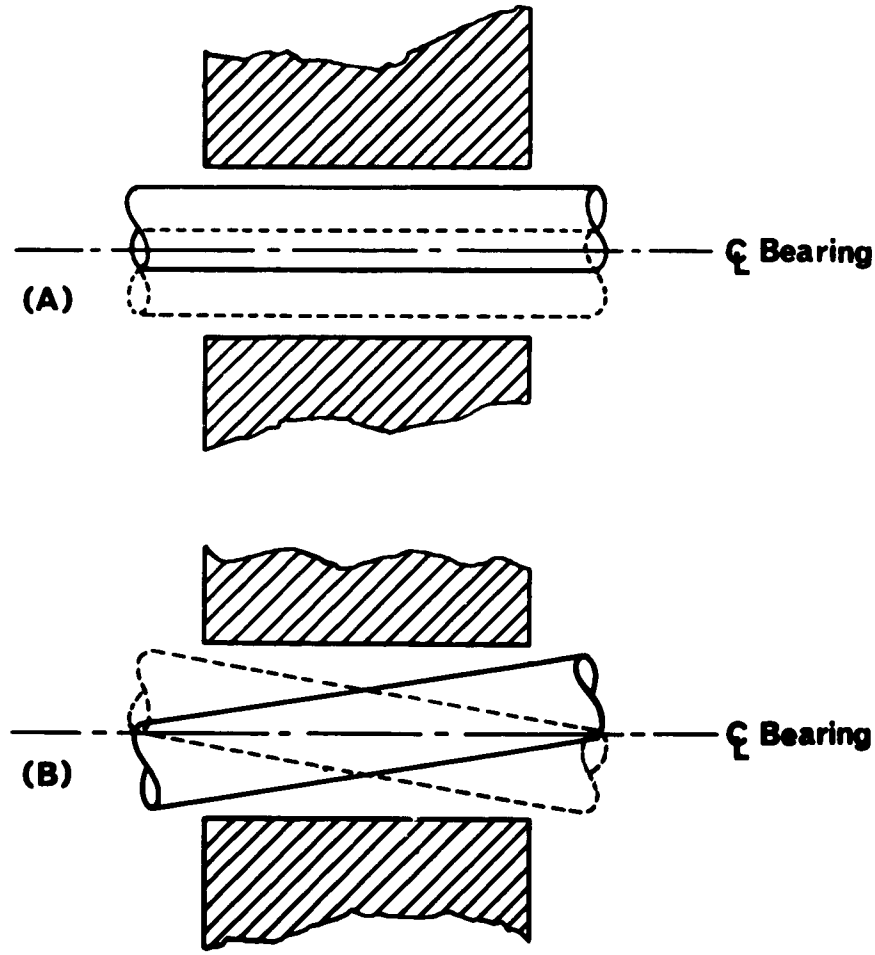

Fig. 39 - Indication of Synchronous Whirl of Shaft in Journal Bearing. (A) Translatory or Cylindrical. (B) Conical.

In translatory, cylindrical, synchronous whirl of the shaft we have the simple case of an undeflected mass on two springs with rigid bearing housings. This has already been described. The conical type of shaft synchronous whirl is illustrated in Figure (39) and also schematically in Figure (40). As has been explained, the springs are not linear, as shown in Figure (38) but by taking a tangent to the load-deflection curve they can be assumed to be linear at the particular point of operation. For conical whirl, the springs develop a restoring moment, and for two springs this becomes $kL^2/2$ (in.lb./radian).

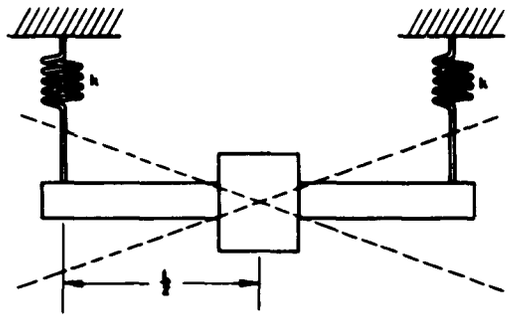

Fig. 40 - Schematic Representation of Shaft Conical Synchronous Whirl.

Then the restoring spring moment equals the inertia moment, or

$$f_{\text{conical shaft}} = \frac{1}{2\pi}\sqrt{\frac{kL^2}{2I_{ts}}} \qquad (21)$$

where I_{ts} is the transverse moment of inertia of the shaft rotor system about a diameter (lb.in.sec^2)

If in the conical whirling motion, the polar moment of inertia of the rotating shaft system is significant compared to the transverse moment of inertia, there could be a gyroscopic effect which would influence the natural frequency of vibration and the critical speed at which resonance takes place. Den Hartog, "Mechanical Vibrations" 4th Edition, McGraw-Hill Publishing Company, shows that if the shaft is whirling (or precessing) in the direction of spin, the gyroscopic inertia moment tends to make the amplitude of vibrations smaller, thus making the effective spring rate higher and in this way raising the natural frequency of vibration. This is the case corresponding to synchronous whirl. Following through Den Hartog's derivation, we have

$$f_{\text{conical shaft}} = \frac{1}{2\pi}\sqrt{\frac{kL^2}{2[I_{ts} - I_{ps}]}} \qquad (22)$$

Where I_{ps} is the polar moment of inertia of the shaft-rotor system.

Synchronous Translatory and Conical Bearing Whirl

(a) Non-Rotating Bearing

Next we consider the case of synchronous bearing whirl. Such an occurrence is common if the bearing is held in flexible supports and can vibrate relative to the spinning shaft. We then have the usual cases of translatory synchronous whirl,(Fig. 41),

$$f_{\text{trans.brg.}} = \frac{1}{2\pi}\sqrt{\frac{k}{m_b}} \tag{23}$$

and for conical whirl

$$f_{\text{conical brg.}} = \frac{1}{2\pi}\sqrt{\frac{k_c}{I_{tb}}} \tag{24}$$

where k_c is the restoring moment produced by the gas film in the bearing and I_{tb} is the transverse moment of inertia of the bearing about a diameter. An expression for k_c can be obtained directly from the translatory k if it is assumed that the gas-film spring action in the bearing is uniformly distributed, neglecting end effects. This assumes that all sections of the bearing, including the ends, contribute equally to the translatory stiffness. This is not true and only in the limit when l/d approaches infinity would it be considered to be a fair representation of the facts. However, using this assumption and integrating across the bearing we find that:

$$k_c = \frac{kl^2}{12} \tag{25}$$

where l is the length of the bearing. Now Equation (25) may in general be written as follows:

$$k_c = \frac{kl^2}{K^*} \tag{26}$$

where K^* is a numerical factor depending upon the l/d ratio of the bearing. Then Equation (24) when combined with (26) becomes

$$f_{\text{conical brg.}} = \frac{1}{2\pi}\sqrt{\frac{kl^2}{K^*I_{tb}}} \qquad (27)$$

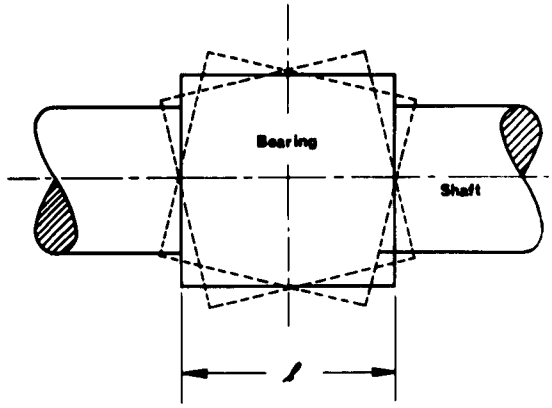

Fig. 41 - Conical Whirl of Bearing With Respect To Shaft.

The number 12 in Equation (25) and K* in Equation (26) may be replaced by modified values obtained from actual experiments such as in Ref. (35). In this paper experimental results are shown for conical whirl of bearings (as contrasted to shaft whirl) in which this numerical factor is evaluated from the observed data.

The following values summarize the results:

TABLE XVI

Experimental Values of K* (Ref.35)

Bearing l/d Ratio	K*
∞	12 (theoretical value)
3	15
2	23
1.5	25
1.0	25

Thus, while these values are experimental and subjected to a number of probable errors they are nevertheless more accurate than the idealized value of K* = 12 computed for the case of l/d of ∞. It is recommended that these experimental values be used in making calculations involving conical bearing whirl and in Equation (27), a number selected from the above table, for the corresponding l/d ratio of the bearing would be used instead of 12.

(b) Rotating Bearing

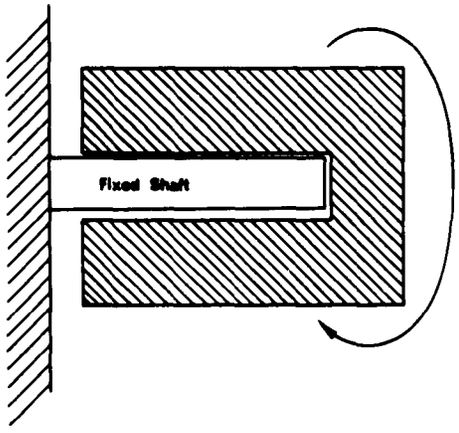

Fig. 42 - Fixed Shaft and Rotating Bearing.

Now Equation (27) for conical whirl of the bearing is applicable to the rocking or oscillating motion of a non-rotating bearing. If the situation that needs to be evaluated is that of a stationary shaft and a rotating bearing, gyroscopic inertia effects of the rotating bearing would need to be included This would correspond physically to an electric motor driven fan, where the "rotor" in the classical sense, is held stationary, and the housing revolves about it. Figure (42).

In this case the polar moment of inertia might be relatively large and should be included. The equation for natural frequency would become

$$f_{\text{conical brg.}} = \frac{1}{2\pi}\sqrt{\frac{k\,l^2}{K^*\,[I_{tb} - I_{pb}]}} \qquad (28)$$

where I_{pb} is the polar moment of inertia of the bearing and K^* is a number taken from Table XVI and which depends upon the l/d ratio of the bearing.

Let us now summarize the discussion so far on synchronous resonant whirl:

1. Translatory synchronous shaft whirl Eq. (20)

2. Conical synchronous shaft whirl
   a. Without gyroscopic effect Eq. (21)
   b. With gyroscopic effect Eq. (22)

3. Translatory synchronous bearing whirl, with rotating or non-rotating bearing Eq. (23)

4. Conical synchronous bearing whirl
   a. Non-rotating bearing Eq. (27)
   b. Rotating bearing Eq. (28)

It is frequently possible to predict which mode of synchronous vibration may be expected to occur first as the speed of a unit is slowly raised. For the case of shaft synchronous whirl we can take the ratio of Equation (20) to Equation (22) and

$$\frac{f_{trans.shaft}}{f_{conical\ shaft}} = \frac{\frac{1}{2\pi}\sqrt{\frac{2k}{m_s}}}{\frac{1}{2\pi}\sqrt{\frac{k\,L^2}{2\,[I_{ts}-I_{ps}]}}}$$

$$\left[\frac{f_{ts}}{f_{cs}}\right]^2 = \frac{2k\ \ 2[I_{ts}-I_{ps}]}{k\ m_s\ L^2}$$

$$\left[\frac{f_{ts}}{f_{cs}}\right]^2 = \frac{4\ [I_{ts}-I_{ps}]}{m_s\ L^2} \qquad (29)$$

Thus, if the right hand side of the equation is greater than one, f_{cs}, conical shaft synchronous whirl will occur at a lower frequency than f_{ts}, translatory shaft synchronous whirl. If the right hand side is less than one then it follows that the translatory mode will have the lower frequency.

In Ref. (31) is data for an electric motor rotor held in two rigid non-rotating bearings so that Equation (29) would be applicable.

Weight of rotor = 17.19 lb.

L (distance between bearings) = 11.75 inches

I_{ts} = 1.91 lb.insec^2

I_{ps} = 0.063 lb.in.sec^2

Substituting in Equation (29)

$$\left[\frac{f_{ts}}{f_{cs}}\right]^2 = \frac{4\ [1.91-0.063]}{17.19/386 \times 11.75^2} = 1.2$$

The results of tests made by the authors of Ref. (31), although performed for half-frequency whirl, did show that conical whirl was observed at a lower speed than translatory whirl, as we would have expected from the ratio of $f_{ts}^2/f_{cs}^2 = 1.2$.

For the case of bearing whirl (non-rotating) we take the ratio of Equation (23) to (27), or

$$\frac{f_{tb}}{f_{cb}} = \frac{\frac{1}{2\pi}\sqrt{\frac{k}{m_b}}}{\frac{1}{2\pi}\sqrt{\frac{k\ l^2}{K^*\ I_{tb}}}}$$

$$\left[\frac{f_{tb}}{f_{cb}}\right]^2 = \frac{K^*\ I_{tb}}{m_b\ l^2} \qquad (30)$$

where values of K* would be obtained from Table XVI.

As part of the experimental work of Ref. (35) it was possible to take a given bearing and add weights to it thus changing the ratio of I_{tb} to m_b in Equation (30) and in turn changing the form of the mode of the lower frequency whirl. The observations were actually made on half-frequency whirl but the general conclusions are valid, for synchronous whirl, with a non-rotating bearing.

Bearing diameter - 2 inches

Bearing length - 6 inches

l/d ratio - 3

K* from Table XVI- 15

Therefore, from right hand side of Equation (30)

$\frac{15\ I_{tb}}{m_b\ l^2}$	Mode of Whirl Predicted	Mode of Whirl Observed
1.305	Conical	-
0.965	Cylindrical	Cylindrical
1.090	Conical	Conical
1.035	Conical	Cylindrical
1.11	Conical	Conical

These results show the general agreement with the predictions of Equation (30).

For the case of bearing whirl, with a stationary shaft but with a rotating bearing, we take the ratio of Equation (23) to Equation (28) and have:

$$\frac{f_{tb}}{f_{cb}} = \frac{\frac{1}{2\pi}\sqrt{\frac{k}{m_b}}}{\frac{1}{2\pi}\sqrt{\frac{k\ l^2}{K^*\ [I_{tb} - I_{pb}]}}}$$

or

$$\left[\frac{f_{tb}}{f_{cb}}\right]^2 = \frac{K^*\ [I_{tb} - I_{pb}]}{m_b\ l^2} \qquad (31)$$

Influence of External Vibration

In the previous section it has been shown that a gas-borne rotating system has at least two resonant synchronous speeds which correspond to natural frequencies of vibration. If such a system is running smoothly, not at one of these "critical speeds", difficulty may arise if the entire structure is shaken or vibrated at a frequency which corresponds to one of these critical speeds. Such resonant external excitations are generally more serious with gas-lubricated bearings than with liquid or oil lubricated bearings because the gas bearing has much less internal damping. Because of this, it is recommended that a bearing not be subjected to a vibration excitation higher than 75 to 85%

of the lowest natural frequency of vibration. In the case of Example 9 for instance, a synchronous resonant shaft frequency was computed as 964 cycles/sec. The recommendation then would be to limit the vibrational excitation of this unit to 725 to 825 cycles per second as a maximum.

If for some reason, perhaps test specifications, it would be necessary to subject the rotor system of Example 9 to say 1000 cycles per second it would be desirable to have the lowest synchronous whirl frequency some 15% to 25% above this value. As shown in Equation (20), or subsequent Equations (21) through (28), whichever would apply, this may be accomplished by increasing the spring rate k or k_c and/or decreasing the mass m or the moment of inertia.

Although the damping in a self-acting bearing of this type is relatively low, it is possible to pass through a synchronous resonant critical speed, if absolutely necessary, and no damage may result providing the amount of unbalance is low and the acceleration rate is high. Under no circumstances however should steady-state operating speed be within approximately 15% of one of the natural frequencies of the system.

In consideration of external vibrations, resonant behavior of self-acting bearings has also been observed at applied vibration frequencies of one half rotational frequency (Ref. 41). Of concern at this condition is the reduction in load capacity of the bearing. Observed increases in eccentricity ratio from 0.05 at a fixed load condition to 0.6 at a sinusoidal load condition and an applied frequency of one half rotational frequency have been recorded.

Experiments conducted by Rotron have indicated that the reduction in load capacity occurs over a rather narrow band around the ratio of applied vibrational frequency to rotating bearing frequency = ½. In the case of one particular unit, a reduction in sinusoidal load capacity from 8 G's to 4 G's was observed at the applied frequency of 125 cps with an operating speed of 250 cps. This decrease in load capacity occurred over the range from 100 to 150 cps

applied frequency. Figure (43) presents a dimensionless plot illustrating the effect of this behavior.

When designing a gas bearing it is quite evident that the designer must carefully review the vibrational requirements that the bearing must withstand. In addition to avoiding vibrational loads of the same frequency as the resonant frequency of the bearing, load capacity must be checked for sustaining vibrational loads at frequencies within 15% of one half rotational frequency.

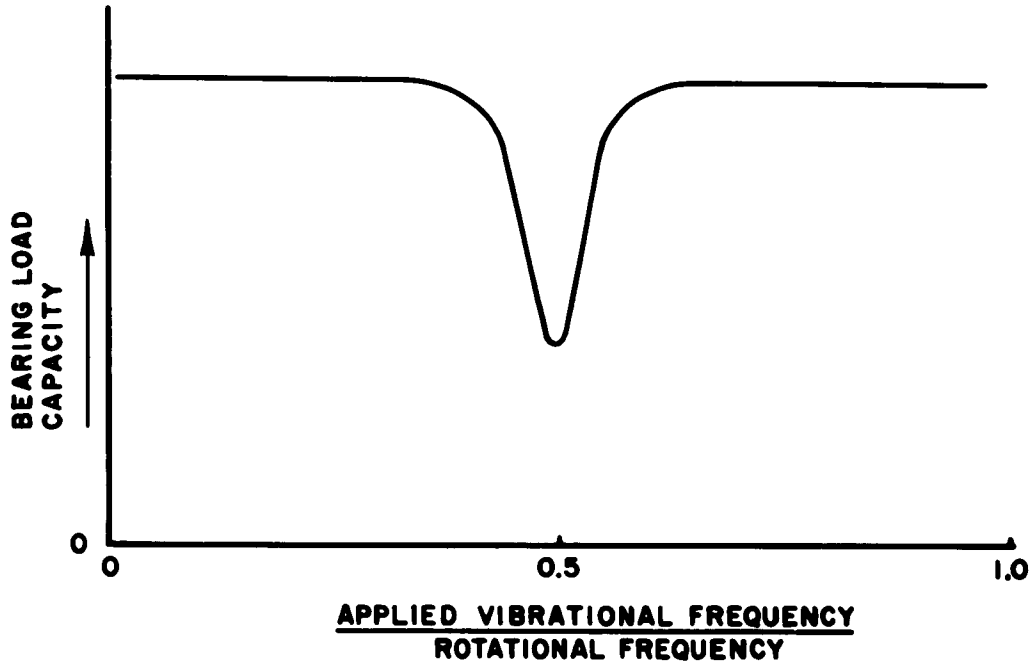

Fig. 43 - Bearing Load Capacity Under Sinusoidal Load Condition.

E. Half-Frequency Whirl

One of the most serious forms of instability encountered in journal bearing operation is known as "half-frequency whirl". The phenomenon is one of self-excited vibration and is characterized by having the center of the shaft orbit around the center of the bearing at a frequency approximately equal to half of the spinning or rotational velocity of the shaft. Under these conditions Hagg (24) has shown that the capacity of the bearing to support radial loads falls to zero. In Figure (44) this half-frequency whirling motion is depicted where Ω is approximately half of ω. Ω is the orbital frequency and ω is the shaft rotational frequency.

The shaft system may be stable as the speed is increased until this threshold is reached. Crossing this threshold with further increase in speed will bring the system into a region of instability which becomes more violent as the penetration becomes deeper until inevitable seizure results. Unlike an ordinary critical speed the shaft cannot pass through this one and attain a region of stability on the other side at a higher speed as with synchronous resonant whirl. A typical instance would be to have a bearing running smoothly without any difficulties at say 40,000 rpm but seize and fail completely at 43,000 rpm. Failure in most instances is instantaneous and complete as the amplitude of vibration becomes equal to the radial clearance in the bearing. It should be pointed out rather emphatically that this type of instability is not peculiar to gas bearings but actually is a serious and continuing problem with high-speed, lightly-loaded, liquid-lubricated bearings as well.

The explanation of this instability and possible methods of predicting its occurrence are based on an understanding of what steady-state positions the journal assumes in the bearing clearance with variations in speed and load. For a given bearing geometry these positions form a path which is predictable and consistent. This path is the attitude-eccentricity locus as described earlier in this manual in Section II C. Referring to Figures (26) and (27), the

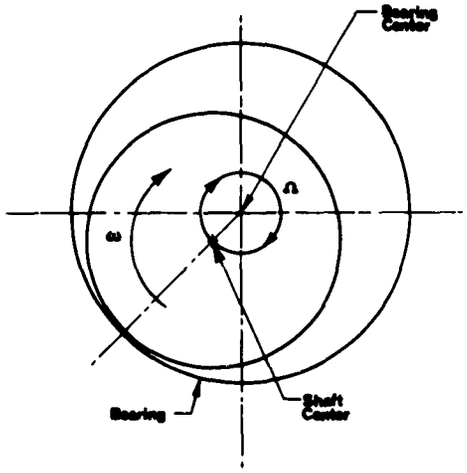

Fig. 44 - Orbital Whirling Velocity of Shaft Center Ω About Center of Bearing Compared to Shaft Spinning Velocity ω.

attitude angle is indicated by the symbol ϕ and for full film, gas-lubricated journal bearings may be obtained from Figures (30) through (34) as a function of bearing compressibility parameter Λ.

Generally at light loads and/or high speeds, the eccentricity ratio ε is small, approaching 0, while the attitude angle approaches 90°. For heavier loads the eccentricity ratio increases and the center of the shaft travels downward along the shaft center locus with the attitude angle approaching zero as the eccentricity ratio approaches one.(Note Fig.26)

Half-frequency whirl is actually the result of a driving force acting on the shaft causing it to whirl or orbit in the same direction as the spin of the shaft. This driving force is a component of the hydrodynamic load-carrying film force that is developed in the clearance space of the bearing. Thus in Figure (45a) with the load applied as shown, the line joining the center of the bearing with the center of the shaft can be drawn. The components of the hydrodynamic film force acting perpendicular to this line of centers can be called F_θ. It is the force F_θ which provides the driving action and which can result in the unstable motion called whirl. In Figure (45b), (c), and (d) it is shown that the location of a shaft center 0' on the attitude eccentricity locus influences the magnitude of F_θ. In Figure (45b) is depicted a position of the shaft where F_r is small and F_θ is rather large. F_θ will therefore tend to cause a high degree of whirl instability.

In Figure (45c) it is assumed that the shaft center is now further down the locus, perhaps midway on the arc. This would result from increasing the external load, for example, or by developing an internal load on the journal through the use of grooves or slots. Now in Figure (45c)

the relationship between F_r and F_θ shows that they are both of comparable magnitude. If the center of the journal now finds itself much further down on the attitude-eccentricity locus as shown in Figure (45d), through modification of either load or geometry, F_r becomes quite small. This means that the driving force F_θ is becoming negligible and that for these conditions the shaft would be very stable.

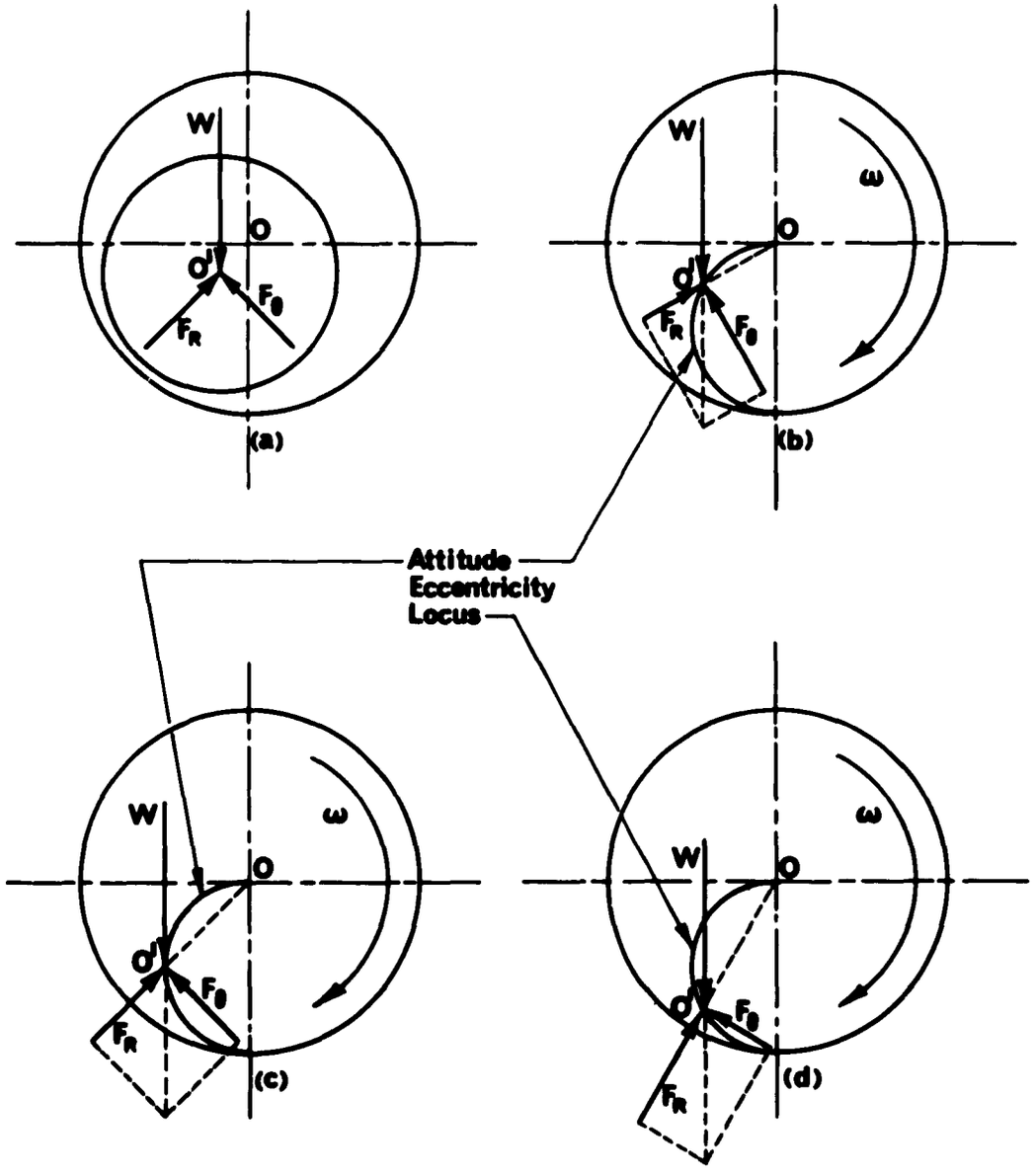

Fig. 45 - Relationship of Radial Force F_R, to Tangential Force F_θ, for Several Values of Eccentricity Ratio.

Thus the angular position of F_θ and its magnitude, or conversely the angular position of F_r and its magnitude will be fundamental parameters in establishing whether half-frequency whirl is a possibility.

Half-Frequency Whirl Stability for Liquid Lubricated Self-Acting Bearings

Poritsky (25), Boeker and Sternlicht (26), refer to the analysis of whirl instability in terms of these forces. The equations of motion are established and these equations are analyzed for stability criteria. A relationship is developed to indicate the threshold of whirl instability as a function of the mass of the system, the spring constant of the shaft itself, and the radial film stiffness of the lubricating film in the bearing as determined by the force F_r that has just been described. If F_r approaches zero the shaft will whirl at all operational speeds. An example of such a case would be a vertical shaft supported by an ungrooved journal bearing where ε would equal to zero and ϕ would be 90°.

The expression derived is as follows, referring specifically to translatory half-frequency whirl of the rotor-shaft system:

$$f_{\frac{ts}{2}} = \frac{2}{2\pi}\sqrt{\frac{1}{\frac{m_s}{2}\left[\frac{1}{K_1}+\frac{1}{K_2}\right]}} \tag{32}$$

where $f_{\frac{ts}{2}}$ = shaft speed at which half-frequency translatory shaft whirl begins (cycles/sec).

m_s = mass of shaft-rotor system (lb.sec^2/in)

K_1 = shaft spring stiffness (lb/in)

K_2 = radial spring stiffness of the bearing film for one bearing, obtained by plotting radial film force F_r against film thickness and evaluating the slope of this curve at the proper eccentricity ratio (lb/in)

For our purposes, where the shaft system is such that operation is well below the first mechanical critical speed (with elasticity of the shaft included), we can properly assume that the shaft stiffness is much greater than the radial stiffness of the gas film, or $K_1 >> K_2$ so that in Equation (32) above $1/K_1 << 1/K_2$ and may be dropped. Therefore, Equation (32) becomes

$$\frac{f_{ts}}{2} = \frac{2}{2\pi}\sqrt{\frac{2K_2}{m_s}} \qquad (33)$$

Use of Equation (33) for liquid-lubricated bearings has shown very satisfactory correlation between predicted whirl threshold speeds and actual speeds at which such instabilities were observed to begin (26,27). More refined analyses involving extended digital computer calculations are available but the justification of this extra involvement and complication has not yet been established (28). It is therefore recommended that Equations (32) or (33) be used for design purposes with liquid-lubricated bearings. The method provides a step-wise sequence of calculations (as shown in Example 10, Steps 1 through 7) in which a physical understanding may be gained of the phenomenon known as half-frequency whirl. With this conceptual understanding there is developed simultaneously the knowledge of the influence of the several variables such as attitude angle, eccentricity ratio, radial and tangential fluid spring forces, speed, clearance ratio and length-to-diameter ratio, on the threshold of half-frequency whirl. It follows that by changing these parameters the threshold speed of instability can also be varied. In this way the design aspects for controlling this phenomenon are established.

This method involving the use of Equations (32) or (33), is also completely general and applies to all sizes and shapes of liquid lubricated journal bearings. If stabilizing forces are introduced, either external to the bearing or arising within the bearing clearance itself, the equations can be used, just as they are, without modification.

The reason this method is being given so much emphasis even though it was developed for bearings using incompressible lubricants, is that it provides the first step in developing a design approach for gas-lubricated bearings. Actually, for values of the compressibility number Λ less than about 1/3,

it may be used directly for gas-lubricated bearings providing that the stability parameter ω_1^* is large, that is to say, equal to or greater than 0.5. This parameter is described by Equation (34). For higher Λ however, two alternate approaches will be suggested.

Half-Frequency Translatory Whirl Analysis for Small Values of Λ

Example 10: This calculation will involve the use of Equation (33) and with it we will attempt to establish whether at a given operating speed the shaft will be stable or not stable to half-frequency whirl.

To provide correlation we will use experimental data from Sternlicht and Winn[29]. For a bearing with the following specifications the onset of half-frequency shaft whirl was observed to occur at 11,800 RPM.

Bearing diameter	2 inches
Bearing length	2 inches
Radial clearance c	0.001643 inches
Viscosity (air)	2.7×10^{-9} lb.sec/in.
P_a	14.7 psia
Radial load on bearing	11.01 pounds
Weight of shaft/bearing	11.01 pounds

Shaft is horizontal and bearing loading is due to gravity

We will begin by assuming that the operating speed is 11,800 RPM. Equation (33) will be evaluated and will yield an answer for the shaft speed $f_{ts/2}$ in cycles per second.

If $f_{ts/2} \times 60 = 11,800$ RPM, this will mean that the design speed is at the threshold of whirl instability.

If $f_{ts/2} \times 60$ is greater than 11,800 RPM, let us say for example 15,000 RPM, this means that the shaft should be free of half-frequency whirl at 11,800 RPM and thus is stable. It does not mean that 15,000 RPM will be a threshold speed.

If $f_{ts/2} \times 60$ is less than 11,800 RPM, say 5,000 RPM, the indication is that this design speed is unstable and that the shaft will be whirling at 11,800 RPM if it hasn't failed before at a lower speed. It does not mean that 5,000 RPM is a threshold speed.

Equation (33) is only a stability indicator. It tells whether the system is stable or unstable at a pre-selected speed. It does not calculate a "critical" speed in the usual sense unless the assumed speed coincides with the calculated value from Equation (33).

Actually it is somewhat similar to a "go"-"no go" gage establishing whether a manufactured part is within acceptable dimensional tolerance. It either is or it isn't. In the same way, Equation (33) shows whether the shaft is stable with respect to half-frequency whirl or it is not, evaluated of course with reference to an assumed operating speed.

Step 1 - Calculate Λ

From Equation (1) $\Lambda = \frac{6\mu\omega}{P_a}\left(\frac{r}{c}\right)^2$

$$\omega = \frac{11,800}{60} \times 2\pi = 1235 \text{ rads/sec.}$$

$$r = 1 \text{ inch}$$

Then $$\Lambda = \frac{6 \times 2.7 \times 10^{-9} \times 1235}{14.7}\left(\frac{1}{1.643 \times 10^{-3}}\right)^2$$

$$\Lambda = 0.504$$

Step 2 - Establish Load-Eccentricity Relationship

From Figure 14, for l/d=1, we obtain the following values at $\Lambda = 0.504$. Value of d x l x P_a = 2x2x14.7 = 58.8

ε	$\frac{W}{dlP_a}$	W(lb)
0	0	0
0.1	0.018	1.059
0.2	0.039	2.293
0.4	0.085	5.0
0.6	0.16	9.4
0.8	0.36	21.3

Step 3 - Determine Attitude Angles

From Figure 33, for l/d = 1, we have the following angles at $\Lambda = 0.504$:

ε	ϕ degrees
0	82.0
0.1	81.5
0.2	81.0
0.4	76.5
0.6	65.5
0.8	41.0

Step 4 - Determine the Component of W acting along the Line of Centers of Bearing and Shaft

Referring back to Figure (25), this is determined as W cos ϕ and acts along the lim of centers OO'. This is also indicated by Equation (16) and by the force F_r in Figure (45), called the radial force or the force that acts along the line of centers.

Actually, steps (2), (3) and (4) can all be combined in one operation by making one large table as shown below. Values of h_o are obtained from Equation (8).

ϵ	dlP_a	W(lb)	ϕdegrees	Cos ϕ	W cosϕ (F_r)(lb)	h_o in.
0	0	0	82.0	0.1392	0	0.001643
0.1	0.018	1.059	81.5	0.1478	0.1565	0.001477
0.2	0.039	2.293	81.0	0.1564	0.359	0.001313
0.4	0.085	5.0	76.5	0.2334	1.167	0.000985
0.6	0.16	9.4	65.5	0.4147	3.90	0.000657
0.8	0.36	21.3	41.0	0.7547	16.07	0.000328

Step 5 - Determine Operating Eccentricity Ratio

The operating ϵ for this bearing with W = 11.01 pounds will be somewhere between ϵ = 0.6 and ϵ = 0.8 judging by the above table. Frequently it is possible to interpolate, by inspection but in this case it will be necessary to plot a curve of W versus ϵ in order to get a sufficiently accurate value.

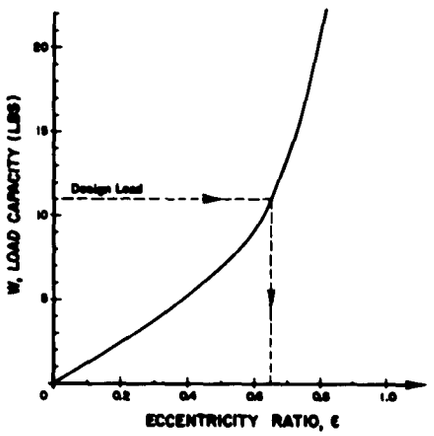

Step 6 - Determine K_2 for Equation (33)

The value of K_2 is obtained by plotting F_r (which is W cos ϕ) versus ϵ and h_o and determining the slope of this curve at the operating value of ϵ.

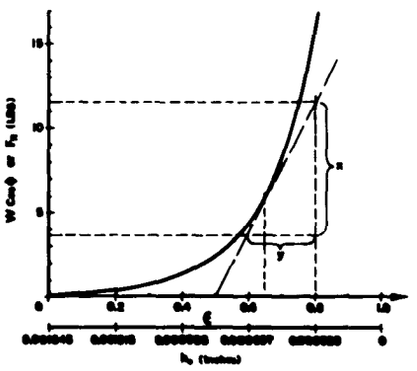

Slope of curve at $\varepsilon = 0.65$ is $\frac{x}{y}$

or $K_2 = \frac{x}{y} = \frac{11.7-3.75}{0.000657-0.000328} = \frac{7.95}{0.000329}$

$K_2 = 24,200$ lb/in at $\varepsilon = 0.65$

Step 7 - Calculate $f_{ts}/2$ from Equation (33)

$$f_{\frac{ts}{2}} = \frac{2}{2\pi}\sqrt{\frac{2K_2}{m_s}} = \frac{1}{\pi}\sqrt{\frac{2K_2}{m_s}}$$

$$f_{\frac{ts}{2}} = \frac{1}{\pi}\sqrt{\frac{24,200}{11.01/386}\times\frac{2}{2}}, \text{where } g = 386 \text{ in/sec}^2$$

$$f_{\frac{ts}{2}} = \frac{1}{\pi}\sqrt{848,000} = \frac{9.2\times10^2}{\pi}$$

$$f_{\frac{ts}{2}} = 293 \text{ cycles/sec.}$$

or $293 \times 60 = 17,600$ cycles per minute.

Now the measured value of threshold speed was 11,900 cycles per minute so that the predicted value based on Equation (33) is higher than the measured value.

$$\text{the ratio "C"} = \frac{\text{Predicted threshold value}}{\text{Measured threshold value}} = \frac{17,600}{11,800} = 1.49$$

This is rather typical of the comparison between theoretical and experimental results for shafts in 360° gas-lubricated journal bearings. The ratio "C" is largely a function of Λ, but not completely, as will be shown below. However, as a general rule, the smaller the value of Λ for a given case, the smaller will be the ratio "C." This means as we approach the incompressible film condition, or as Λ approaches zero, Equation (33) becomes more accurate.

For example, the graph (Figure 46) shows the results of a number of calculations similar to that of Example 10. The trend in the relationship between the factor "C" and the value of Λ is indicated.

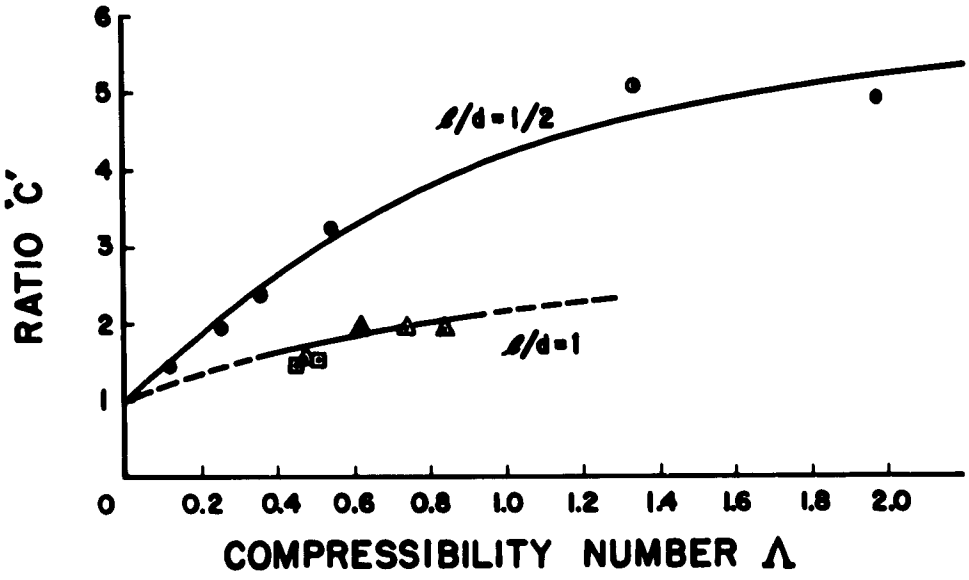

Fig. 46 - Ratio C Plotted Against Compressibility Number for Two l/d Ratios.

Although Figure (46) shows the trend of actual observed threshold speeds compared to predicted values using Equation (33), there is another parameter that is significant in establishing the stability characteristics of gas-lubricated journal bearings. This is called the stability parameter and has been given several forms depending upon the investigator (Refers. 32, 33, and 34).

The form of the stability parameter that appears most useful from a bearing design point of view is ω_1^*. This is found in Ref. (33) and (34)

$$\omega_1^* = \omega\sqrt{\frac{cM_1}{w}} \qquad (34)$$

where ω is the shaft speed, (radians/sec)
c is the radial clearance in the bearing (in.)
M_1 is the mass per unit length ($lb.sec^2/in^2$)
w is the load per length (lb/in)

The values of ω_1^* can be calculated for the data in Table XVII using Equation (34). The results are presented in Table XVIII.

TABLE XVII

Calculated and Observed Threshold Speeds

No.	Source Ref.	l(in)	d(in)	c(in)	Observed Threshold Rads/Sec	λ	Predicted Threshold Rads/Sec(eq.33)	Ratio Pts.on "C" Fig.46
1	(30)	0.5	1.0	0.000533	584	0.549	1765	3.02
2	(30)	0.5	1.0	0.000284	572	1.89	2830	4.94
3	(30)	0.5	1.0	0.001175	584	0.113	844	1.44
4	(30)	0.5	1.0	0.000284	402	1.33	2040	5.07
5	(30)	0.5	1.0	0.000533	383	0.360	900	2.35
6	(30)	0.5	1.0	0.000533	218.9	0.206	427	1.94
7	(31)	2.5	2.5	0.00125	680	0.736	1338	1.965
8	(31)	2.5	2.5	0.00125	560	0.604	1100	1.97
9	(31)	2.5	2.5	0.00125	440	0.475	684	1.55
10	(31)	2.5	2.5	0.00125	785	0.847	1557	1.985
11	(29)	2.0	2.0	0.001643	1235	0.504	1840	1.49
12	(29)	2.0	2.0	0.001643	1095	0.455	1595	1.39

Example 11: Consider the bearing which is described as No. 1 of Table XVII, for $\Lambda = 0.549$, the mass of the shaft is obtained from the weight of the shaft associated with one bearing. This weight was 0.33 pounds. The bearing was 1/2 inch long. The weight per unit length was thus 0.33 x 2 = 0.66 pounds/inch. The mass per unit length

$$M_1 = \frac{0.66}{386} = \frac{\text{lb.sec}^2}{\text{in.x in.}}$$

$$M_1 = 0.00171 \text{ lb.sec}^2/\text{in}^2$$

The shaft was not horizontal so that the load on the bearing was less than the weight of the shaft.

Load on bearing $w = 0.2795$ lbs.(given)
Long per unit length $= 0.2795 \times 2$
$= 0.559$ lb./in.

The observed threshold speed (or in general the intended operating speed) = 584 rads/sec.

Substituting in Equation (34)

$$\omega_1^* = 584 \quad \frac{0.000533 \times 0.00171}{0.559}$$

$$\omega_1^* = 584 \quad 1.63 \times 10^{-6}$$

$$= 584 \times 1.75 \times 10^{-3}$$

$$\omega_1^* = 0.745$$

Thus we have an additional parameter ω_1^* to describe the stability behavior of the bearing.

Making similar calculations, as Example 11 above, for the remainder of the bearings in Table XVII we have the following data, presented in Table XVIII.

TABLE XVIII

Stability Data

No.	Source Reference	l/d	Λ	"C"	ω_1*
1	(30)	½	0.549	3.02	0.745
2	(30)	½	1.89	4.94	0.498
3	(30)	½	0.113	1.44	1.435
4	(30)	½	1.33	5.07	0.416
5	(30)	½	0.360	2.35	0.646
6	(30)	½	0.206	1.94	0.513
7	(31)	1	0.736	1.965	1.312
8	(31)	1	0.604	1.97	1.195
9	(31)	1	0.475	1.55	1.115
10	(31)	1	0.847	1.985	1.410
11	(29)	1	0.504	1.49	2.55
12	(29)	1	0.455	1.39	2.42

From Table XVIII it is possible to cross-plot and average the values of Λ versus "C" and ω_1* for values of l/d of ½ and l/d of 1. Tables XIX and XX present the results of the cross-plotted data.

TABLE XIX

Cross-Plotted Stability Data vs "C" and ω_1* for l/d=½

"C"	Λ for ω_1*=0	Λ for ω_1*=0.5	Λ for ω_1*=1.0
1	0	0	0
2	0	0.20	0.30
3	0	0.44	0.65
4	0	0.88	1.30
5	0	1.68	2.65

TABLE XX

Cross-Plotted Stability Data vs "C" and ω_1^* for l/d=1

"C"	for ω_1^*=0	for ω_1^*=1.0	for ω_1^*=1.5
1	0	0	0
2	0	0.7	0.97
3	0	1.8	0.20

The data from Tables XIX and XX are plotted in Figures (47) and (48). The original data points from Table XVIII before cross-plotting are also shown to provide an indication of the averaging that was necessary.

Example 12: As an example of the use of this method, consider a case taken from Reference (30). This has previously been considered in Example 11.

Bearing length = 1/2 inch
Bearing diameter = 1 inch
Radial clearance = 0.000533 inches
Mass of rotor per bearing = 0.333/386 = 0.000862 $lb.sec^2/in$
Force on bearing = 0.279 lbs.
Observed whirl threshold speed = 93 cycles/sec.
Lubricant is air with $\mu = 2.65 \times 10^{-9}$ reyns

The calculations were made following the pattern used in Example 10, with the following results:

$A = 0.549$

$\frac{W}{dlP_a} = 0.0380$

ϵ under static conditions at 93 cycles/sec.= 0.45

$K_2 = 672$ lbs/in

$f_{\frac{ts}{2}}$ = from Eq. (33) = 281 cycles/sec, predicted threshold without modification.

Now modify this value of predicted threshold in accordance with Equation (34) and Figure (47) as was done in Example 11.

$$\omega_1^* = \omega\sqrt{\frac{cM_1}{w}} \qquad (34)$$

where M_1 = mass/unit length = $\frac{0.000862}{0.5} = 0.001724$ $lbs.sec^2/in^2$

and $\omega = 93 \times 2\pi = 584$ radians/sec

So $\omega_1^* = 584\sqrt{\frac{0.000533 \times 0.001724}{0.549}}$

$\omega_1^* = 0.748$

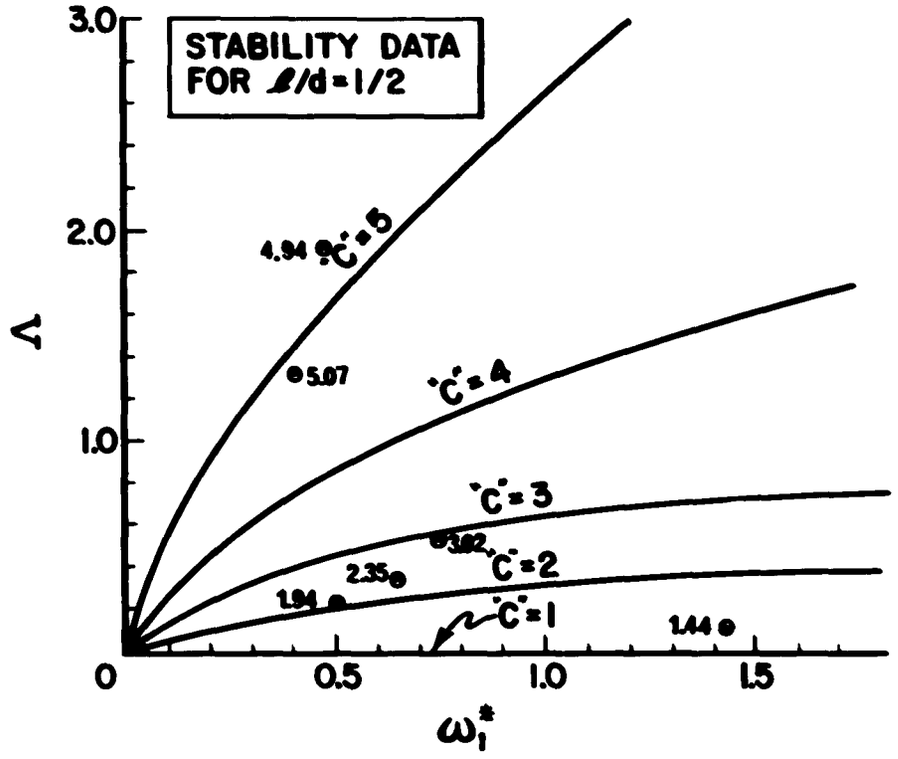

Fig. 47 - C Plotted Against Δ and ω_1^* for $l/d=\frac{1}{2}$.

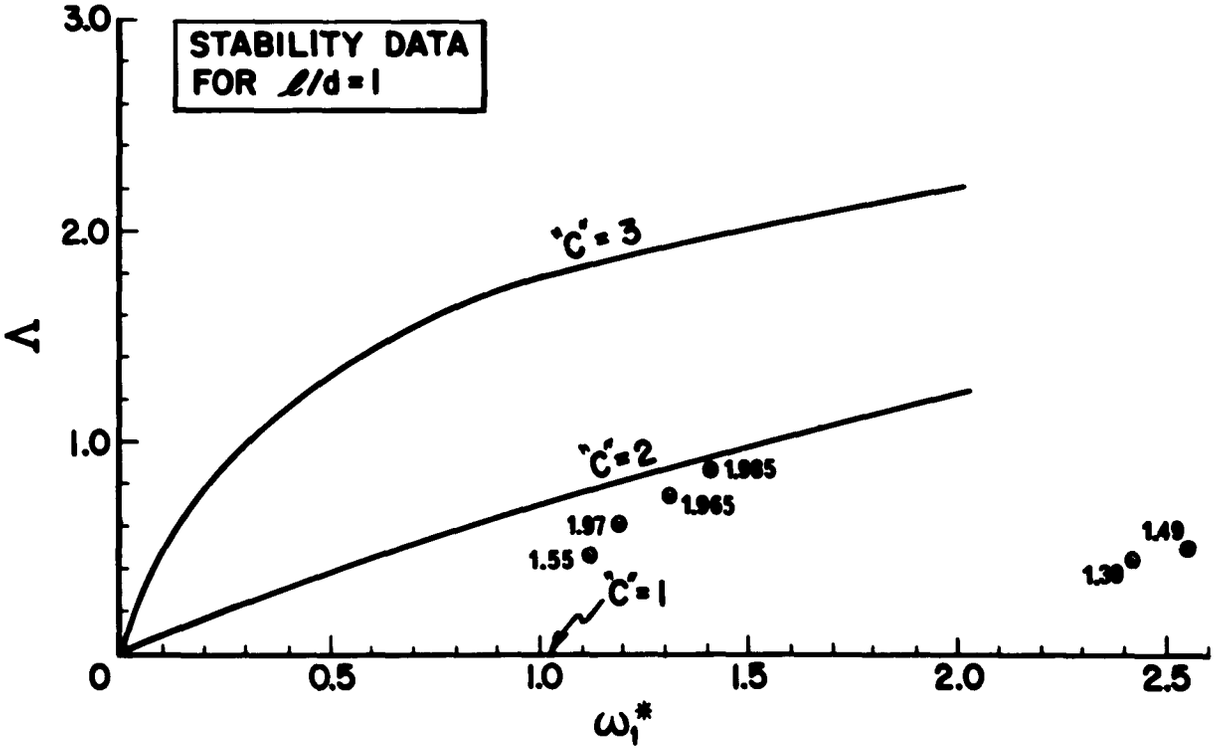

Fig. 48 - "C" Plotted Against Δ and ω_1^* for $l/d=1$

Now enter Figure (47) for $1/d = \frac{1}{4}$, with $\omega_1^* = 0.748$ and $A = 0.549$ and the intersection will occur very closely to the line where $C = 3$.

Therefore divide 281 cycles/sec from above, by 3 and the result will be

$$\frac{281}{3} = 93.6 \text{ cycles/sec}$$

This would indicate that the half-frequency whirl threshold was very close to the operating speed and that instability would be expected.

Half-Frequency, Translatory Whirl of a Shaft in Infinitely Long, Cylindrical Journal Bearings

For this approach we utilize Reference (34), a doctoral dissertation by Professor V. Castelli at Columbia Undersity. This manuscript provides an analytical evaluation of translatory half-frequency whirl of shafts in cylindrical, 360° journal bearings of infinite length. Although it applies particularly to bearings of infinite length, it appears to have some accuracy in predicting the stability threshold for shafts in very long bearings, such as for example where 1/d values may be 2.5, 3 or larger.

It also appears to be conservative for all 360° bearings of finite length providing that the eccentricity ratio for static loads, ε_o, is calculated for an equivalent bearing of infinite length. This can be done through the use of Figure (11) with a unit load on the bearing, lbs/in , corresponding to that of the finite length bearing.

Thus, if such a calculation for a bearing of finite length, let us say 1/d = 2, using the above approach based on infinite length, showed that for the selected operating conditions the shaft was on the threshold of instability, the shaft would in all probability actually be stable since it has finite length and not infinite length.

The finite length bearing has side flow and the actual value of ε would be greater than ε_o as calculated for the equivalent infinite length bearing. There would be a resultant improvement in the attitude angle for the finite length bearing over the infinite length bearing and in addition there would probably be more damping than for the infinite case.

All of these factors would tend to increase the stability and raise the threshold speed over that calculated for the equivalent bearing of infinite length.

The procedure is to make a plot of Λ versus ω_1^* for several values of ε_o. These curves represent the threshold of instability. ε_o is computed on a static load basis.

A tabulation of the stability data from Ref. 34 is shown in Table XXI.

A sample curve for $\varepsilon_o = 0.1$ is shown in Figure (49).

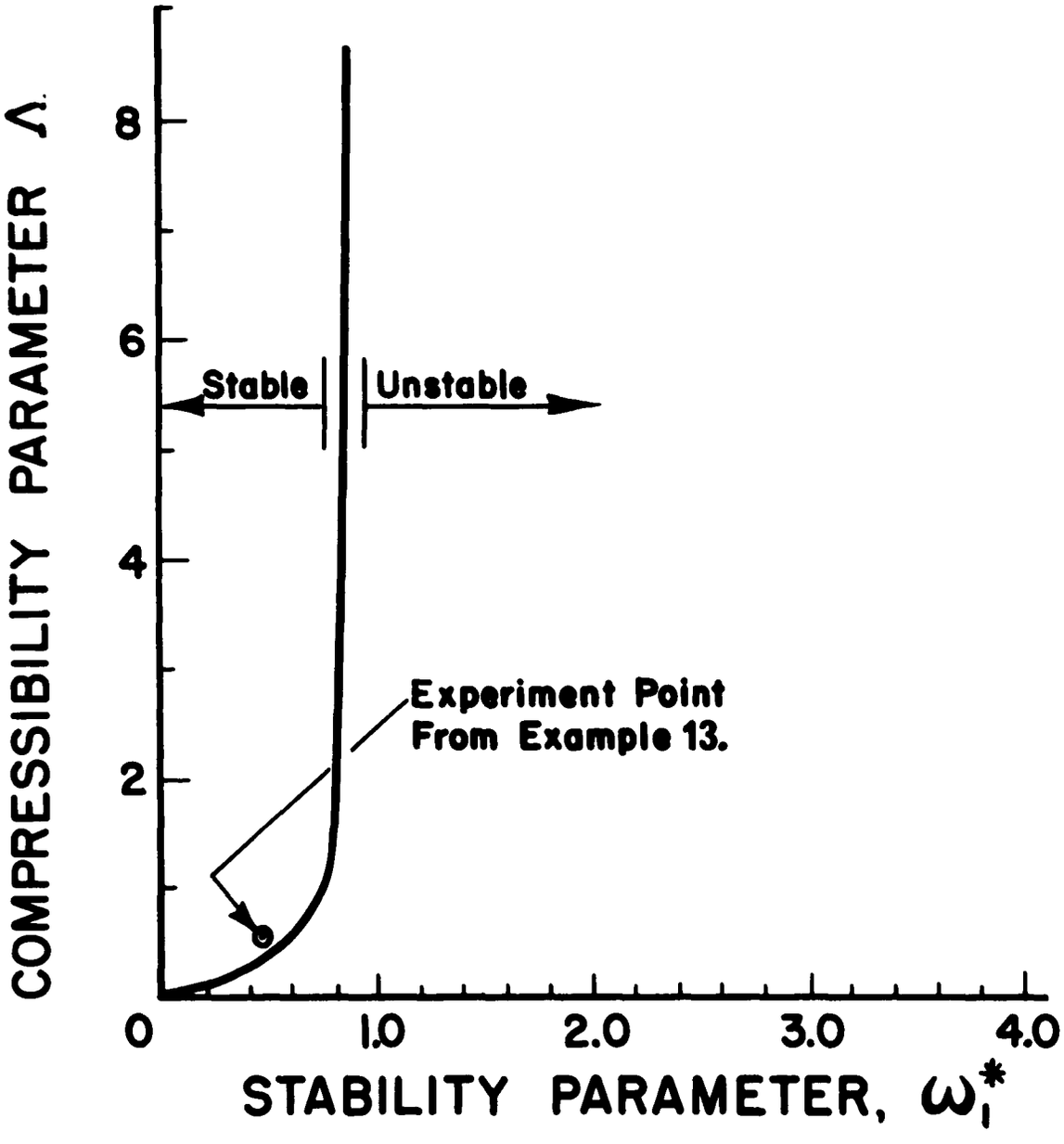

Fig. 49 - Half Frequency Whirl Stability Plot for $\epsilon_o = 0.1$

TABLE XXI

Stability Data From Ref. 34 for Half-Frequency, Translatory Shaft Whirl, in 360° Cylindrical Journal Bearings of Infinite Length

ε_o	ω_1^*	Λ
0.1	0.838	8.016
0.1	0.826	4.004
0.1	0.819	1.996
0.1	0.750	1.0
0.2	0.98	0.9622
0.2	1.09	1.979
0.2	1.06	4.0126
0.2	1.10	8.058
0.4	1.40	0.8209
0.4	1.62	1.859
0.4	1.52	3.9754
0.4	1.52	8.110
0.6	2.14	0.5418
0.6	2.07	1.460
0.6	1.94	3.643
0.6	1.91	7.781
0.8	4.27	0.2052
0.8	4.27	0.6348
0.8	2.68	2.379
0.8	2.32	6.256
0.9	10.05	0.0722
0.9	40.1	0.2221
0.9	13.9	1.017
0.9	3.11	4.246

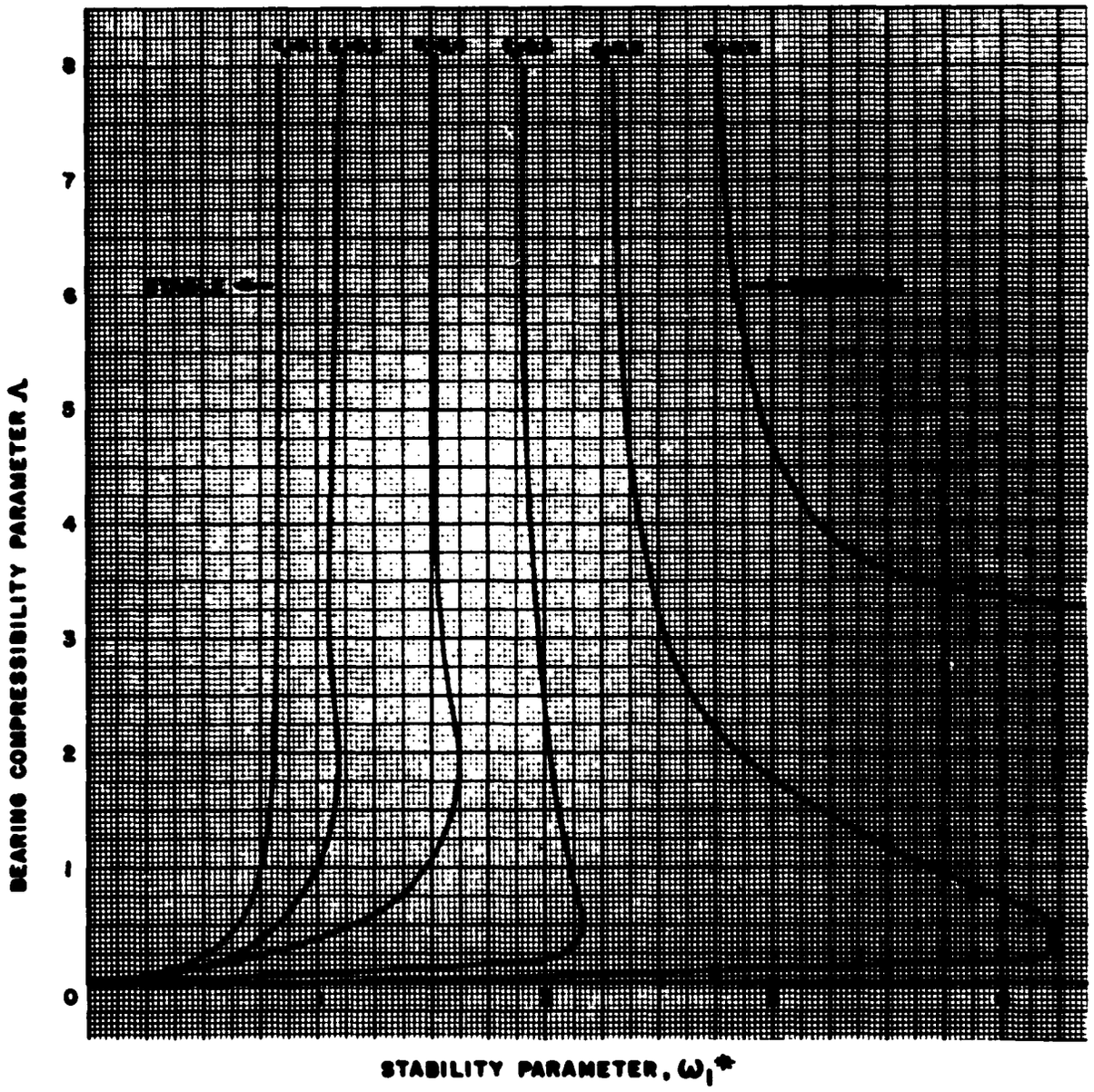

Fig. 50 - Plot of Half-Frequency Translatory Whirl Threshold for Infinite Length 360° Journal Bearing.

Example 13: To illustrate the use of this curve let us calculate the predicted half-frequency whirl threshold speed for a point of experimental data from Ref. 29. The data are as follows:

$$d = 2 \text{ in.}$$
$$l = 4 \text{ in.}$$
$$l/d = 2$$
$$c = 0.000771 \text{ in.}$$
$$\text{Wgt/brg} = 11.01 \text{ lb/brg.}, \quad w = \frac{11.01}{4} = 2.752 \text{ lb/in}$$
$$\mu = 2.7 \times 10^{-9} \text{ reyns (lb.sec/in}^2\text{)}$$
$$P_a = 14.7 \text{ psia}$$
$$A = 0.62$$
$$M_1 = \frac{11.01}{386 \times 4} = 0.00713 \quad \frac{\text{lb.sec}^2}{\text{in}^2}$$

Observed threshold speed for half-frequency whirl 3,200 RPM

or $\omega = 335$ radians/sec.

Calculated value of ω_1^* from Equation (34)

$$\omega_1^* = 335\sqrt{\frac{0.000771 \times 0.00713}{2.752}}$$

$$\omega_1^* = 335\sqrt{1.995 \times 10^{-6}}$$

$$\omega_1^* = 0.473$$

Now to calculate a value of ϵ_o for the equivalent bearing of infinite length, turn to Figure (11).

Value of $\frac{W}{dlP_a}$ for this bearing is $\frac{11.01}{2 \times 4 \times 14.7} = 0.0936$

In Figure (11) with $A = 0.62$ and $\frac{W}{dlP_a} = 0.0936$, ϵ_o is very close to 0.1.

Now locate the intersection of ω_1^* and A in Figure (49). It is slightly to the left of the threshold line for the bearing of infinite length and lies therefore in the stable region. If the point had fallen to the right of this line the indication would have been for unstable operation. Thus the line represents the threshold between stable and unstable shaft rotation.

Notice, however, that the point from Example 11, plotted in Figure (49), is very close to the threshold line showing that the operating condition is somewhat marginal as far as stability is concerned. Actually, as noted previously, this data point was identified with a measured speed of threshold instability.

Instead of having a separate stability plot for each value of ϵ_o similar to Figure (49), it is convenient to combine all data points from Table XXI on a single graph as shown on Figure (50).

It is understood that only one of these curves will be pertinent for any particular stability evaluation and the same conclusions will be valid as outlined in Example 11; namely, if the calculated point falls to the left of the threshold line the operating condition should be stable, and to the contrary, if the calculated point falls to the right of the threshold line operation should be unstable.

Summary of Discussion on Half-Frequency, Translatory Shaft Whirl

The physical explanation for this instability phenomenon begins under Section E and describes the action of the fluid film forces tending to drive the shaft in an orbital fashion about the center of the bearing.

A method of analysis and prediction for rigid-shaft, translatory half-frequency whirl is described and presented as Equation (33). This equation applies to liquid lubricants but has limited use for gaseous lubricants providing Λ is small, perhaps less than 1/3, and if ω_1^* is relatively large, perhaps greater than 1/2. The use of Equation (33) with a gas bearing is demonstrated in detail by Example 10. Figure (46) indicates the approximate error that may be incurred by this method in predicting threshold speeds if Λ grows in magnitude.

In Equation (34) the stability parameter ω_1^* is introduced and then the above method of calculation for finite length journal bearings is modified through the use of this stability parameter, with Example 11 and Table XVIII showing the end results. These are shown graphically in Figures (47) and (48) for bearings of $l/d = \frac{1}{2}$ and $l/d = 1$ respectively. Use of the graphs and the correction factor "C" for improved accuracy is shown in Example 12.

Finally, a method for the prediction of half-frequency, translatory whirl of a shaft in infinitely long, cylindrical journal bearings for any value of Λ and ω_1^* is presented in Figure (50). This method can be applied to bearings with l/d ratios of perhaps 2.5 to 3.0 and larger and may also be used, with some discretion, for shorter bearings. Example (13) and Figure (49) demonstrate the procedure.

Conical Half-Frequency Shaft Whirl Rotating Journal (Rigid Body Condition)

Conical, half-frequency whirl is somewhat similar to the conical synchronous resonant whirl described earlier by Equations (20) through (31) except of course that now the orbital frequency is about half of the spinning frequency and also the spring rate instead of being k as defined in Figure (38) is now K_2 as defined in Eq. (32).

Thus, like Equation (21), we will have for conical half-frequency shaft whirl

$$f_{\frac{cs}{2}} = \frac{1}{\pi}\sqrt{\frac{K_2 L^2}{2\ I_{ts}}} \tag{35}$$

L is the distance between bearings as shown in Figure (40)

I_{ts} is the transverse moment of inertia of the shaft rotor system about a diameter ($lb.in.sec^2$)

With conical motion of the shaft, there may be gyroscopic moment contributions to increase the apparent stiffness of the shaft, especially if the mass is concentrated in the shape of discs or rotors. Following the direction of Den Hartog in "Mechanical Vibrations", 4th Edition,

McGraw-Hill Book Company, we arrive at Equation (36) for conical half-frequency shaft whirl.

$$\frac{f_{cs}}{2} = \frac{1}{\pi}\sqrt{\frac{K_2 L^2}{2\,[I_{ts} - 2\,I_{ps}]}} \tag{36}$$

where I_{ps} is the polar moment of inertia of the shaft-rotor system.

Conical Half-Frequency Bearing Whirl (Rotating and Non-Rotating Bearings)

Next we consider the case of half-frequency bearing whirl. This can occur (as with synchronous whirl) if the bearing is held in flexible supports and moves relative to the spinning shaft. With translatory half-frequency whirl of the bearing we have Equation (37)

$$\frac{f_{tb}}{2} = \frac{1}{\pi}\sqrt{\frac{K_2}{m_b}} \tag{37}$$

For conical whirl of a non-rotating bearing we have Equation (38)

$$\frac{f_{cb}}{2} = \frac{1}{\pi}\sqrt{\frac{K_{2c}}{I_{tb}}} \tag{38}$$

$$\text{where } K_{2c} = \frac{K_2 l^2}{K^*} \tag{39}$$

where K^* is a numerical factor determined from Table XVI.
l is the length of the bearing as shown in Fig. (41)
I_{tb} is the transverse moment of inertia of the bearing about a diameter.

Therefore, Equation (38) becomes

$$f_{\frac{cb}{2}} = \frac{1}{\pi}\sqrt{\frac{K_2\ l^2}{K^*\ I_{tb}}} \qquad (40)$$

And finally, for the case of a stationary shaft and a rotating bearing as shown in Figure (43)

$$f_{\frac{cb}{2}} = \frac{1}{\pi}\sqrt{\frac{K_2\ l^2}{K^*\ [I_{tb} - 2\ I_{pb}]}} \qquad (41)$$

Let us now summarize the various equations that apply to half-frequency whirl:

1. Translatory, half-frequency shaft whirl small values of Λ - Equation (33)

2. Correction Factors, Figures (47) and (48)

3. Translatory, half-frequency shaft whirl, infinitely long bearings - Figure (50).

4. Conical, half-frequency shaft whirl
   (a) Without gyroscopic action - Eq. (35)
   (b) With gyroscopic action - Eq. (36)

5. Translatory, half-frequency bearing whirl, with rotating or non-rotating bearing - Eq. (37)

6. Conical, half-frequency bearing whirl
   (a) Non-rotating bearing - Eq. (40)
   (b) Rotating bearing - Eq. (41)

As with synchronous whirl it is frequenly possible to predict which mode of half-frequency vibration may be expected to occur first as the speed of a unit is slowly raised. For the case of shaft half-frequency whirl we may take the ratio of Equation (33) to Equation (36)

$$\frac{f_{\frac{ts}{2}}}{f_{\frac{cs}{2}}} = \frac{\frac{1}{\pi}\sqrt{\frac{2K_2}{m_s}}}{\frac{1}{\pi}\sqrt{\frac{K_2 L^2}{2[I_{ts}-2I_{ps}]}}}$$

$$\left[\frac{f_{\frac{ts}{2}}}{f_{\frac{cs}{2}}}\right]^2 = \frac{2K_2\ 2[I_{ts}-2\ I_{ps}]}{m_s\ K_2 L^2}$$

Assuming that the value of K_2 at translatory and conical operating speeds is the same

$$\left[\frac{f_{\frac{ts}{2}}}{f_{\frac{cs}{2}}}\right]^2 = \frac{4[I_{ts}-2\ I_{ps}]}{m_s\ L^2} \qquad (42)$$

Thus, if the right hand side of Equation (42) is greater than one, then $f_{cs/2}$, the conical shaft half-frequency whirl, will occur at a lower speed than $f_{ts/2}$, the translatory shaft half-frequency whirl. If the right hand side is less than one it follows that the translatory mode will have the lower frequency.

Repeating the calculations shown in the section on synchronous whirl for an electric motor rotor held in two rigid non-rotating bearings (Ref. 31), we have the following:

Weight of rotor = 17.19 lb.
L (distance between bearings) = 11.75 inches
I_{ts} = 1.91 lb. in.sec^2
I_{ps} = 0.063 lb.in.sec^2

Substituting in Equation (42),

$$\left[\frac{f_{\frac{ts}{2}}}{f_{\frac{cs}{2}}}\right]^2 = \frac{4\ [1.91 - 2(0.063)]}{17.19/386 \times 11.75^2} = 1.16$$

The results of tests made by the authors of Ref. 31 showed that conical half-frequency whirl was observed at a lower speed than translatory whirl as would have been expected with a ratio of $[f_{ts/2}/f_{cs/2}]^2 = 1.16$.

For the case of a non-rotating bearing, we take the ratio of Equation (37) to Equation (40).

$$\frac{f_{\frac{tb}{2}}}{f_{\frac{cb}{2}}} = \frac{\frac{1}{\pi}\sqrt{\frac{K_2}{m_b}}}{\frac{1}{\pi}\sqrt{\frac{K_2\, l^2}{K^*\, I_{tb}}}}$$

and

$$\left[\frac{f_{\frac{tb}{2}}}{f_{\frac{cb}{2}}}\right]^2 = \frac{K^*\, I_{tb}}{m_b\, l^2} \tag{43}$$

This is the same as Equation (30) for synchronous whirl and the experimental data taken from Ref. 35 establish the validity of Equation (43).

For the case of bearing half-frequency whirl with a stationary shaft but with a rotating bearing we take the ratio of Equations (37) to (41).

$$\frac{f_{\frac{tb}{2}}}{f_{\frac{cb}{2}}} = \frac{\frac{1}{\pi}\sqrt{\frac{K_2}{m_b}}}{\frac{1}{\pi}\sqrt{\frac{K_2 l^2}{K^*\,[I_{tb}-2I_{pb}]}}}$$

yielding

$$\left[\frac{f_{\frac{tb}{2}}}{f_{\frac{cb}{2}}}\right]^2 = \frac{K^*\,[I_{tb}-\,2\,I_{pb}]}{m_b\, l^2} \tag{44}$$

Example 14: Experiments at the Rotron Manufacturing Company with a stationary shaft and rotating bearing of the following dimensions have shown that the mode of half-frequency whirl observed is conical. Let us substitute the particular values into Equation (44) to see if this would have been predicted. For a hollow circular cylinder we have the following relationships. The symbols are shown in Figure (52) and the schematic representation in Fig.(51):

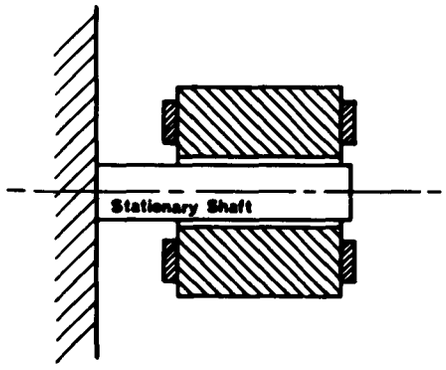

Fig. 51 - Schematic Representation of Rotating Bearing On Stationary Shaft.

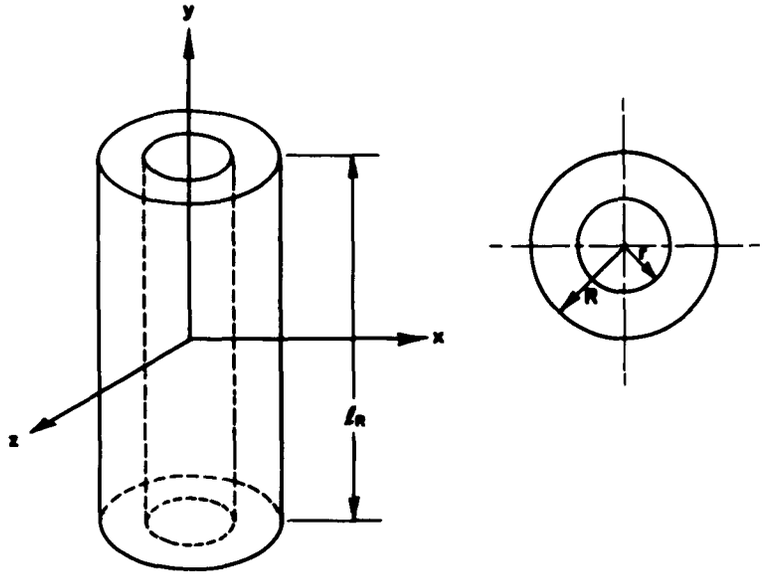

Fig. 52 - Dimensions of Hollow Cylinder for Equations. (45) and (46).

$$I_{xx} = I_{tb} = \frac{W}{g}\left[\frac{\ell_R^2}{12} + \frac{(R^2 + r^2)}{4}\right] \qquad (45)$$

where W is the weight of the bearing.

$$I_{yy} = I_{pb} = \frac{W}{2g} [R^2 + r^2] \qquad (46)$$

$R = 0.456$ in.
$r = 0.225$ in.
$W = 0.342$ lbs.
$l_R = 2.50$ in.

Substituting in Equation (45)

$$I_{tb} = \frac{0.342}{386} \left[\frac{2.50^2}{12} \quad \frac{(0.456^2 + 0.225^2}{4}\right]$$

$$I_{tb} = 0.000519 \text{ lb.in.sec}^2$$

Next, substituting in Equation (46)

$$I_{pb} = \frac{0.342}{2x386} [0.456^2 + 0.225^2]$$

$$I_{pb} = 0.0001144 \text{ lb.in.sec}^2$$

The actual l/d ratio for this bearing is 3.33. From Table XVI K* is approximately 15. Substituting into Equation (44) we have

$$\left[\frac{f_{\frac{tb}{2}}}{f_{\frac{cb}{2}}}\right]^2 = \frac{15 x [0.000519 - 2 \times 0.0001144]}{\frac{0.342}{386} \times 1.25^2}$$

Note: The actual length of bearing inside of cylinder is 1.25 inches therefore l = 1.25 and the l/d ratio is 3.33.

$$\left[\frac{f_{\frac{tb}{2}}}{f_{\frac{cb}{2}}}\right]^2 = \frac{15 \times 0.0002902 \times 386}{0.342 \times 1.25^2}$$

$$= 3.15$$

So that the translatory mode would occur at a higher speed than the conical mode. This was observed experimentally.

For this bearing then:

$$\frac{f_{\frac{tb}{2}}}{f_{\frac{cb}{2}}} = \sqrt{3.15} = 1.775$$

This would mean, $f_{\frac{tb}{2}} = 1.78 \times f_{\frac{cb}{2}}$

Next let us attempt to predict the actual whirl threshold speed for this bearing, using the method involving Figure (50).

Example 15: If the bearing of Example 14 has a diametral clearance of 0.00066 inches and the actual bearing bore is 0.375 inches, using air as the lubricant, what would be the predicted threshold speed for initiation of conical, half-frequency whirl? For correlation with analytical prediction, we have a measured threshold of 3900 RPM.

Let us consider a speed of 7200 RPM. Assuming the viscosity of air as 2.7×10^{-9} lbs.sec/in^2, then from Equation (1)

$$A = \frac{6\mu\omega}{P_a}\left(\frac{r}{c}\right)^2$$

$$\omega = \frac{2\pi N}{60} = \frac{2\pi \times 7200}{60} = 755 \text{ rads/sec.}$$

Therefore:

$$A = \frac{6 \times 2.7 \times 10^{-9} \times 755}{14.7}\left(\frac{0.1875}{0.00033}\right)^2$$

$$A = 0.268$$

$$\frac{W}{dlP_a} = \frac{0.342}{0.375 \times 1.25 \times 14.7} = 0.0496$$

From Figure (11), for an equivalent bearing of infinite length with $A = 0.268$ and $W/dlP_a = 0.0496$ we have $\epsilon_o = 0.13$.

In order to make use of the stability curves Figure (50), it is necessary to determine ω_1^* from Equation (34) where:

$$\omega_1^* = \omega\sqrt{\frac{cM_1}{W}}$$

For the case of just a simple gravity load of the rotor on the bearing, Equation (34) becomes:

$$\omega_1^* = \omega\sqrt{\frac{cW}{Wg}} = \omega\sqrt{\frac{c}{g}} \qquad (34A)$$

Therefore

$$\omega_1^* = 755\sqrt{\frac{0.00033}{386}} = 755 \times 0.925 \times 10^{-3}$$

$$\omega_1^* = 0.698$$

In Figure (50) there is no stability curve for the calculated ϵ_o of 0.13 and it is necessary therefore to estimate the location of this line. We are interested in determining whether the value of $\omega_1^* = 0.698$ and $A = 0.268$ on Figure (50) is located to the left (stable region) or to the right (unstable region) of the $\epsilon_o = 0.13$ stability line. If we plot the point for $A = 0.268, \omega_1^* = 0.698$, it would appear to fall on the estimated 0.13 stability line. This would indicate that the threshold of translatory bearing whirl would be very close to 7200 RPM. From Example 12, concerning this bearing, it was determined that conical bearing whirl would be encountered before translatory whirl with the following relationship:

$$f_{\frac{tb}{2}} = 1.78\, f_{\frac{cb}{2}}$$

Therefore the threshold of half-frequency conical whirl would be predicted as:

$$f_{\frac{cb}{2}} = \frac{7200}{1.78} = 4050 \text{ RPM}$$

As was stated, the measured value was 3900 RPM.

III. SELF-ACTING THRUST BEARINGS

Self-action thrust bearings may be of many types. All of the usual varieties may be employed with gaseous lubricants. These are the classical, pivoted-pad type, the tapered land with fixed geometry, the Rayleigh step bearing and various forms of the pocket bearing. Figure (53).

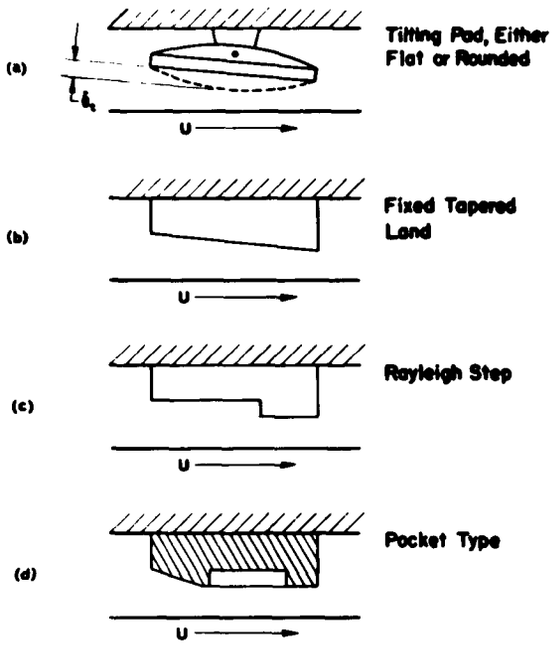

Fig. 53 - Typical Forms of Self-Acting Thrust Bearing. (Ref. 21).

In addition, the spiral or herringbone grooved pumping plate may be used, which is in essence a modification of the Rayleigh step as applied to circular geometry. See Figure (54) and also Figure (5), which is reproduced for convenience as Figure (55).

The choice among these bearings will depend upon the relative ease of physical construction, practicability of installation in a given machine, and ability to carry the specified loads within the limits of available space. The tilting-pad type of bearing is self-aligning but does not equalize the loads on each shoe of the bearing. The other types are not self-aligning and usually require some type of gimbal, pivoted or flexible mounting to perform this function. Many of the comments previously made for self-acting journal bearings apply equally as well to thrust bearings. Pressures are developed in the same fashion and a typical pattern for a tilting pad type is shown in Figure (56). In a qualitative way Figure (56) shows the difference between the pressure rise for a compressible and an incompressible lubricant. Figure (57) shows quantitative values for such a bearing.

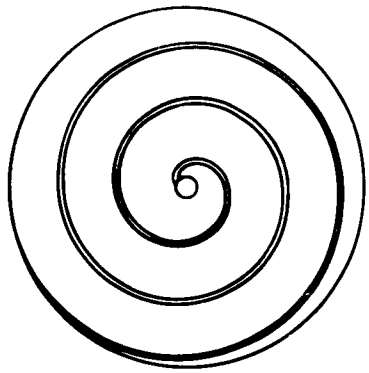

Fig. 54 - Grooved Pumping Plate With Either Logarithmic or Archimedean Spiral.

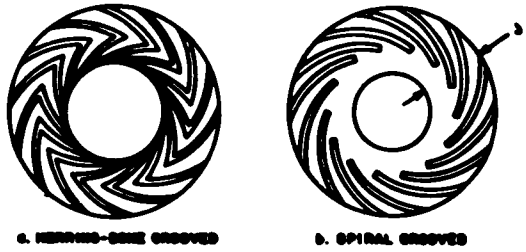

Fig. 55 - Grooved Thrust Bearings.

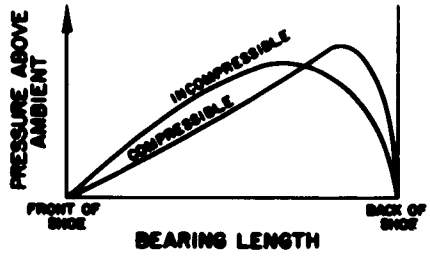

Fig. 56 - Comparative Pressure Distribution for Compressible and Incompressible Lubrication. (From Gross, Ref. 36).

Note that for high values of Λ (see Eq.2)(or in this case as the ambient pressure falls) the center of pressure moves toward the trailing edge or the back of the pad. For each such operating condition the pivot must be located at the center of pressure. Where the ambient pressure or speed are likely to change considerably (Λ varies over a fairly wide range) this would be a disadvantage.

Thrust shoes made of fixed tapered lands, Rayleigh steps or pockets, would not be sensitive to this situation.

The literature is quite complete on the analysis and design of the tilting-pad thrust bearings (Ref. 11). However, they will not be considered here because of the practical limitations imposed by the small size of the blowers toward which this design manual is pointed. A lower limit on the size of a tilting-pad thrust bearing with an equalizer system would be about 1½ inches outside diameter. They can, of course, be made smaller but the cost of manufacture would make them impractical for use in commercially competitive equipment.

Instead, design procedures for the spiral grooved pumping plate will be described as shown in its optimized form in Figure (55b).

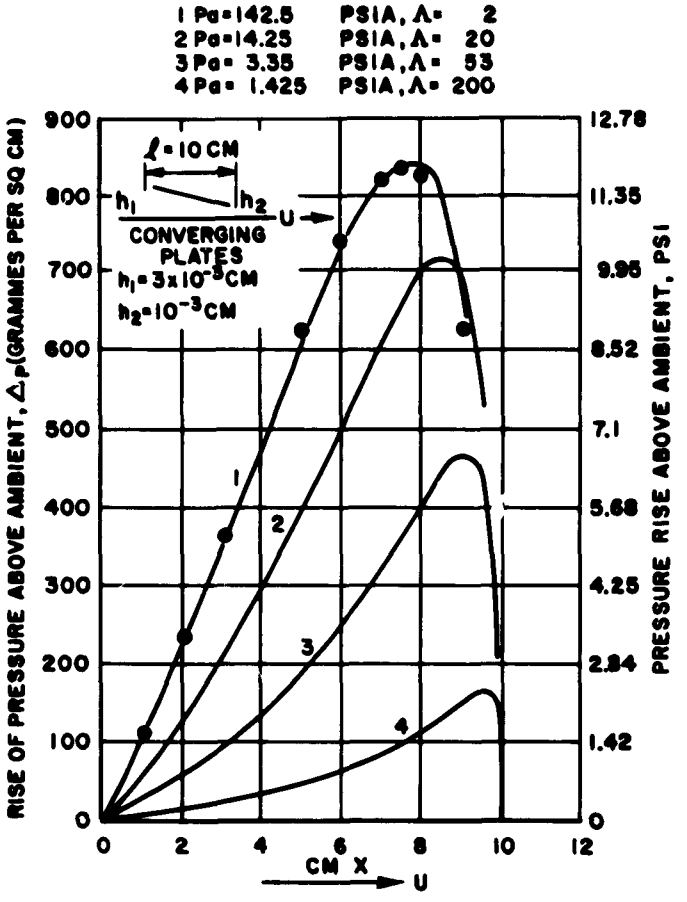

Fig. 57 - Gas Pressure Distribution in Flat Tilted Pad Bearing.

This is based on the principle of the Rayleigh step bearing, Figure (53c), where gas is dragged into a slot by a moving runner. The exit end of the slot has a restrictor or dam so that the escape of gas from the slot is retarded. The runner continues to pump gas into the entrance of the slot due to viscous drag and as a consequence the pressure in the slot builds up and the bearing has the capacity to carry load with a gas film separating the surface. Fig.(58).

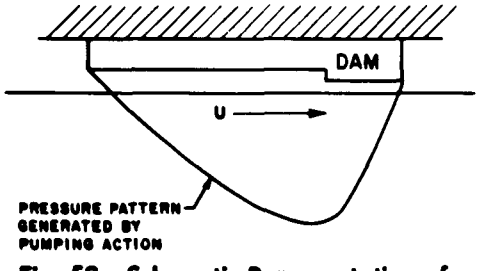

Fig. 58 - Schematic Representation of a Pumping Groove.

Reasonably high pressures can be generated and since the surface area on such a pumping plate-thrust bearing is large, the load-carrying capacity is surprisingly high.

A detailed hydrodynamic theory for the spiral grooved thrust plate has been worked out by Whipple (37). This theory includes the types shown in Figure (55a) and (b). He has shown that for the herringbone thrust plate the pressure rise developed by the grooving is independent of compressibility effects. For the spiral grooved thrust plate Whipple indicates that compressibility effects do occur but the effects are not significant until the pressure rise developed by the grooves is three or four times the ambient pressure. For applications in normal atmospheres such limits are not generally exceeded and as a consequence the solution of the equations based on an incompressible lubricant may be used. This may be measured in terms of another form of the compressibility bearing parameter Λ . For thrust plates Λ may be described as:

$$\Lambda = \frac{6\mu UJ}{h^2 P_a} \qquad (3)$$

where J is the radial dimension of the thrust plate.

The data show that for values of Λ up to 30 very little difference is discernable between solutions for incompressible and compressible lubricants as applied to the spiral grooved pumping plate.

Dr. Boeker (38), reports on a detailed calculation for a grooved thrust plate of this type having an outside diameter of four inches and an inside diameter of 2.5 inches, operating in air at atmospheric pressure. With a running film thickness of 0.0003 inch and a speed of 10,000 RPM and using the optimized geometry recommended by Whipple, the average film pressure developed is about 4.6 psi. With an effective plate area of 7.65 square inches, the load-carrying capacity is calculated to be about 35 pounds.

Whitley and Williams (39) indicate however, that unless the plates of the thrust bearing are especially rigid, distortions and deflections of the plates will reduce the estimated load-carrying capacity. Depending upon the degree of distortion the measured load has ranged from ½ to 3/4 of the predicted theoretical load. Other investigators show results ranging mostly from 3/4 up to the full theoretical value of load.

A. Design of Self-Acting, Spiral Grooved Thrust Bearings

A single spiral groove, as shown in Figure (54), will produce a pressure rise and some load-carrying capacity. However, if the design is optimized for maximum load-carrying ability a multiplicity of shorter grooves will be indicated. This has been done by Whipple (37).

He concludes that there should be 18 grooves of width a_1. The land width between grooves is a_2. See Figure (59).

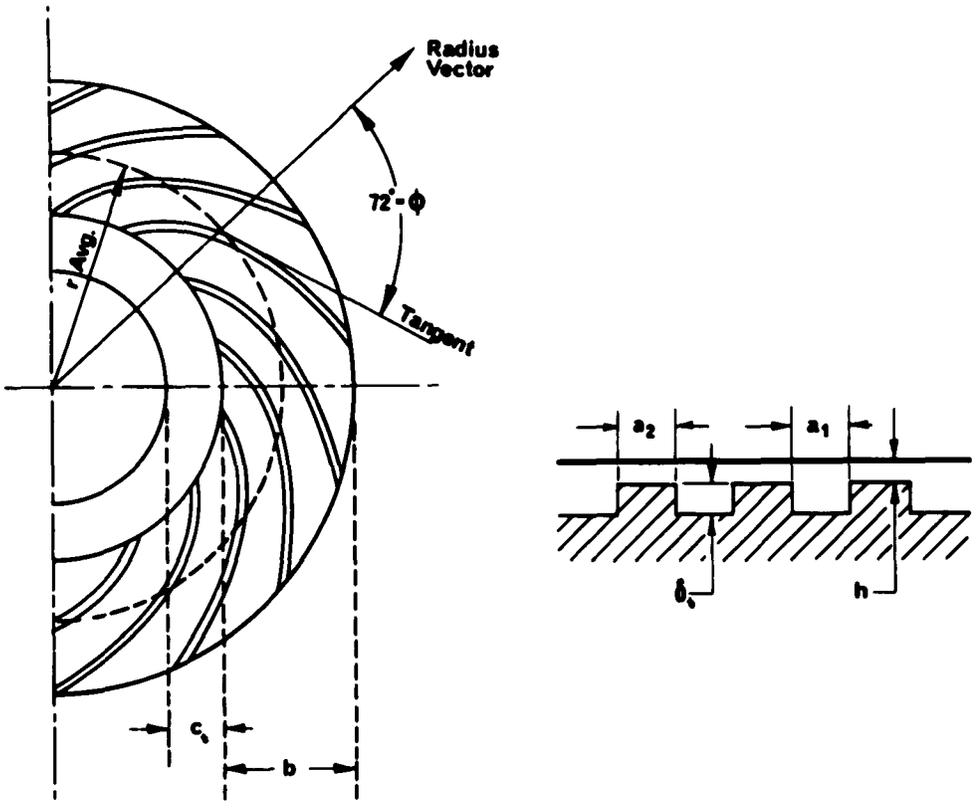

Fig. 59 - Optimized Configuration for Spiral-Grooved Pumping Plate. (37).

Dimension c_t is an ungrooved annulus known as the seal belt. This corresponds to the dam or flow restrictor in the Rayleigh step bearing, Figure (58). In this case, shown in Figure (59), the bearing is considered an inward pumping surface with the direction of rotation of the mating thrust plate CCW. If the direction of rotation is reversed and the seal belt located toward the outer diameter of the thrust plate we would obtain an outward pumping thrust surface.

In Figure (59):

(δ_t) is the depth of the groove
(h) is the film thickness of the bearing measured between the top of the land and the thrust face.

Whipple has established that for optimum load-carrying capacity the following relationships should be satisfied.

$$\frac{\delta t}{h} = 3.05 \tag{47}$$

$$a_1 = 1.8\ a_2 \tag{48}$$

$$\frac{b}{b+c_t} = 0.7 \tag{49}$$

$$\phi = 72^{o}$$

Slight deviations from the optimized parameters are possible without too significant a change in performance. For greater variations actual evaluations by testing is recommended.

Two parameters for the analysis of these optimized bearings have been developed by Whipple. They are:

$$\theta = \frac{T}{(b+c)\ P_a} \tag{50}$$

$$\tau = \frac{1}{1.145}\ \frac{\mu\ u_o (b+c)}{h^2\ P_a} \tag{51}$$

where the individual variables are described as follows:

T = thrust capacity per inch of mean circumference (lb/in)

u_o = the linear velocity at the mean radius (in/sec)

Values of τ and θ are given in Table XXII.

TABLE XXII

Values of Spiral-Grooved Thrust Plate Parameters, θ and τ (Ref.37)

τ	θ
10	2.62
8	2.25
6	1.78
4	1.26
2	0.70
0	0

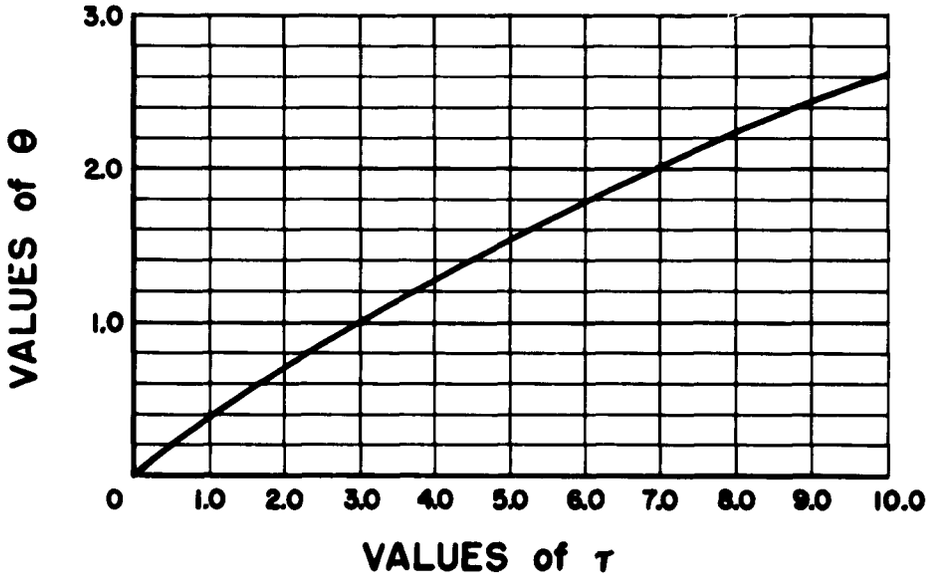

Fig. 60 - Spiral-Grooved Thrust Plate Parameters from Table 20. (37).

Example 16: To illustrate the design approach established by Whipple let us determine the load-carrying capacity of a particular thrust bearing geometry having an outside diameter of 1.365 inches and an inside diameter of 0.420 inches. Rotor speed 3450 RPM. Rotor weight 0.388 lbs. Magnetic thrust load 0.30 lbs. Referring to Figure (59),

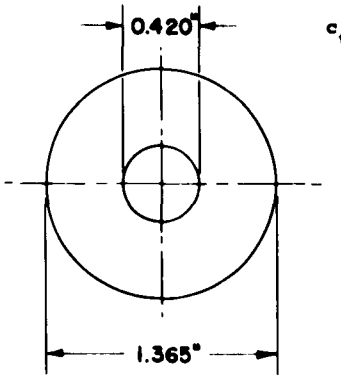

$$c_t + b = \frac{1.365-0.420}{2} = 0.473"$$

From Equation (49),

$$b = 0.7(b+c_t) = 0.7(0.473) = 0.3311"$$

or $c_t = 0.473-0.3311 = 0.142"$

Mean radius $r_m = \frac{1.365}{2} - \frac{0.420}{2} + 0.210$

$$r_m = 0.446"$$

Mean Circumference = $2\pi r_m$

Mean Circumference = $2\pi \times 0.446$

Mean Circumference = 2.80"

With 18 grooves, $a_1 + a_2 = \frac{2.80}{18}$

$$a_1 + a_2 = 0.1555"$$

From Equation (48) $1.8\, a_2 = a_1$

Substituting in above

$$1.8\, a_2 + a_2 = 0.1555"$$

$$2.8\, a_2 = 0.1555"$$

$$a_2 = 0.0556"$$

and $a_1 = 0.0999"$

Now with air having a viscosity of 2.86×10^{-9} reyns, we will next evaluate the parameter τ. The peripheral speed at the mean radius is

$$u_o = \frac{3450}{60} \times 2\pi \times 0.446 = 161 \text{ in/sec.}$$

Then in Equation (51),

$$\tau = \frac{1}{1.145} \frac{\mu u_o (b+c_t)}{h^2 P_a}$$

$$\tau = \frac{1}{1.145} \frac{2.86 \times 10^{-9} \times 161 \times 0.473}{h^2 \times 14.7}$$

$$\tau = \frac{12.98}{h^2} \times 10^{-9}$$

assume $h = 0.0001"$

then $\tau = \frac{12.98 \times 10^{-9}}{(1 \times 10^{-4})^2} \quad \frac{12.98 \times 10^{-9}}{10^{-8}} = 1.298$

and from Figure (60) $\theta = 0.454$

For small values of τ and θ straight line interpolation may be made with good accuracy since the plot in Figure (60) is essentially linear for this range of variables. For example,

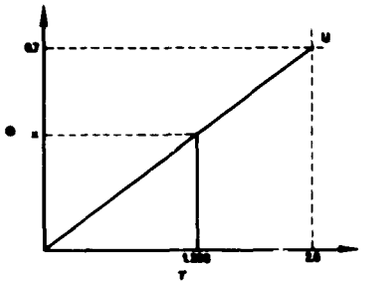

$$\frac{x}{1.298} = \frac{0.7}{2.0}$$

$$x = \frac{0.7}{2.0} \times 1.298$$

$$x = 0.454 = \theta$$

Then from Equation (50):

$$\theta = \frac{T}{(b+c_t)P_a}$$

$$T = \theta (b+c_t) P_a$$

$$T = 0.454 \times 0.473 \times 14.7$$

$$T = 3.16 \text{ lbs/in. thrust capacity per inch of mean circumference}$$

Total thrust capacity $= T \times 2\pi r_m$

$$= 3.16 \times 2.80$$

$$= 8.85 \text{ lbs with } h = 0.0001"$$

If this were the applied thrust load, then the groove depth would be determined by Equation (47),

$$\delta_t = 3.05\, h$$

In this case $\delta_t = 3.05 \times 0.0001$

$$\delta_t = 0.0003 \text{ inches}$$

However, it is desirable to develop a more complete picture of the bearing performance. This can be done by assuming different values for h and computing the corresponding values of τ, θ, T and total thrust capacity, as shown in Table XXIII.

Table XXIII

Computed Values of Thrust Capacity

h inches	τ	θ	T lbs/in	T total lbs.
0.0001	1.298	0.454	3.16	8.85
0.0002	0.3245	0.1137	0.792	2.215
0.0003	0.1443	0.0505	0.353	0.984
0.0004	0.0811	0.0284	0.198	0.554
0.0005	0.0519	0.01815	0.1265	0.354
0.0006	0.0360	0.0126	0.0878	0.246
0.0007	0.0265	0.00926	0.0645	0.1807
0.0008	0.0203	0.0071	0.0495	0.1385
0.0009	0.01603	0.00561	0.0391	0.1095

Figure (61) depicts a plot of the total load-carrying capacity of such a thrust bearing. On the same plot is also shown a superposition of two of these curves, back to back, as would be the case with a double acting thrust bearing having a total clearance ($h_1 + h_2$) of 0.001 inches. The configuration of such a double acting bearing is shown schematically in Figure (62).

Consider first that we have only a single thrust bearing, the left hand bearing. With a thrust load of 0.3 pounds the operating film thickness would be about 0.0005 inches.

With a double acting bearing and the same external thrust load the operating film thickness would be a little less because the second thrust bearing, while not carrying any external load, would nevertheless impose an additional force upon the thrust face that is already carrying load. The magnitude of this additional internal thrust load will depend upon the total clearance designed into the double acting thrust bearing. This is the clearance designated as $h_1 + h_2$ inches. Figure (62). If a bearing is built with a total clearance of 0.001 inches as depicted in Figure (61), then the net load-carrying load-capacity of the left hand bearing would be given by Table XXIV.

Table XXIV

Load Capacity of Double Acting Thrust Bearing

h inches	T total Left brg. lb.	T total Right brg. lb.	T Net lbs.
0.0001	8.85	0.1095	8.74
0.0002	2.215	0.1385	2.076
0.0003	0.984	0.1807	0.8033
0.0004	0.554	0.246	0.308
0.0005	0.354	0.354	0
0.0006	0.246	0.554	-0.308
0.0007	0.1807	0.984	-0.8033
0.0008	0.1385	2.215	-2.076
0.0009	0.1095	8.85	-8.74

These values are shown in Figure (63).

It should be noted that when the runner is centered in the double acting thrust bearing, corresponding to the case of $h_1 = h_2$ in Figure (62), the load-capacity of the thrust bearing is zero as illustrated on Figure (63) for a film thickness of 0.0005 inches.

If there is a thrust force of 0.3 pounds acting to the left, in Figure (63), the film thickness for the double acting thrust bearing is 0.0004 inches. For the single acting thrust bearing with the same magnitude of load the film thickness would be 0.0005 inches, as was pointed out previously in conjunction with Figure (61).

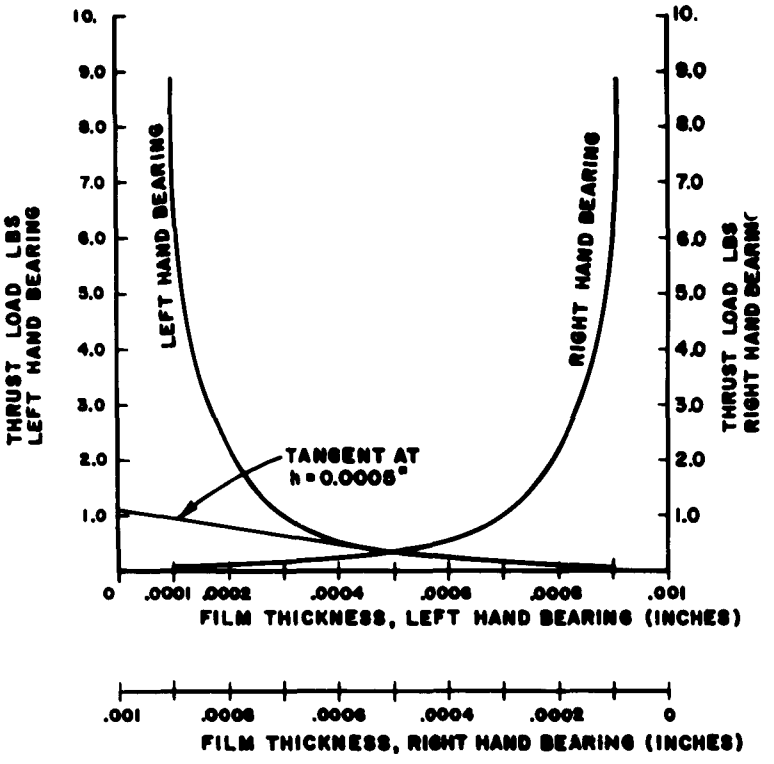

Fig. 61 - Thrust Bearing Capacity of a Single Bearing and Also of a Double Acting Bearing with a Total Clearance of 0.001 Inches.

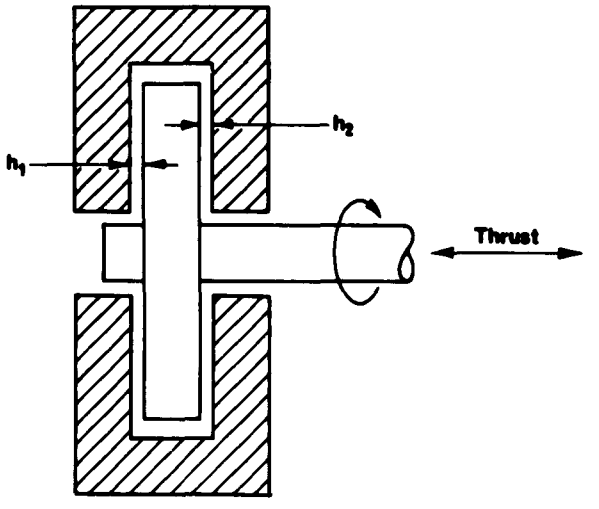

Fig. 62 - Schematic Diagram of Double Acting Thrust Bearing.

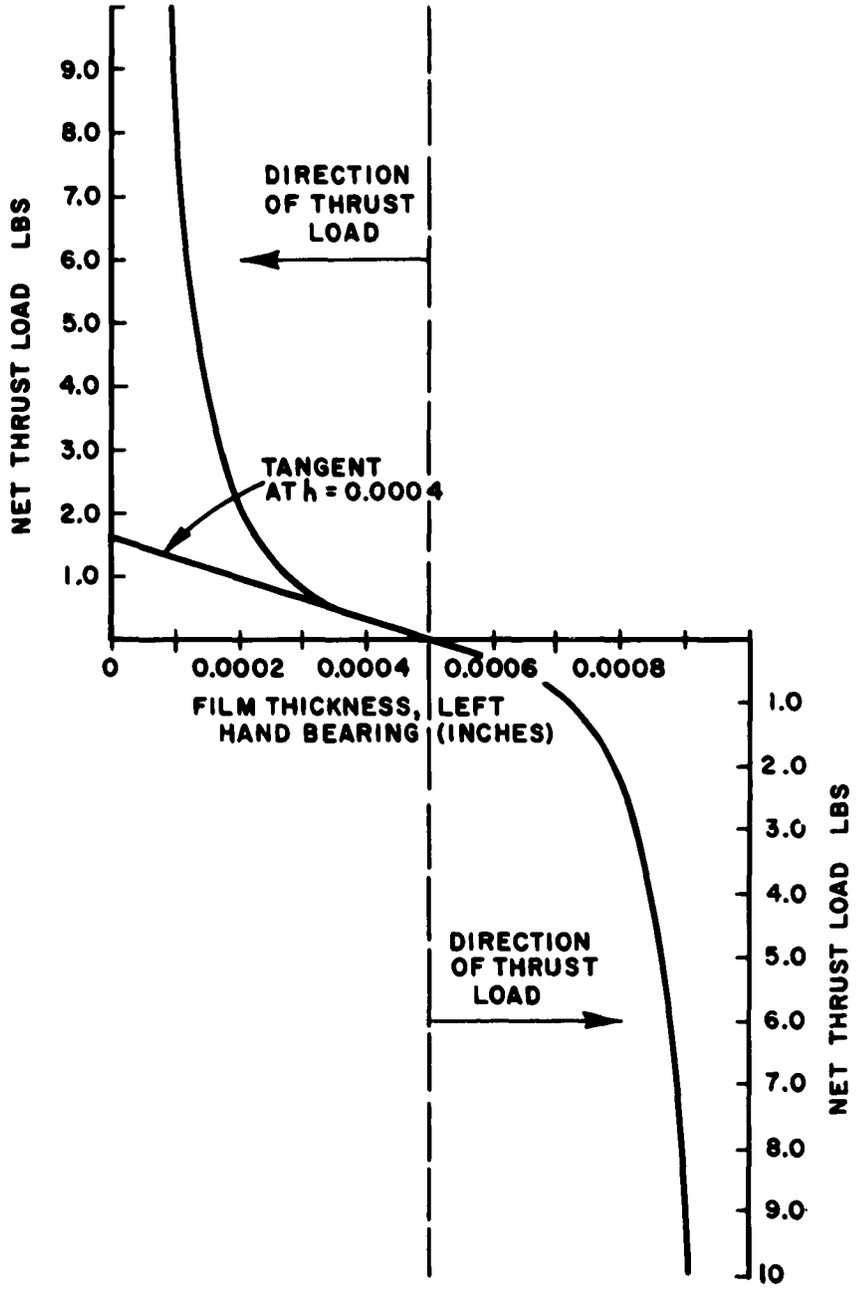

Fig. 63 - Thrust Load Characteristics of Double Acting Bearing With Total Clearance of 0.001 Inches.

Film Stiffness in Spiral Grooved Thrust Bearings

Where the dynamics of the thrust bearing-rotor assembly must be considered, it is necessary to evaluate the stiffness of the gas film in the bearing. This stiffness is defined as the rate of change of thrust capacity with respect to change in film thickness or dT/dh, where T is the thrust load in pounds and h is the film thickness in inches. The units of dT/dh are lbs/in. so that we are dealing with the property of the gas film that behaves like a spring. This characteristic was evaluated earlier for the journal bearing when synchronous whirl in its various forms was investigated.

Referring back to Example 14 and Figure (61), with a thrust load of 0.3 pounds the expected film thickness will be 0.0005 inches. If we draw a tangent to the load-film thickness curve at h = 0.0005 inches, the slope of the curve will be a quasi-static version of the film stiffness which should be satisfactory for the determination of the dynamic characteristics of the system in the axial direction. For example, the slope of the tangent in Figure (61) at h = 0.0005 in. is

$$\frac{1.15-0.354}{0.0005} = \frac{0.796}{0.0005}$$

therefore

$$k = \frac{0.796}{0.0005} = 1592 \text{ lbs/in.}$$

The natural frequency of axial vibration can then be estimated, knowing that weight of the rotor is 0.388 lbs., by using Equation (20) after substituting the appropriate terms.

Thus,
$$f = \frac{1}{2\pi}\sqrt{\frac{1592 \times 386}{0.388}}$$

$$f = 200 \text{ cycles/sec. (axial natural frequency for single-acting bearing)}$$

Now consider the double-acting thrust bearing for the same loading and mass condition. A tangent will be drawn to the curve at a film thickness of 0.0004 inches. The slope of this tangent becomes

$$\frac{1.17}{0.0005} = 3400 \text{ lbs./in.}$$

It becomes evident that the effect of the additional thrust bearing is to apply what might be termed a "preload" to the unit and in this way make the film stiffer and thus raise the natural frequency of vibration of the rotor system.

It follows then that:

$$f = \frac{1}{2\pi}\sqrt{\frac{3400 \times 386}{0.388}}$$

f = 292 cycles/sec.(axial natural frequency for double-acting thrust bearing.)

Using a total clearance less than 0.001 inch would increase the magnitude of the "preload" and thus raise the natural frequency of vibration.

The most complete collection of references on all phases of gas-lubricated analysis and design is Ref. (40), which contains 464 abstracts of papers in this field.

IV. BEARING LOADS

The determination of bearing loads is an important aspect of gas bearing design. The rotating mass load and mass unbalance load are readily attainable by calculation. However, it is also necessary to consider radial loads produced by the motor itself. Of primary concern is the magnetic force produced by an eccentric air gap between the motor stator and the motor rotor.

A. Magnetic Radial Bearing Loads

The three most common types of eccentricity occuring in the fabrication of the motor are:

a. Displacement of the motor stator centerline from the motor rotor centerline.

b. Rotation of the motor rotor around a center other than its geometrical center.

c. A combination of (a) and (b).

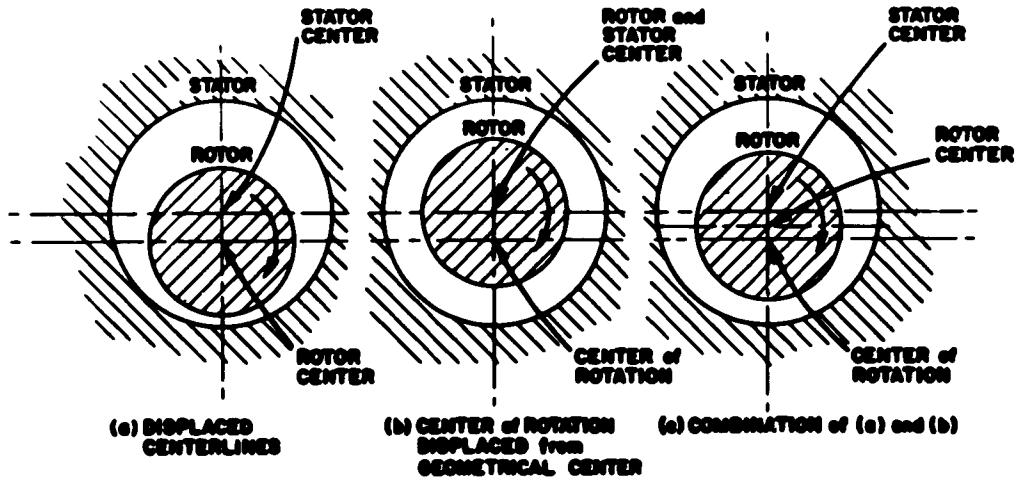

Fig. 64 - Motor Stator to Rotor Eccentricity.

In either of the three cases depicted in Figure (64) the eccentricity produces an unequal air gap between the motor stator and rotor which results in a magnetic radial force. This force is due to an unbalance in the radial direction of the linking of flux lines in the motor gap region. In the case of a two pole motor, the flux lines link the stator north and south poles through the rotor and the stator as shown on Figure (65). The magnetic field rotates at a frequency equal to line frequency. At the instant of time when the stator poles are in position (65a) there is equal linking of the flux lines through the rotor and no radial forces exist. As the field rotates to position (65b), due to the eccentric rotor condition, there is an unbalance of flux lines through the rotor producing unbalanced radial magnetic force in the direction indicated by the vector F. The force drops to zero with an additional 90° rotation of the field (65c) and peaks to a maximum again at 270° total rotation (65d). It can be seen, therefore, that the magnetic radial force is a sinusoidal directional force acting at the minimum motor air gap region at a frequency twice line frequency. The magnitude of the force is a function of the eccentricity and can be described analytically as:

$$F = 17.42 \times \left(\frac{B}{10,000}\right)^2 \times D \times l_m \times \sigma \quad (52)$$

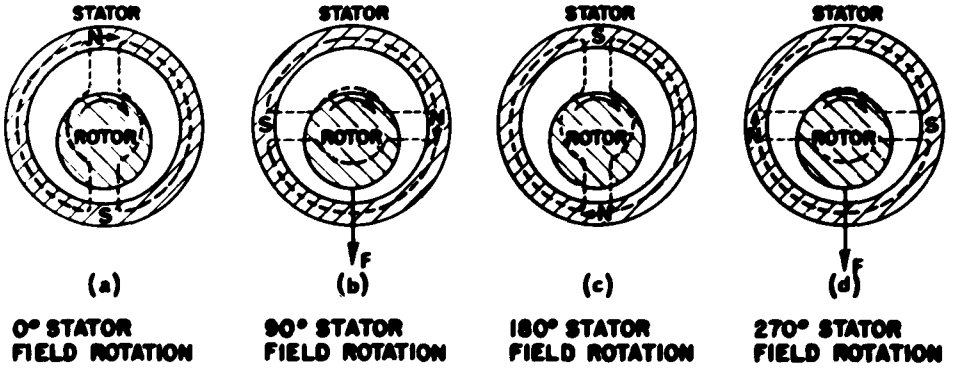

Fig. 65 - Flux Lines Linking Motor Rotor and Stator for Angular Positions of Stator Magnetic Field.

where F = Force (peak value)-lbs.

B = Flux Density -lines per sq.in.

D = Rotor Diameter - inch.

l_m = Rotor Stack Length - inch

$$\sigma = \frac{1}{2\gamma^3}\left[\frac{2-\gamma^2}{2\ 1-\gamma^2}\right] - 1 \qquad (53)$$

$$\gamma = \frac{\text{eccentricity}}{2\ \Delta} \quad \text{(eccentricity = 2 x distance between rotor and stator centers)} \qquad (54)$$

Δ = Average motor radial air gap - inch.

The force described by this formula is a peak value varying from zero to a maximum sinusoidally. The average force acting on the rotor is one half the peak value (F/2).

If the case of Figure (64b) is considered, i.e. the rotor rotating about a center other than it's geometrical center, then the location of minimum air gap rotates about the stator at rotor rotational frequency. In an induction motor the rotor rotates at a frequency less than the stator field rotational frequency. The difference between stator and rotor frequencies is the slip frequency of the motor. As seen on Figure (65), the radial magnetic force occurs when the stator poles are at right angles to the point of minimum motor air gap. This point of minimum motor air gap is rotating at slip frequency in relation to the stator field rotation, and therefore the radial magnetic force rotates at slip frequency.

The most common type of eccentricity encountered in electrical motors is a combination of both displaced rotor and stator centerlines and rotation of the rotor about a center other than its geometrical center. The resultant force varies in magnitude at slip frequencies from a maximum when both eccentricity effects are additive to a minimum when both effects are subtractive.

The significance of these forces can be shown in the following example for a 2 pole, 60 cycle induction motor:

Motor Length (L) = 1.250 inch
Motor Diameter (D) = 0.923 inch
Flux Density (B) = 25,000 lines per inch
Average Motor Air Gap (A) = .0075 inch
Eccentricity due to misalignment of rotor and stator centerlines = .001 TIR (inch)
Runout of Rotor O.D. to Bore = .0005 TIR (inch)
Total Eccentricity = 0.001 + 0.005 = 0.0015

Example 17:

From Equation (52) $F = 17.42 \left(\frac{B}{10,000}\right)^2 \times D \times L_m \times \sigma$

$$Y_{max} = \frac{0.0015}{2\ A} = \frac{0.0015}{2(.0075)} = 0.1 \text{ max.}$$

$$Y_{min} = \frac{0.0005}{2(.0075)} = 0.033 \text{ min.}$$

$$F_{max} = 17.42 \left(\frac{25,000}{10,000}\right)^2 \times 1.250 \times 0.923$$

$$F \left(\frac{1}{2(0.1)} 3 \left[\frac{2-(0.1)^2}{2\ 1-0.1^2} 2 -1\right]\right)$$

$$F_{max} = 0.793 \text{ pounds (peak)}$$

$$\text{Avg.}F_{max} = 0.397 \text{ pounds}$$

$$F_{min} = 0.261 \text{ pounds}$$

$$\text{Avg.}F_{min} = 0.131 \text{ pounds}$$

The average force therefore is in the direction of minimum motor air gap occuring at 120 cycles per second and pulsating at an average force level of 0.397 pounds maximum and 0.131 pounds minimum at slip frequency of the motor.

Bearing Moment Loads

Another condition that can be encountered in electrical motors is the non-parallelism of the stator and rotor centerlines. As shown on Figure (66) this condition creates an eccentric air gap at one end of the rotor 180 degrees out of phase with the eccentricity at the other end of the rotor, thus producing a moment on the rotor. As can be seen from Equation (52), the magnetic force due to motor air gap eccentricity varies directly with both the rotor length and the parameter σ For low eccentricities, at least below .004 inch TIR, σ can be assumed to vary directly with the eccentricity. Table I presents the magnetic force versus eccentricity for Example 15 and indicates very slight deviation from a straight line relationship between force and eccentricity to eccentricities of .004 inches.

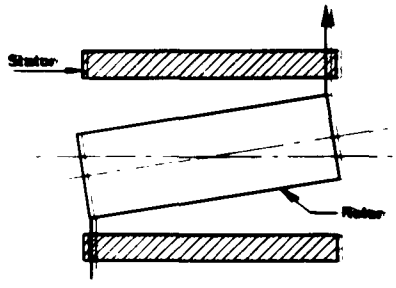

Fig. 66 - Moment Produced By Non-Parallel Motor Rotor and Stator Centerlines.

TABLE I

Eccentricity of Motor Air Gap T.I.R.(in)	Magnetic Force (peak) Pounds
.0005	.26115
.001	.52632
.0015	.79300
.0020	1.0657
.003	1.6354
.004	2.2630

Considering that the magnetic force varies directly with rotor length and eccentricity from Figure (67), the average eccentricity from (a) to (b) is $\sigma_{max}/2$. The force (F_b) at one end of the rotor therefore is:

$$F_b = 17.42 \left(\frac{B}{10,000}\right)^2 \times D \times \frac{1}{2}\ell \times \frac{\sigma_{max}}{2} = \frac{F}{4}$$

The location of this force is two thirds the distance from (a) to (d) or $2/3 \times l_m/2 = l_m/3$.

The force F is a peak to peak value. Therefore the average force = 1/2 x F/4 = F/8. The total moment becomes

$$\text{Moment (in.lbs)} = F/8 \times 2/3\ l_m = \frac{Fl_m}{12}$$

where F = Force at max. eccentricity (lbs)

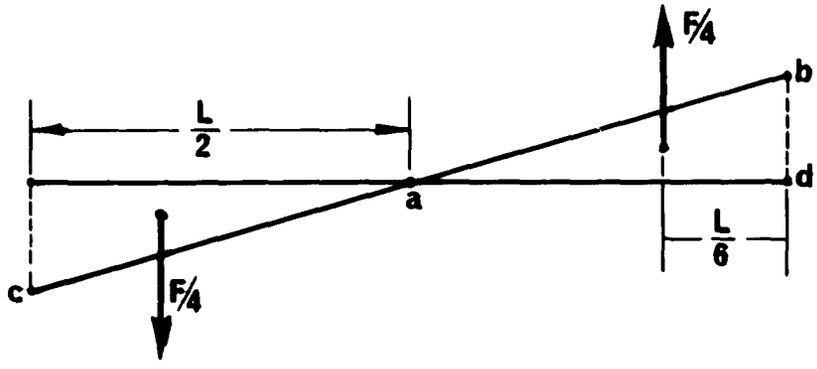

Fig. 67 - Magnetic Force Producing Moment Diagram.

V. BIBLIOGRAPHY

1. Drescher, H., "Air Lubricated Bearings", The Engineer's Digest, Vol. 15, March 1954, pp. 103-107, Abstracted from Zeit. V.D.I., Vol.95, Dec. 11, 1953, pp. 1182-1190.

2. Ford, G. W. K., Harris, D. M., and Pantall, D.,"Principles and Applications of Hydrodynamic-Type Gas Bearings", Proceedings of The Institution of Mechanical Engineers, Vol. 171, No. 2, 1957, pp. 93-113. Discussion, pp. 113-128.

3. Cole, J. A., and Kerr, J., "Observations on the Performance of Air-Lubricated Bearings", Proceedings, Conference on Lubrication and Wear, London, 1957, pp. 164-170.

4. Harrison, W. J., "The Hydrodynamical Theory of Lubrication with Special Reference to Air as a Lubricant", Trans. Cambridge Phil. Soc., Vol. 22, 1912-1923, pp. 39-54.

5. Ausman, J. S., "Theory and Design of Self-Acting, Gas-Lubricated Journal Bearings Including Misalignment Effects", Proceedings, First International Symposium on Gas-Lubricated Bearings, Oct. 1959, pp. 161-192. Superintendent of Documents, U. S. Government Printing Office, Washington, 25, D.C. ACR-49.

6. Pantall, D., and Robinson, C. H., "Gas-Lubricated Bearings in Nuclear Engineering", Nuclear Engineering, Feb. 1959, pp. 53-58.

7. Burgdorfer, A., "The Influence of the Molecular Mean Free Path on the Performance of Hydrodynamic Gas-Lubricated Bearings", Trans. A.S.M.E., Journal of Basic Eng'g., March 1959, pp. 94-100.

8. Wildmann, M., "Experiments on Gas-Lubricated Journal Bearings", A.S.M.E. Paper No. 56-Lub-8.

9. Fuller, D. D., "Theory and Practice of Lubrication for Engineers", John Wiley & Sons, New York, 1956, 432 pages.

10. Elrod, H. G., Jr., and Burgdorfer, A., "Refinements of the Theory of the Infinitely-Long, Self-Acting, Gas-Lubricated Journal Bearing", Proceedings, First International Symposium on Gas-Lubricated Bearings, Oct. 1959, pp. 93-118. Superintendent of Documents, U.S. Government Printing Office, Washington 25, D.C., ACR-49.

11. Gross, W. A., "Gas Film Lubrication", John Wiley & Sons, New York, 1962, p. 238. 413 pages.

12. Elrod H. G., Jr., and Malanoski, S. B., "Theory and Design Data for Continuous-Film, Self-Acting Journal Bearings of Finite Length", Report I-A 2049-13, Nov. 1960, The Franklin IInstitute Laboratories for Research and Development.

13. Elrod, H. G., Jr., and Malanoski, S. B., "Theory and Design Data for Continuous Film, Self-Acting Journal Bearings of Finite Length", (Supplement to Report I-A 2049-13), Report I-A 2049-17, June 1962, The Franklin Institute Laboratories for Research and Development.

14. Raimondi, A. A., "A Numerical Solution for the Gas-Lubricated, Full Journal Bearing of Finite Length", Trans. American Society of Lubrication Engineers, April 1961, Vol. IV, pp. 131-155.

15. Hays, D. F., "A Variational Approach to Lubrication Problems and the Solution of the Finite Journal Bearing", Trans. A.S.M.E., Vol. 81, No.1, March 1959, pp. 13-23.

16. Iwasaki, H., "Measurement of Viscosities of Gases at High Pressure, Part I", Sci. Reports, Research Institute, Tohoku University, Ser. A, 3,pp. 247-257.

17. Kestin, J., and Pilarczyk, K., "Measurement of the Viscosity of Five Gases at Elevated Pressures by the Oscillating Disc Method", Trans. A.S.M.E., Vol. 76, pp.987-999.

18. Ausman, J. S., "Theory and Design of Self-Acting Gas-Lubricated Journal Bearings Including Misalignment Effect", Proceedings, First International Symposium on Gas-Lubricated Bearings, Oct. 1959, pp. 161-192, Superintendent of Documents, U. S. Government Printing Office, Washington 25, D.C., ACR-49.

19. Smith, M. I., and Fuller, D. D.,"Journal Bearing Operation at Superlaminar Speeds", Trans. A.S.M.E., Vol. 78, April 1956, pp. 469-474.

20. Sternlicht, B., and Elwell, R. C.,"Synchronous Whirl in Plain Journal Bearings", A.S.M.E. Paper Preprint 62-Lub-19, 11 pages.

21. Fuller, D. D., "General Review of Gas-Bearing Technology", Proceedings, First International Symposium on Gas-Lubricated Bearings, Oct. 1959, pp. 1-29. Superintendent of Documents, U. S. Government Printing Office, Washington 25, D.C., ACR-49.

22. Fischer, G. K., Cherubim, J. L., and Fuller, D. D., "Some Instabilities and Operating Characteristics of High-Speed, Gas-Lubricated Journal Bearings", A.S.M.E. Paper No. 58-A-231.

23. Fischer, G. K., Cherubim, J. L., and Decker, O.,"Some Static and Dynamic Characteristics of High-Speed Shaft Systems Operating with Gas-Lubricated Bearings", Proceedings, First International Symposium on Gas-Lubricated Bearings , Oct. 1959, pp. 383-417. Superintendent of documents, U. S. Government Printing Office, Washington 25, D.C., ACR-49.

24. Hagg, A. C., "The Influence of Oil-Film Journal Bearings on the Stability of Rotating Machines", Trans. A.S.M.E., Jl. Applied Mechanics, Vol. 68, 1946, pp. A211-A220, Discussion Vol. 69, March 1947, pp. A77-A78.

25. Poritsky, H., "A Contribution to the Theory of Oil Whip", Trans. A.S.M.E., Vol. 75, 1953, pp. 1153-1161.

26. Boeker, G. F., and Sternlicht, B., "Investigation of Translatory Fluid Whirl in Vertical Machines", Trans.A.S.M.E. Vol. 78, 1956, pp. 13-19.

27. Sternlicht, B., "Experimental Verification of Theoretical Investigations into Half-Frequency Whirl", Trans. A.S.M.E.

28. Pinkus, O., and Sternlicht, B.,"Theory of Hydrodynamic Lubrication", McGraw-Hill Book Co., New York, N.Y., 1961, 465 pages.

29. Sternlicht, B., and Winn, L. W., "On the Load Capacity and Stability of Rotors in Self-Acting Gas-Lubricated Plain Cylindrical Journal Bearings", A.S.M.E. Paper No. 62-Lub-8, presented at A.S.ME.-A.S.L.E. Lubrication Conference, Oct. 16-18, 1962, Pittsburgh, Pa.

30. Reynolds, D. B., and Gross, W. A., "Experimental Investigation of Whirl in Self-Acting, Air-Lubricated Journal Bearings", A.S.L.E. Preprint No. 62AM IA-4 presented at the A.S.L.E. Annual Meeting, May 1962, St. Louis, Mo.

31. Elwell, R. C., Hooker, R. J., and Sternlicht, B.,"Gas Bearing Stability Study - Vertical Rotor Investigation", General Electric Tech. Report, May 20, 1960, for Office of Naval Research,General Electric Co., Schenectady, N.Y.

32. Pan, C. H.T., and Sternlicht, B., "On the Translatory Whirl Motion of a Vertical Rotor in Plain Cylindrical Gas-Dynamic Journal Bearings", Trans. A.S.M.E., Jl. of Basic Eng'g., March 1962, pp. 152-158.

33. Cheng, H. S., and Trumpler, P. R., "Stability of High-Speed Journal Bearing under Steady Load. 2. The Compressible Film", A.S.M.E. Paper No. 62-WA-101, presented at the Annual Meeting, November 25-30, 1962, at New York, N.Y.

34. Castelli, V., "Solution of the Stability Problem for 360° Self-Acting, Gas-Lubricated Bearings", Doctoral Dissertation, Columbia University, November 1962.

35. Whitley, S., Bowhill, A. J., and McEwan, P., "Half-Speed Whirl and Load Capacity of Hydrodynamic Gas Journal Bearings", Preprint for March 1962 Meeting of Institution of Mechanical Engineers, (London).

36. Gross, W. A. "Film Lubrication Part II", I.B.M. Research Paper RJ-RR-117-2, March 17, 1958.

37. Whipple, R. T. P., "Theory of the Spiral Grooved Thrust Bearing with Liquid or Gas Lubricant", Atomic Energy Research Establishment T/R 622, 1951.

38. Boeker, G. F., Fuller, D. D., and Kayan, C. F., "Gas-Lubricated Bearings, A Critical Survey", WADC Tech. Report 58-495, Wright Air Development Center, July 1958. ASTIA Document No. AD 216 356.

39. Whitley, S., and Williams, L. G., "The Gas-Lubricated Spiral Groove Thrust Bearing", United Kingdom Atomic Energy Authority (I.G.) Report: IG Report 28(RD/CA), 1959.

40. Peters, A. and Sciulli, E. B., edited by D. D. Fuller, "A Bibliography (with abstracts) on Gas-Lubricated Bearings - Revised", The Franklin Institute Report No. I-A2049-16, Oct. 15, 1961. ASTIA No. AD 264 965.

41. Simons, E. M., "Hydrodynamic Lubrication of Cyclically Loaded Bearings", Trans. A.S.M.E., Vol. 74, August 1952.